Terms and Conditions of Use of Digitised Theses from Trinity College Library Dublin

Copyright statement

All material supplied by Trinity College Library is protected by copyright (under the Copyright and Related Rights Act, 2000 as amended) and other relevant Intellectual Property Rights. By accessing and using a Digitised Thesis from Trinity College Library you acknowledge that all Intellectual Property Rights in any Works supplied are the sole and exclusive property of the copyright and/or other IPR holder. Specific copyright holders may not be explicitly identified. Use of materials from other sources within a thesis should not be construed as a claim over them.

A non-exclusive, non-transferable licence is hereby granted to those using or reproducing, in whole or in part, the material for valid purposes, providing the copyright owners are acknowledged using the normal conventions. Where specific permission to use material is required, this is identified and such permission must be sought from the copyright holder or agency cited.

Liability statement

By using a Digitised Thesis, I accept that Trinity College Dublin bears no legal responsibility for the accuracy, legality or comprehensiveness of materials contained within the thesis, and that Trinity College Dublin accepts no liability for indirect, consequential, or incidental, damages or losses arising from use of the thesis for whatever reason. Information located in a thesis may be subject to specific use constraints, details of which may not be explicitly described. It is the responsibility of potential and actual users to be aware of such constraints and to abide by them. By making use of material from a digitised thesis, you accept these copyright and disclaimer provisions. Where it is brought to the attention of Trinity College Library that there may be a breach of copyright or other restraint, it is the policy to withdraw or take down access to a thesis while the issue is being resolved.

Access Agreement

By using a Digitised Thesis from Trinity College Library you are bound by the following Terms & Conditions. Please read them carefully.

I have read and I understand the following statement: All material supplied via a Digitised Thesis from Trinity College Library is protected by copyright and other intellectual property rights, and duplication or sale of all or part of any of a thesis is not permitted, except that material may be duplicated by you for your research use or for educational purposes in electronic or print form providing the copyright owners are acknowledged using the normal conventions. You must obtain permission for any other use. Electronic or print copies may not be offered, whether for sale or otherwise to anyone. This copy has been supplied on the understanding that it is copyright material and that no quotation from the thesis may be published without proper acknowledgement.

Resonances and Lattice Field Theory

by
Darran MacMaghnusa
B.Sc., M.Sc.

A Project submitted to
The University of Dublin
for the degree of
Doctor in Philosophy

School of Mathematics
University of Dublin
Trinity College

February 2012

Declaration

I declare that this thesis has not been submitted as an exercise for a degree at this or any other university and it is entirely my own work. I agree to deposit this thesis in the University's open access institutional repository or allow the Library to do so on my behalf, subject to Irish Copyright Legislation and Trinity College Library conditions of use and acknowledgement.

Signature of Author_

Summary

In this thesis, we look at the extraction of resonance parameters in lattice field theory. In particular we detail two major methods of dealing with resonances and consider them in a perturbative and nonperturbative context. We also explore a third method in less detail in a nonperturbative context.
The first method is the well known Lüscher's method, which relates the infinite volume phase shift, $\delta(p)$, of two particle scattering states to the energies of those states in a finite volume. It is possible to extract resonance parameters via a fit to some expression for phase shift.
The second method is a recently proposed method which we call the histogram method. Here we construct a histogram which profiles the relative density of free and interacting two particle scattering states. It can be shown that this histogram is related to the phase shift and so provides an alternative to Lüscher's method.
We investigate first the performance of the two methods in a perturbative setting, using an effective version of the theory used in the nonperturbative calculations. We find that both methods give similar results for the resonance parameters and, furthermore, that these results agree with the actual parameters computed in Minkowski space. The two particle spectrum, required as an input for both methods, is computed through the evaluation of a single finite volume Feynman diagram.
We then investigate the methods nonperturbatively, in a Monte Carlo simulation of the lattice $O(4)$ linear sigma model. We detail the application of both methods in a numerical context, as well as the relative strengths and weaknesses of each. Similar to the perturbative case, we find that both methods agree regarding the resonance parameters, provided the resonance is not too broad. For broad resonances we find that Lüscher's method provides better results.
We investigate a third method, which attempts to treat resonances on a similar setting to other states in lattice field theory. For the case of a narrow resonance we find a good agreement with the other two methods.
Finally we compare and contrast each of the methods.

Acknowledgements

First of all, I would like to thank all the members of the Lattice Group, Mike, Stefan and Sinéad for giving me the opportunity to do this work and all their help over the years. In particular, I'd like to thank my supervisor Dr. Mike Peardon, without whom I couldn't have done any of this. Also I'd like to thank the School of Maths.

Táim fíorbhuíoch dearna daoinib a bhaileadar umam le linn mo chuid léiginn. Aoife, Sheum, Pietro, Pol agus Paula, Goidé mar féadaid furil agus gáirí déanamh, agus níor chuigear leat cóir mairt bunúr na firince fanamh aitin dom iad, Coimeádfaidís tú go hoíche ag abcóidíocht agus cur thé céile.

Táim buíoch leis dem' máthair agus de m'athair ar a ngháir, agus dem' dhíorfúin Ciara agus mo bheirt dhíoltáin Conor agus Déaglán, 's é mo leóg, mo ghille mear.

Fé deire, ba mhaith liom m'aidiún a chur in iúl do eimíle. Do deinir a lán neithe do chabhraig go mór liom chun an faothar fo a chíochnú, Notchanaimm!

Contents

1 Introduction **1**

1.1 Lattice Field Theory 5

2 Resonances and the Lattice **13**

2.1 Resonance Theory 13

2.1.1 Example of a resonance 16

2.1.2 Resonances and scattering 17

2.1.3 Resonances on the Lattice 21

2.2 Lüscher's Method 25

2.2.1 Finite volume mass shift 25

2.2.2 Finite volume effects on scattering states 28

2.2.3 Consequences of Lüscher's formula 38

2.2.4 Limitations of Lüscher's formula. 39

2.3 Histogram Method 42

3 Perturbative Calculations **47**

3.1 The model 47

3.2 Renormalisation 48

3.3 Finite volume Feynman rules 50

3.4 Computing the self-energy 50

3.5 The two particle spectrum 57

3.6 Comparison with Minkowski case 61

4 Numerical Simulations **64**

4.1 The model 64

4.2 Extracting the spectrum 69

4.3 Choosing parameters 71

4.4 Numerical application of Lüscher's Method 78

4.5 Numerical application of the Histogram Method 90

4.6 Discussion and comparison of methods 105

5 Correlator method **110**
5.1 Asymptotic form of the correlator at small times 110
5.2 The Fit 114

6 Conclusions **116**

References **119**

List of Figures

1 Finite volume spectrum of a theory without a resonance . . . 38
2 Finite volume spectrum of a theory with a resonance 40
3 Behaviour of modified Bessel functions 55
4 Perturbative spectrum 57
5 Perturbative spectrum without a resonance 58
6 Free spectrum and perturbative interacting spectrum 60
7 Perturbative histogram 61
8 Perturbative phase shift 62
9 Two particle effective mass plot 72
10 Numerical Spectrum of theory with narrow resonance 73
11 Numerical Spectrum of theory with medium width resonance . 74
12 Numerical Spectrum of theory with broad resonance 75
13 Numerical Spectrum of theory with inelastic resonance 76
14 Phase shift for narrow resonance 81
15 Plot of the Lüshcer formula function, $\phi(\kappa)$ 82
16 Comparison of lattice and continuum dispersion relations . . . 86
17 Phase shift for narrow and broad resonances. 87
18 Inelastic region phase shift 88
19 Narrow resonance spectrum extended to all values of L 91
20 Narrow resonance histogram 92
21 Narrow resonance free spectrum continued 93
22 Narrow resonance histogram after continuation of free spectrum 94
23 Narrow resonance spectrum with two levels removed. 95
24 Narrow resonance histogram after removal of energy levels . . 96
25 Region of narrow resonance histogram used for fitting 97
26 Histogram for medium width resonance 98
27 Modified medium width resonance histogram and fitting region 99
28 Broad resonance histogram 100
29 Modified broad resonance histogram 101
30 Inelastic histogram 102
31 Modified inelastic histogram 103

32 Correlator method fit 113

List of Tables

1 Lüscher's method results with lattice dispersion relations . . . 84
2 Lüscher's method results with continuum dispersion relations . 85
3 Comparison of results from Lüscher's method and the Histogram Method 105

1 Introduction

Particle physics is currently described using the framework of quantum field theory. Quantum field theory provides a mathematical structure which unifies quantum mechanics and special relativity. It was developed initially in the late 1920s and early 1930s by Heisenberg, Pauli, Jordan and Dirac. There were problems with its initial formulation however and quantum field theory as we know it today comes into being in the late 1940s from the work of Schwinger, Feynman, Tomonaga and Dyson.

Although there are other possibilities for a relativistic quantum theory, quantum field theory is in some sense the most natural possibility. A short argument for quantum field theory is as follows:

QFT1 We wish to retain the basic formulation of quantum mechanics. A Hilbert space of states $\mathcal{H}$ and unitary operator on $\mathcal{H}$ implementing time evolution, given by $U(t) = e^{-i\int_0^t H(t')dt'}$, where H is known as the Hamiltonian operator. The time evolution of operators in the Heisenberg picture is given by $U^\dagger(t)\widehat{\mathcal{O}}U(t)$.

QFT2 We need to implement relativistic covariance.

QFT3 The theory should have the clustering property. This means that particle clusters at large space-like distance from each other should be independent.

To satisfy property [QFT3], all operators on the Hilbert space should be functions of a basic set of creation and annihilation operators a_p, a_p^* obeying either of:

$$\left[a_q, a_p^*\right] = \delta^3(q-p), \tag{1.1}$$

$$\left\{a_q, a_p^*\right\} = \delta^3(q-p), \tag{1.2}$$

where $q, p \in \mathbb{R}^3$.

However to satisfy [QFT2] the operators should be functions of Minkowski

spacetime transforming as Tensor or Spinor fields. The simplest way to satisfy [QFT2] and [QFT3] is to express all operators as functions of basic Tensor/Spinor field operators whose Fourier components are the a_p, a_p^* operators, these operators being known as quantum fields. The Hamiltonian is then a function of these quantum fields and this, combined with the Heisenberg equations of motion for operators, which follow from [QFT1], imply that the fields obey local field equations. A much more complete version of this argument can be found in Chapters 2-5 of [1].

One of the many formulations of quantum field theory is the path integral formalism. In this approach one calculates expectation values of quantum mechanical observables by integrating over some space of all possible field configurations. Formally:

$$\left(\Omega, \widehat{\mathcal{O}}(\phi)\Omega\right)_{\mathcal{H}} = \int_{\mathcal{S}} \mathcal{O}(\phi) e^{iS_M(\phi)} \mathcal{D}\phi. \tag{1.3}$$

On the left hand side of Eq.(1.3), $\widehat{\mathcal{O}}(\phi)$ is an operator representing some observable, Ω is the vacuum and $\mathcal{H}$ is the Hilbert space. On the right hand side $\mathcal{S}$ is the space of field configurations, $\mathcal{O}$ is the functional on this space corresponding to $\widehat{\mathcal{O}}(\phi)$, $S_M(\phi)$ is the action and $\mathcal{D}\phi$ is the measure on the space of fields. ϕ is left unspecified and may be a collection of a number of fields, each in different representations of the Lorentz group and the various internal symmetry groups. We use S_M for the action to denote that it is currently formulated in Minkowski space. We will switch to Euclidean space shortly.
The action $S_M(\phi)$ is given by

$$S_M(\phi) = \int \mathcal{L}_M(\phi) d^4x, \tag{1.4}$$

where $\mathcal{L}_M(\phi)$ is known as the Lagrangian density. Commonly a quantum field theory is specified by its Lagrangian density. Hereafter, as is typical, we will call the Lagrangian density just the Lagrangian.
When $S_M(\phi)$ contains no interaction terms the integral can be performed

exactly, since it is, in some sense, an infinite dimensional version of Gaussian integration. When $S_M(\phi)$ contains interaction terms one commonly applies perturbation theory. The action is split into two parts, $S_M(\phi) = S_0(\phi) + S_{int}(\phi)$, where S_0 is the action of a free theory and S_{int} contains the interactions:

$$\int_{\mathcal{S}} \mathcal{O}(\phi) e^{iS_0(\phi)+iS_{int}(\phi)} \mathcal{D}\phi. \tag{1.5}$$

The coefficients of the interacting terms in $S_{int}(\phi)$ are known as coupling constants. Perturbation theory consists of expanding the exponential $e^{iS_{int}(\phi)}$, which produces a series of free path integrals which can be performed exactly.

$$\begin{aligned} \int_{\mathcal{S}} \mathcal{O}(\phi) e^{iS_0(\phi)+iS_{int}(\phi)} \mathcal{D}\phi = & \int_{\mathcal{S}} e^{iS_0(\phi)} \mathcal{O}(\phi) \mathcal{D}\phi \\ & + \int_{\mathcal{S}} e^{iS_0(\phi)} \mathcal{O}(\phi) iS_{int}(\phi) \mathcal{D}\phi \\ & + \int_{\mathcal{S}} e^{iS_0(\phi)} \mathcal{O}(\phi) \frac{1}{2} (iS_{int})^2(\phi) \mathcal{D}\phi + \cdots \end{aligned} \tag{1.6}$$

An additional complication occurs in these computations beyond those of non-relativistic quantum mechanics, known as renormalisation. In brief, most of the terms in perturbation theory are infinite when computed naively. The solution to this problem involves realising that the coefficients appearing in the Lagrangian, the masses and coupling constants, are not the same as the physical values of these quantities. The physical values being shifted or renormalised away from their "bare" values in the Lagrangian. Renormalisation consists of a systematic replacement of the bare quantities with their physical counterparts, which, for certain theories, completely removes the infinities. An interesting consequence of this procedure is the discovery that the coupling constants are not fixed, but rather are a function of the energy scale.

The current knowledge of particle physics is encoded in the quantum field theory known as the Standard Model. The Standard Model was developed in the early 1970s and describes the Strong, Weak and Electromagnetic forces,

ignoring only gravity. It has withstood every experimental test to date, [2]. The only one of its main predictions still untested is the existence of the Higgs boson.

For electromagnetic processes, perturbation theory provides results in excellent agreement with experiment. Similarly for weak processes and high-energy strong processes. However, for low energy strong processes, those most relevant for nuclear physics and meson and baryon properties, perturbation theory can not be used.

The sub-component of the Standard Model which describes the strong force is known as Quantum Chromodynamics (hereafter QCD) and is described by the following Lagrangian:

$$\mathcal{L} = -\frac{1}{2g_0^2}\,\mathrm{Tr}\left(F_{\mu\nu}F^{\mu\nu}\right) + \sum_{i=1}^{6}\overline{\psi}_i\left(\not{D} - m_i\right)\psi_i, \tag{1.7}$$

$$\not{D} = \gamma^\mu\left(\partial_\mu - iA_\mu\right).$$

The ψ_i are six fermion fields transforming under the fundamental ($\underline{\mathbf{3}}$) representation of $SU(3)$, as well as a single Lie-algebra-valued ($\mathfrak{su}(3)$-valued) field, $\mathbf{A}$, transforming under the adjoint ($\underline{\mathbf{8}}$) representation. g_0 is known as the bare strong coupling constant.

As mentioned above coupling constants are actually energy dependent, due to renormalisation. The strong coupling, g, grows as energy is decreased. This implies that the terms on the right hand side of Eq.(1.6) do not decrease in value for the case of the QCD Lagrangian, Eq.(1.7), and an observable $\mathcal{O}(\phi)$ corresponding to low energy physics. In addition to this the asymptotic Hilbert spaces suggested by the perturbative method are not the correct ones. One would imagine $\mathcal{H}_{in/out}$ to be quark-gluon Fock spaces. However, due to nonperturbative effects, quarks and gluons are confined and the physical Hilbert space is spanned by Hadron states, so one should be dealing with $\mathcal{F}_{hadron}$ as the asymptotic Hilbert space, with $\mathcal{F}$ denoting a Fock space built

over the appropriate one-particle states. Hence perturbation theory cannot be used for low energy QCD.

In this case one needs to evaluate the integral in Eq.(1.5) directly. However there is no general theory of such integrals, meaning it is often impossible to analytically solve them or estimate them. Hence we turn to a numerical evaluation of these integrals known as Lattice Field Theory, which is the main focus of this work.

1.1 Lattice Field Theory

The first step to making the path integral numerically tractable is to reduce it from an infinite dimensional integral to a finite dimensional one. To do this, spacetime is reduced from the continuum $\mathbb{R}^4$ to the discrete set $\mathbb{Z}^4$. This reduces the integration variables from $\phi(x)$ to $\phi(n)$, where $n \in \mathbb{Z}^4$. The discrete set $\mathbb{Z}^4$ is known in this context as "the lattice" from which the method gets its name. The distance between the points of $\mathbb{Z}^4$ is known as the lattice spacing, labelled a hereafter.
Even on $\mathbb{Z}^4$ the path integral is infinite-dimensional (although countably so). To reduce it to a finite dimensional integral, space and time are given a finite extent, labelled L and T respectively in the rest of this work. These two steps produce a reduced version of spacetime on which the path integral is finite dimensional:

$$\int_{\mathcal{S}} \mathcal{O}(\phi(n)) e^{iS_M(\phi)} \mathcal{D}\phi(n), \tag{1.8}$$

$$\mathcal{D}\phi(n) = \prod_n d\phi(n), \tag{1.9}$$

$$n \in \Lambda, \qquad \Lambda \subset \mathbb{Z}^4, \qquad |\Lambda| < \infty. \tag{1.10}$$

In this work we will continue the fields periodically in both time and space:

$$\phi(x + Lan_\mu) = \phi(x), \tag{1.11}$$

where n_μ is a unit vector in the μ-direction and $\mu = 0, 1, 2, 3$. In this sense we are working with fields which live on a discrete version of $\mathbb{T}^4$. The reasons for periodicity in space will be explained in Sec. 2.2.2. It should be noted that when using fermionic fields, the fields must be anti-periodic in time. However we shall not use fermionic fields in this work.
As it stand the integral Eq.(1.8) is not well defined, which is due to the oscillating exponential $e^{iS_M(\phi)}$. The action will involve terms polynomial in the field, for example:

$$e^{i\sum_x \phi^n(x)} = e^{i\|\phi^n\|_1}. \tag{1.12}$$

Since there will be fields for which $\|\phi^n\|_1$ is arbitrarily large, we do not expect that this integral will converge.
For this reason Lattice field theory is formulated in Euclidean space, produced by sending $t \to -it$, to give the Euclidean lattice path integral:

$$\int_S \mathcal{O}(\phi(n))e^{-S_E(\phi)}\mathcal{D}\phi(n), \tag{1.13}$$

where $S_E(\phi)$ refers to the Euclidean action. Here the path integral features a damped exponential $e^{-S_E(\phi)}$, which produces a mathematical well defined integral. From here on we refer to $S_E(\phi)$ as simply $S(\phi)$.
It also has additional benefit of producing an integral of a type which can be evaluated with Monte Carlo techniques. A justification of the continuation of the path integral to Euclidean space can be found in [3], with a full proof given in [4] and Chapter 19 of [5].

The actual numerical calculation of the expectation values $< \mathcal{O} >$ of an observable consist in generating an ensemble of field configurations, weighted by the probability distribution $e^{-S(\phi)}$, and taking the ensemble average of $\mathcal{O}(\phi)$.

$$\int_S \mathcal{O}(\phi(n))e^{-S(\phi)}\mathcal{D}\phi(n) \approx \frac{1}{N}\sum_{\phi_i \in \mathcal{E}} \mathcal{O}(\phi_i) + \frac{1}{\sqrt{N}}, \tag{1.14}$$

ϕ_i being a single sample configuration and $\mathcal{E} = \{\phi_i\}$ being the sample set of configurations generated with probability $e^{-S(\phi)}$. Generating the configurations with this probability ensures that our sample configurations are ones which dominate the path integral.

To place a scalar field theory on the lattice one discretises the derivatives that appear in the action. These appear in the free part of the Lagrangian:

$$\mathcal{L}_0 = \frac{1}{2}\phi(-\Delta + m^2)\phi. \tag{1.15}$$

The Laplacian is discretised as:

$$\Delta\phi(x) = -\sum_{\mu=0}^{3} \frac{1}{a^2}\left(2\phi(x) - \phi(x + a\widehat{\mu}) - \phi(x - a\widehat{\mu})\right). \tag{1.16}$$

There are some additional complications when putting a gauge theory on the lattice. Unlike the continuum case, one does not use the connections A_μ, instead using the parallel transporters U_μ defined as:

$$U_\mu(n) = e^{ig_0 a_\mu A_\mu(n)}, \tag{1.17}$$

$$a_\mu = a n_\mu, \tag{1.18}$$

where g_0 is the bare coupling constant and n_μ is the displacement vector in the $\widehat{\mu}$ direction. The U_μ link two nearby sites n and $n + \widehat{\mu}$. In this sense they are said to live on lattice links instead of lattice sites. A single gauge configuration is given by the values of $U_\mu(n)$ on every link. The U_μ take values in the compact space of the gauge group, unlike the A_μ which take values in the non-compact Lie Algebra. This has two advantages. First of all it means that the lattice path integral measure, given by

$$\prod_b dU_b, \tag{1.19}$$

where b is a lattice link between two points and dU is the Haar measure, is automatically finite. Secondly it means there is no need for gauge fixing,

hence eliminating the delicate issues found in continuum gauge theories such as Fadeev-Poppov ghosts.
Using the U_μ one can construct the holonomy, the parallel transporter from a point back to itself along some curve. The simplest such holonomy is one where the curve is just a square loop of one lattice spacing in extent, known as a plaquette, given by:

$$U_p(n) = U_\mu(n)U_\nu(n+\widehat{\mu})U_\mu^\dagger(n+\widehat{\nu})U_\nu^\dagger(n), \tag{1.20}$$

where p labels the plaquette. It is a fundamental result in the theory of fiber bundles that the holonomy about a square path of size a^2 is proportional to the curvature:

$$Tr(U_p(n)) = e^{-a^2 F_{\mu\nu}(n)+\mathcal{O}(a^3)}, \tag{1.21}$$

which gives

$$\frac{1}{2}Tr(U_p(n) + U_p^{-1}(n)) = Tr(\Re e(U_p)) = \tag{1.22}$$

$$= Tr(1) + a^4 Tr(F_{\mu\nu}F_{\mu\nu}(n)) + \mathcal{O}(a^5). \tag{1.23}$$

Since the continuum action involves $F_{\mu\nu}F_{\mu\nu}(n)$, as can be seen in Eq.(1.7), one choice for the lattice action is the Wilson action:

$$S(U) = \beta \sum_p \left\{ 1 - \frac{1}{N}\Re e(Tr(U)) \right\}, \tag{1.24}$$

with $\beta = \frac{2N}{g_0^2}$. Using Eq.(1.23) it can be seen that:

$$S(U) = \beta \sum_p \left\{ 1 - \frac{1}{N}\Re e(Tr(U)) \right\} = -\frac{1}{2g_0^2}\sum_{n,\mu\nu} a^4 Tr(F_{\mu\nu}F_{\mu\nu}(n)) + \mathcal{O}(a^5), \tag{1.25}$$

and thus the continuum limit of this action is the pure gauge part of Eq.(1.7).

As for the fermion part of the QCD Lagrangian, in the continuum it ap-

pears as $\overline{\psi}\left(\not{D}\right)\psi$. The fermion fields are placed on the lattice the same way as scalar fields with $\psi(x) \to \psi(n)$. The main subtlety is related to the discretisation of the Dirac operator $\not{D}$. Any discretisation of the Dirac operator which is hermitian and leaves the lattice action local and translationally invariant, either breaks chiral symmetry or produces extra unphysical fermion species called doublers, a result known as the Nielsen-Ninomiya theorem, [6, 7].

Quite often the observables $\mathcal{O}(\phi)$ used in Lattice field theory are products of some local field, $\mathcal{A}(x)$, composite or elementary, at two different space time points:

$$\mathcal{O} = \mathcal{A}(x)\mathcal{A}(y), \tag{1.26}$$

whose expectations values are known as correlation functions.

The advantage of using these operators is that their correlation functions decay exponentially in time proportional to the masses of the particles which carry the quantum numbers of $\mathcal{A}$. This can be seen by using the completeness relation:

$$\langle \mathcal{A}(0)\mathcal{A}(t)\rangle = \sum_i \left(\Omega\mathcal{A}(0), \Phi_i\right)\left(\Phi_i, \mathcal{A}(t)\Omega\right), \tag{1.27}$$

where the state Φ_i is the i-th state with the quantum numbers of $\mathcal{A}$. Other states are excluded since for a state Ψ with different quantum numbers:

$$(\Psi, \mathcal{A}(0)\Omega) = 0. \tag{1.28}$$

If we allow the contraction operator e^{-tH}, which gives Euclidean time evolution, to act on the states Φ_i

$$\sum_i \left(\Omega \mathcal{A}(0), \Phi_i\right) \left(\Phi_i, e^{-tH} \mathcal{A}(0)\Omega\right) = \tag{1.29}$$

$$\sum_i \left(\Omega \mathcal{A}(0), \Phi_i\right) \left(\Phi_i, \mathcal{A}(0)\Omega\right) e^{-E_i t}, \tag{1.30}$$

we obtain the general time dependence of the correlator

$$\langle \mathcal{A}(0)\mathcal{A}(t)\rangle = \sum_i A_i e^{-E_i t}, \tag{1.31}$$

$$A_i = \left|\left(\Psi_i, \mathcal{A}(0)\Omega\right)\right|^2. \tag{1.32}$$

Hence measuring the correlation functions on the lattice provides a nonperturbative method of extracting the spectrum of the theory and particularly the masses of particles. Using three-point functions or more general objects it is possible to get at other physics besides the particle masses. This is important in QCD where we are interested in the nonperturbative physics of low energy strong processes and particles.

The formulation of a field theory in a finite volume has some interesting properties which affects the physics of particles. First of all there is the effect of the finite volume on the range of possible momenta. Instead of taking values in $\mathbb{R}^3$, particle momenta can only take a discrete set of values based on the finite volume of the lattice:

$$\mathbf{p} = \frac{2\pi \mathbf{n}}{L}, \tag{1.33}$$

$$\mathbf{n} \in \mathbb{Z}^3. \tag{1.34}$$

This restriction of momenta values affects the analytic properties of correlation functions. The Fourier transform of the correlation function

$$\langle \mathcal{A}(0)\mathcal{A}(t)\rangle = \int D(i\omega, \mathrm{k}) e^{-i\omega t - i\mathrm{kx}} d\omega d^3k, \tag{1.35}$$

can be written as an integral over what is known as the Källén-Lehmann spectral function, ρ:

$$D(i\omega, \mathbf{k}) = \int_0^\infty \frac{d\omega'^2}{\omega'^2 + \omega^2} \rho(\omega', \mathbf{k}). \tag{1.36}$$

It is a basic result of infinite volume field theory, assuming a mass gap, that the spectral function has a branch cut at ω_* which corresponds to the lowest energy multiparticle state. This branch cut is a result of the continuum of multiparticle states, in contrast to the isolated poles in the spectral function due to single particle states or bound states. However in a finite volume, the restriction on the momenta means that the set of multiparticle states is discrete, not continuous and hence the multiparticle branch cut dissolves into a sequence of isolated poles. This effect will be important in what follows.

As well as this, the discretisation of the spacetime means that the momenta can only assume a finite range, hence providing an ultraviolet cutoff, but this effect is not important in this work.

Another effect of the Lattice is the reduction of the full spatial rotation group $O(3)$ down to the cubic group O_h. This affects the quantum numbers of the particles as they appear on the lattice, since the representations of the cubic group do not have a one-to-one correspondence with those of $O(3)$.

The constructions above provide a nonperturbative numerical method of calculating low-energy strong force processes and masses. However there is a type of particle for which the above methods can not be applied directly. These particles are resonances, unstable particles which only manifest in the scattering processes of other particles. The two major quantities of interest for resonances are their masses, M_R, and their widths or inverse lifetimes, Γ_R. Resonances are quite common in QCD, for example the ρ resonance, hence the difficulty of accessing resonances is a major drawback in the numerical study of strong processes. The difficulty of analysing resonances by the usual methods of lattice field theory is two-fold:

1. Ultimately resonances are related to the dynamical process of scattering, something which is not preserved in Euclidean space, due to a result known as the Maiani-Testa theorem.

2. In finite volume the above mentioned restriction on momenta means that it is not possible for the resonance to decay, since conservation of momentum may require it to decay into particles having a value of momentum outside the set of discrete values. In this case the resonance will become a stable state. However due to presence of interactions it will mix with other stable states.

For these reasons we need some method of accessing resonance data on the lattice. In what follows we will compare and contrast two main methods, as well as, in less detail, a recently proposed third method. The two main methods are the well known Lüscher's formula, first applied to resonances in four dimensional field theory in [8](although the main ideas had been explored earlier, [9, 10, 11]) and a method we call the Histogram method proposed in [12]. The main aim is to understand the relative strengths and weaknesses of these methods.

In order to study resonances and how it may be possible to extract their properties in the finite volume world of lattice field theory, we turn now to the theoretical background of resonances and finite volume field theory.

2 Resonances and the Lattice

2.1 Resonance Theory

Resonances are basically unstable particles and due to this they cannot appear as either ingoing or outgoing scattering states and can only be detected by their effects on the scattering cross-sections of stable particles. Commonly this effect manifests as a rapid variation in the cross-section at energies near the mass of the resonance. A proper explanation of resonances in the context of scattering theory will be necessary in the rest of the thesis, so we will begin with a description of non-relativistic scattering theory, for a full treatment see [13]. The non-relativistic theory will be used to derive various results important for the field theory case.

A quantum mechanical system is specified by two features, the Hilbert space of states and the Hamiltonian which governs time evolution. In non-relativistic quantum mechanics the Hilbert space can be taken to be $\mathbb{L}^2\left(\mathbb{R}^{3N}\right)$ where N is the number of particles. The Hamiltonian governing the time evolution commonly has the general form:

$$H = \sum_i -\Delta_i + W(\mathbf{r}_i) + \sum_{i,j;i<j} V(\mathbf{r}_i - \mathbf{r}_j), \tag{2.1}$$

where Δ_i is the Laplacian on the space of coordinates of the i-th particle, $V(\mathbf{r}_i - \mathbf{r}_j)$ is the inter-particle potential and $W(\mathbf{r}_i)$ is the single particle potential exerted on the particles by some external force.
A Hamiltonian will typically have a set of states known as bound states. These are states obeying the eigenvalue equation $H\psi = E\psi$. These states correspond to the point spectra of H. There are also the scattering states $\mathcal{R}_-$ and $\mathcal{R}_+$, these are defined to be the set of states whose time evolution approaches that of a free state in either the far future or the far past, specifically

$$\lim_{t\to\pm\infty} \|U(t)\psi - U_0(t)\psi_0\| = 0. \tag{2.2}$$

ψ_0 is known as the in/out asymptote and $U_0(t)$ is the free time evolution operator. The whole Hilbert space can be decomposed as $\mathcal{H} = \mathcal{B} \oplus \mathcal{R}$, where $\mathcal{B}$ is the set of all bound states and $\mathcal{R}$ is the set of all scattering states. Usually the assumption of asymptotic completeness is made:

$$\mathcal{R}_- = \mathcal{R}_+ = \mathcal{R}. \tag{2.3}$$

So that all states have in and out asymptotes. The map between in and out states

$$S : \mathcal{R}_- \to \mathcal{R}_+, \tag{2.4}$$

is known as the S-operator. Assuming asymptotic completeness, the S-operator is unitary.

The collection of matrix elements of the S-operator, $(\psi, S\phi)$, are known as the S-matrix. A useful decomposition of the S-matrix is to look at restrictions of it to states with a specific angular momentum, $s_l(p)$, with p being the momentum of the in-going state and l the angular momentum. Since resonances, being particles, have a fixed angular momentum l this decomposition is more useful in their study. An important property of the S-matrix can be seen by decomposing it into a ratio involving the Jost function, $j_l(p)$

$$s_l(p) = \frac{j_l(-p)}{j_l(p)}. \tag{2.5}$$

In loose terms, the Jost function $j_l(p)$ measures the out-going scattering wave, while $j_l(-p)$ measures the in-going scattering wave. In quantum mechanics bound states are typically given negative energies and scattering states positive energies. In terms of momentum, a bound state with $E < 0$, corresponds to purely imaginary momentum $\overline{p} = i\alpha$. Considering this, if the momentum of the Jost function takes on an imaginary value corresponding to one of the energy eigenstates, then $j_l(i\alpha)$ will vanish, since a bound state has no out-going scattering wave. Hence, by Eq.(2.5), there will be a pole in $s_l(p)$ at these momenta. Hence a bound state appears as a pole of the S-matrix in the region $\{p : \Im(p) > 0\}$ of the complex momentum plane.

More precisely a potential

$$V(r) \in \mathcal{O}(r^{-1-\eta}), \qquad \eta > 0, \tag{2.6}$$

has a solution regular at the origin, namely

$$\chi_{pl} = \alpha_l(p)\chi^-_{pl}(r) - \beta_l(p)\chi^+_{pl}(r), \tag{2.7}$$

with α and β functions depending only on p and $\chi^\pm_{pl}$ having the asymptotic behaviour

$$\chi^\pm_{pl} \approx e^{\pm i(pr - \frac{\pi l}{2})}. \tag{2.8}$$

In all these formula l is the angular momentum. χ^+ corresponds to an ingoing scattering wave and χ^- and outgoing wave. If the potential $V(r)$ possesses a bound state with energy $-E$, this corresponds to momentum $p = \pm i\sqrt{2mE}$. Giving the asymptotic solutions the form:

$$\chi^\pm_{pl} \approx e^{\mp r\sqrt{2mE}} e^{-\frac{\pi l}{2}}, \tag{2.9}$$

for iE and

$$\chi^\pm_{pl} \approx e^{\pm r\sqrt{2mE}} e^{-\frac{\pi l}{2}}, \tag{2.10}$$

for $-iE$.

In the first case we see that the function χ^- may not enter the asymptotic expression for the wavefunction or else it would not be normalisable, so we see that we must have $\alpha_l(p) = 0$. In the second case χ^+ cannot enter, so we must have $\beta_l(p) = 0$. Using the fact that the S-matrix can be written as:

$$\frac{\beta_l(p)}{\alpha_l(p)}, \tag{2.11}$$

we see that the bound state produces a pole in the upper-half plane and a zero in the lower half plane.
Of course this still leaves open the issue of poles in the lower half plane $\{p : \Im(p) < 0\}$. These poles are the resonances, the unstable particles we are looking for. First we will give a physical example of a resonance.

2.1.1 Example of a resonance

As an example of a resonance we shall take the Helium Atom, treated in much more detail in [14]. The Helium atom has the Hamiltonian

$$H = H_0 + V(\mathbf{r}_1, \mathbf{r}_2), \tag{2.12}$$

$$H_0 = -\Delta_1 - \frac{1}{\mathbf{r}_1} - \Delta_2 - \frac{1}{\mathbf{r}_2}, \tag{2.13}$$

$$V(\mathbf{r}_1, \mathbf{r}_2) = \frac{1}{|\mathbf{r}_1 - \mathbf{r}_2|}. \tag{2.14}$$

The interactions between the electrons in the helium atom are given by the potential $V(\mathbf{r}_1, \mathbf{r}_2)$. First let us look at the spectrum of the Hamiltonian, H_0, which is essentially two copies of the hydrogen atom. The bound state spectrum for the hydrogen atom, with Hamiltonian

$$H_h = -\Delta - \frac{1}{\mathbf{r}}, \tag{2.15}$$

is given by

$$E_n = \left\{ -\frac{1}{n^2} \right\}_{n=1}^{\infty}, \tag{2.16}$$

So the bound state spectrum of H_0 is

$$E_{n,m} = \left\{ -\frac{1}{n^2} - \frac{1}{m^2} \right\}_{n,m=1}^{\infty}. \tag{2.17}$$

The scattering states for the Hydrogen atom are basically those with energies above the bound states, so we have $\mathcal{R}(H_h) = [0, \infty)$, where $\mathcal{R}(A)$ is the continuous spectrum of the operator A. If we think of H_0 as two copies of the hydrogen atom, there can be scattering states in the interval $[-1, 0]$ by

placing the first atom in its ground state and the second in a scattering state. Hence the scattering spectrum for H_0 is given by

$$\mathcal{R}(H_0) = [-1, \infty)\,. \tag{2.18}$$

Comparing the two spectra for bound states, Eq.(2.17), and scattering states, Eq.(2.18), it can be seen that the bound states with $n \geq 2, m \geq 2$ are embedded inside the scattering spectrum.
When we include the interaction $V(\mathbf{r}_1, \mathbf{r}_2)$ and obtain the total Hamiltonian H, these bound states inside the scattering spectrum will be lost, since the interaction will couple them to the scattering states and they will evolve, that is decay, into those scattering states given enough time. These "lost" bound states are the most typical example of resonances.

2.1.2 Resonances and scattering

We have mentioned that resonances correspond to poles of the S-matrix in the lower half plane $\{p : \Im(p) < 0\}$, similar to how bound states are poles in the upper half-plane and that resonances can be produced by the loss of bound states, such as in the example above. This leads to the typical picture of resonances as near bound states or metastable states. This also explains their effect on the scattering cross-section since the in-going particles will momentarily be bound in the metastable state of the resonance before it decays into out-going particles. A mathematically clearer example of this can be given by writing the Hamiltonian in a form where the potential can be modified:

$$H = H_0 + \lambda V, \tag{2.19}$$

where we take the potential to be negative for $\lambda = 1$.
Let us assume that we start at some value of λ where the Hamiltonian has a bound state, producing a pole in $s_l(p)$ in the upper half plane. As λ is varied this pole must move, if λ is increased the potential becomes more attractive and the bound state will decrease in energy, moving the pole further into the

upper half plane. However if λ is decreased the potential is become less attractive and the pole will move toward the real axis. Eventually it will move into the lower half plane when the potential is weak enough that the state is no longer a permanently bound state. At this point it will be a resonance.

Instead of using momentum, a more useful picture for the methods we will use shall be the complex energy plane. The relationship between energy and momentum in non-relativistic physics is provided by $E = \frac{p^2}{2m}$. In terms of the whole complex plane, it can be seen that the momentum plane maps twice onto the energy plane. In terms of functions like the $s_l(p)$ this means that there will be two Riemann sheets when they are expressed as functions of energy $s_l(E)$. The first Riemann sheet corresponds to the upper-half plane and the real axis $\{p : \Im(p) \geq 0\}$ of the momentum plane. This is known as the physical sheet, since the bound states and scattering states are located on it. The second Riemann sheet corresponds to the lower half plane and contains the resonance poles.

The branch cut between the two sheets is located on the real axis. In this way $s_l(E)$ has poles, the bound states, at negative energy and another set of poles found by continuing through the branch cut, which are the resonances. In the example of the Helium atom above, prior to the inter-particle interaction being turned on the resonances appear as stable bound state poles on the physical sheet. When the interaction is turned on these poles move through the branch cut and into the second Riemann sheet. We will label the position of a resonance pole as $\overline{E} = E_R - i\frac{\Gamma}{2}$

A quantity which is crucial in this work is the phase shift $\delta_l(E)$. The scattering phase shift measures the shift in the phase of a scattering wave of a given angular momentum l as it passes through a potential. It is related to the S-matrix in the elastic region via

$$s_l(E) = e^{2i\delta(E)}. \tag{2.20}$$

Using the Schwartz reflection principle, Eq.(2.5) and Eq.(2.20) its relation to the Jost function can be given as:

$$j_l(E) = |j_l(E)|\, e^{-i\delta(E)}, \tag{2.21}$$

from which we can see that

$$\delta(E) = -\arg(j_l(E)). \tag{2.22}$$

If the energy E of the ingoing particle is near a resonance pole, $\overline{E} = E_R - i\frac{\Gamma}{2}$, then Jost function can be expanded about the pole with the linear approximation being reasonably accurate. The Jost function vanishes at the resonance position, since a pole of the S-matrix is a zero of the Jost function, meaning the expansion is

$$j_l(E) = \left.\frac{dj_l}{dE}\right|_{E=\overline{E}} (E - \overline{E}) + \mathcal{O}((E - \overline{E})^2). \tag{2.23}$$

Then the scattering phase shift is

$$\delta(E) = -\arg(j_l(E)) = \delta_{bg}(E) + \delta_{res}(E), \tag{2.24}$$

$$\delta_{res}(E) = -\arg((E - \overline{E})), \tag{2.25}$$

$$\delta_{bg}(E) = -\arg\left(\left.\frac{dj_l}{dE}\right|_{E=\overline{E}}\right). \tag{2.26}$$

δ_{bg} is the part of the phase shift due to direct scattering between the particles without an intermediate resonance state being formed. $\delta_{res}(E)$ is the part of the scattering entirely due to the resonance, from Eq.(2.25) it can be derived that it has the form:

$$\delta_{res}(E) = \arctan\left(\frac{\Gamma}{E_R - E}\right) \tag{2.27}$$

or equivalently

$$\delta_{res}(E) - \frac{\pi}{2} = \arctan\left(\frac{E_R - E}{\Gamma}\right). \tag{2.28}$$

It can be seen from Eq.(2.27) that the scattering cross section will rapidly vary by π as the energy passes near the resonance energy E_R.

Finally a physical interpretation of the parameters E_R and Γ are necessary. If we take the resonance as a state Φ we may imagine it as an eigenstate of the Hamiltonian with energy $\overline{E} = E_R - i\frac{\Gamma}{2}$, then it evolves in time as:

$$e^{-iHt}\Phi = e^{-iE_Rt}e^{-\frac{\Gamma}{2}t}\Phi. \tag{2.29}$$

In this equation E_R appears as the energy of the resonance, while Γ appears in a factor damping the wave-function, causing it to die off at large times. This die off may be seen as the decay of the resonance and hence Γ is the inverse life time of the resonance. A more rigorous analysis [13] involving the scattering wave-function shows that Γ and E_R are indeed the inverse lifetime and the energy of the resonance respectively.

This quantum mechanical analysis of resonances is necessary in what follows, but when it comes to obtaining the resonance parameters on the lattice the resonances in that context are relativistic. It is somewhat more difficult to obtain the analogues of Eq.(2.27) and Eq.(2.28) in relativistic field theory, since there is no Jost function. However the S-matrix in field theory is related to residue of the correlation functions at on-shell four-momenta through the LSZ reduction formula. In this manner, in the relativistic theory, resonances can be found as a pole in the correlation function on the second Riemann sheet. As mentioned in Sec.1.1, the branch cut in this case is due to the multiparticle continuum. The relativistic analogues of Eq.(2.27) and Eq.(2.28)

are then:

$$\delta_{res}(p) = \arctan\left(\frac{M_R\Gamma}{M_\sigma^2 - E^2}\right) \tag{2.30}$$

and

$$\delta_{res}(p) - \frac{\pi}{2} = \arctan\left(\frac{4p^2 + 4M_\pi^2 - M_R^2}{M_R\Gamma_\sigma}\right). \tag{2.31}$$

We use M_R rather than E_R in the relativistic context as there the energy of the resonance is just its mass.

2.1.3 Resonances on the Lattice

We now come to the difficulty of obtaining information on resonances on the lattice. The difficulties specific to resonances are due to the use of Euclidean spacetime and a finite volume.

The discretisation of the spectrum due to the finite volume has a drastic effect on the Källén-Lehmann spectral function. As mentioned previously the multiparticle branch cut in the spectral function dissolves into a series of isolated poles. In other words, the spectral function will now be a meromorphic function, this function will have no branch cuts and so no additional Riemann sheets. As resonances are poles on the second Riemann sheet this effectively eliminates them. From a more physical point of view it has already been pointed out that the resonances cannot decay since in a finite volume this would involve a violation of conservation of momentum.

Hence in a finite volume the resonance appears as a stable eigenstate of the Hamiltonian. However due to the fact that there are terms in the Hamiltonian coupling the resonance to the multiparticle states which would be its decay products in infinite volume, the eigenstates of the finite volume Hamiltonian will be linear combination of these multiparticle states and the resonance state. Essentially the multiparticle sector will have absorbed the resonance.

Of course, *a priori*, this may not pose any difficulty provided there is some observable which can be measured on the lattice which is connected to infinite volume scattering processes. Unfortunately, the use of Euclidean spacetime makes it difficult to extract information on scattering processes due to a result known as the Maiani-Testa theorem [15].

In Sec.1.1, in Eq.(1.31), we have seen that the Euclidean correlator contains information on the particle masses. Following this line of thought one would expect to be able to extract scattering information from a three-point, or higher, correlation function. If we imagine a scattering process with two particles of the same species, π, in the final state, we may model the initial state via some local operator $J(x)$ with the correct quantum numbers. We will take the final state to have zero total momentum, since this will be the case in the simulations which follow. One would expect to measure scattering processes numerically by evaluating the following correlation function on the lattice:

$$G(t_1, t_2; q) = \langle \phi(q, t_1)\phi(-q, t_2)J(0)\rangle. \tag{2.32}$$

Where ϕ is the field associated with the outgoing particles and q their momentum.

Using the completeness relation, in analogy with Eq.(1.31), this can be shown to have the asymptotic form

$$\lim_{\substack{t_1\to\infty \\ t_2\to-\infty}} G(t_1, t_2; q) = \frac{Z}{2E_q}\langle \pi, q|J(0)|\pi, q\rangle + \cdots \tag{2.33}$$

Where Z is the field strength factor given by $\langle \pi, q|\phi|\Omega\rangle = \sqrt{Z}$ and $E_q = 2\sqrt{q^2 + m^2}$.

This does not contain the quantity of interest, namely the amplitude

$$\langle \pi, q; \pi, -q; out|J(0)|0\rangle. \tag{2.34}$$

However this is not the region of the t_1, t_2 plane explored by lattice simulations. Instead lattice simulations will take place in the region $0 \ll t_2 \ll t_1$ and so we need the asymptotic form there.
The form for $0 \ll t_1$ can be obtain through the limit $t_1 \to \infty$,

$$\lim_{t_1 \to \infty} G(t_1, t_2; q) = \frac{\sqrt{Z}}{\sqrt{2E_q}} e^{-E_q t_1} F_q(t_2), \tag{2.35}$$

$$F_q(t_2) = \langle \pi, q | \phi_q(t_2) J(0) | 0 \rangle. \tag{2.36}$$

The function F_q can be separated into it's connected and disconnected parts

$$F_q(t_2) = \frac{\sqrt{Z}}{\sqrt{2E_q}} \langle \pi, q; \pi, -q; out | J(0) | 0 \rangle + F_q^{conn}(t_2). \tag{2.37}$$

The connected component itself contains a term arising from a pole at $E = 2E_q$ which produces a factor containing an ingoing matrix element and a second term $P_q(t_2)$. The three-point function is then

$$\lim_{\substack{t_1 \to \infty \\ t_2 > 0}} G(t_1, t_2; q) = \tag{2.38}$$

$$\frac{Z}{2E_q} e^{-E_q t_1} e^{-E_q t_2} \left[\frac{1}{2} \left(\langle \pi, q; \pi, -q; out | J(0) | 0 \rangle + \langle \pi, q; \pi, -q; in | J(0) | 0 \rangle \right) + P_q(t_2) \right]. \tag{2.39}$$

For $q \neq 0$ the function $P_q(t_2)$ is of the form

$$P_q(t_2) \approx \mathcal{F} e^{2(E_q - m_\pi) t_2}, \tag{2.40}$$

where the coefficient $\mathcal{F}$ is related to an off-shell amplitude. It can be seen from this form that $P_q(t_2)$ contains no information on physical scattering. For the first term in Eq.(2.39), containing the average of the matrix elements, the term that one would wish to extract, namely $\langle \pi, q; \pi, -q; out | J(0) | 0 \rangle$, does appear. However as it appears in an average with the in-going matrix elements, the overall contribution is purely real and so it is not possible to extract scattering information, which is associated with the complex phase

of the S-matrix elements. Only at the two particle threshold, $q = 0$, can any information be obtained, as there the coefficient $\mathcal{F}$ of $P_q(t_2)$ is related to the threshold scattering amplitude. This is the result known as the Maiani-Testa theorem. Fundamentally the theorem arises due to the loss of the complex phase in the form factor of the three-point function. This phase contains the scattering phase shift between in and out states, as proven in [16]. The Euclidean three-point function is purely real (up to trivial phases) and hence cannot contain this information. Only at threshold, where the Minkowski three-point function is itself real, can any information be extracted.

Hence the finite volume prevents the extraction of resonance data as it merges the resonance with the rest of the spectrum. However, more fundamentally, the Maiani-Testa theorem appears to prevent any direct method of measuring scattering data via the appropriate n-point functions. For this reason it is necessary to have some indirect method of evaluating the scattering parameters. The main idea in all the methods investigated here is that the resonances, having merged with the two-particle states, will have some effect on the spectra of the theory in a finite volume.
Since the resonance has merged with the rest of the spectrum its parameters will be difficult to extract in a single volume. However the fact that the multiparticle states are not bound states, but scattering states will affect their dependence on the volume in a critical way. As a function of the volume the energies of single particle states and bound states, $E_n(L)$, will decay as an exponential in the volume. Two particle state energies however will decay as inverse power of L and the dependence will involve the infinite volume phase shift $\delta(p)$.
The idea is to use the finite volume of the lattice world as a method to probe the scattering information of the field theory. This is the foundation of the first method of analysing resonances on the lattice, Lüscher's method.

2.2 Lüscher's Method

The most obvious effect on the spectrum of imposing a finite volume is that it becomes discrete. However Lüscher has shown that there are other consequences. The behaviour of the finite volume spectrum is related to infinite volume quantities otherwise inaccessible in Euclidean space. So rather than just being a source of systematic error, the finite volume can be used as a probe of the system. There are two major finite volume effects.

2.2.1 Finite volume mass shift

The finite volume effects on single particle states and bound states was first described in [17]. Here it was found that the shift in the mass of a stable particle in a spatial box with periodic boundary conditions and infinite temporal extent was related to the forward scattering amplitude.

In infinite volume and finite volume the mass of a particle is found through the following respective equations for the poles of the correlation function:

$$p^2 + m^2 - \Sigma(p) = 0, \tag{2.41}$$

$$p^2 + m^2 - \Sigma(p)_L = 0. \tag{2.42}$$

Where $\Sigma(p)_L$ and $\Sigma(p)$ are the finite and infinite volume self-energies.

The solutions to these equations are m^2, the infinite volume mass and M^2, the finite volume mass. The mass shift in finite volume is then $\delta m = M - m$. Taking the finite volume pole equation (2.42) and expanding in powers of δm, ignoring terms of $\mathcal{O}(\delta m^2)$, the mass shift is

$$\delta m = -\frac{\Sigma(\hat{p})_L}{\left(2m + i\frac{\partial}{\partial p^0}\Sigma(\hat{p})_L\right)} + \mathcal{O}(\delta m^2), \tag{2.43}$$

$$\hat{p} = (im, \underline{0}). \tag{2.44}$$

Hence to estimate δm one only needs knowledge of the behaviour of the finite-volume self-energy at $\hat{p}$. It is difficult to analyse $\Sigma_L(p)$ on its own. However, since the infinite volume self-energy vanishes at $\hat{p}$, due to the standard renormalisation conditions

$$\Sigma(\hat{p})_L = 0, \tag{2.45}$$

$$\frac{\partial}{\partial p^0}\Sigma\left(\hat{p}\right) = 0, \tag{2.46}$$

it is possible to analyse $\Sigma(\hat{p}) - \Sigma(\hat{p})_L$ and $\frac{\partial}{\partial p^0}\Sigma(\hat{p}) - \frac{\partial}{\partial p^0}\Sigma_L(\hat{p})$ instead.

Using $\Sigma(\hat{p}) - \Sigma(\hat{p})_L$ the cause of the mass shift becomes explicit. The Feynman diagrams contributing to the self-energy are almost identical in the infinite and finite volume cases, since the vertices are unaffected by the volume size. The only difference is that in addition to the standard Feynman propagator lines, the finite volume Feynman diagrams have other topological classes of propagators not possible in the infinite volume case. Namely propagators that encircle the world. The difference between the infinite and finite volume cases is then entirely due to these propagators, their effect being known as "virtual polarisation around the world". A series of estimates on the size of Feynman diagrams containing these "around the world" propagators[1] shows that only the diagrams with one propagator going around the world once contribute significantly. The same estimates also provide the following bounds:

$$\Sigma(\hat{p}) - \Sigma(\hat{p})_L = \mathcal{O}(e^{-\frac{\sqrt{3}}{2}mL}), \tag{2.47}$$

$$\frac{\partial}{\partial p^0}\Sigma(\hat{p}) - \frac{\partial}{\partial p^0}\Sigma_L(\hat{p}) = \mathcal{O}(e^{-\frac{\sqrt{3}}{2}mL}). \tag{2.48}$$

using these bounds on Eq.(2.44) reduces the expression for the mass shift to

$$\delta m = -\frac{1}{2m}\Sigma(\hat{p})_L + \mathcal{O}(e^{-\sqrt{3/2}mL}). \tag{2.49}$$

[1]The theory behind these estimates are covered in [18]

In any self-energy Feynman diagram, isolating a single line divides the diagram into a part that contributes to the four-point function and a part that contributes to the two point function, a proof can be found in [18]. Hence if one isolates the only around-the-world propagator in each diagram and sums over all diagrams, the following result is obtained

$$\Sigma(\hat{p})_L = \int \frac{d^4q}{(2\pi)^4} G_L(q,-q)G_4(p,q,-p,-q), \tag{2.50}$$

G_4 is the four-point function. G_L is the two point function with L denoting the fact that one of its external lines has gone around the world, which gives it faster decay properties. The contour of the integral in Eq.(2.50) can be shifted due to the analyticity of the three point vertex Γ_3 and four point vertex Γ_4 functions which make up $G_4(p,q,-p,-q)$. This shift in the contour basically eliminates G_2^L and replaces it with an exponentially decaying factor, leaving only this factor and $G_4(p,q,-p,-q)$. However $G_4(p,q,-p,-q)$ is just the Wick rotation of the forward scattering amplitude $F(\nu)$, with ν the crossing variable

$$\nu = \frac{E_{\underline{p}}E_{\underline{q}} - \underline{p}\cdot\underline{q}}{m}. \tag{2.51}$$

Hence one has

$$\delta m = -\frac{3}{16\pi m^2 L}\left\{\lambda^2 e^{-\frac{\sqrt{3}}{2}mL} + \frac{m}{\pi}\int_{-\infty}^{\infty} dy F(iy) e^{-\sqrt{m^2+y^2}L}\right\} + \mathcal{O}(e^{-\sqrt{\frac{3}{2}}mL}), \tag{2.52}$$

with λ the three-particle coupling constant and y the parameter on the imaginary axis in the complex ν-plane.

So with a detailed knowledge of how the mass of a stable particle changes with the volume, the behaviour of the forward scattering amplitude can be obtained. Although this effect is not explicitly related to resonances, it is important to have knowledge of it. This is because when deriving the relevant

formula for resonances in Sec.2.2.2 we use a contour shift valid only on the infinite volume propagator, so we must replace the finite volume propagator with the infinite volume one. The explicit formula for the mass shift controls this error. To estimate the size of the effect one often needs the simpler estimate:

$$\delta m = \mathcal{O}(e^{-\frac{\sqrt{3}}{2}mL}). \tag{2.53}$$

This estimate is obtained through pushing the contour of integration around the real-axis in the complex ν plane. $F(\nu)$ has poles at $\nu = \pm\frac{1}{2}m$ and branch cuts starting at $\nu = \pm m$, a result which can be seen by decomposing the four-point function into a sum of one-particle irreducible functions. In terms of y these poles occur at $y = \pm\frac{i}{2}m$, so picking up the contributions at the poles, which dominate over those of the branch cut (as y appears in a decaying exponential) we have the estimate Eq.(2.53).
This estimate is the one we use in the numerical analysis of resonances.

2.2.2 Finite volume effects on scattering states

We now come to Lüscher's fundamental results about the behaviour of scattering states in a finite volume. The results will only apply to two particle scattering states. The energies of these states are altered by the finite volume in two ways. First of all each individual particle in the pair has the virtual polarisation discussed above. However there is also a second effect resulting from their direct interaction with each other. It is this effect that is related to resonances.

This effect is derived in [19], although there was earlier work by DeWitt [20] on the quantum mechanical case in a spherical box[2]. In this case one obtains a relation between the infinite volume scattering phase shift and the finite volume energy spectrum.

To derive this effect it is necessary to consider the case of non-relativistic Quantum Mechanics and treat the Field Theory case by relating it back to

[2]A similar relation to the scattering phase shift is derived in DeWitt's work.

the non-relativistic one. It is simpler to understand the two-dimensional version of the effect, as derived in [21], so we will start there.

The two particle wave-function of two bosons in one spatial dimension is given by $\psi(x, y)$. If the total momentum vanishes $P = 0$, then the wave-function $\psi(x, y)$ is only a function of the relative coordinate, $r = x - y$. If the two particles are placed in a finite volume then the phase of the wave-function $\psi(r)$ will be altered in two ways.
First the phase will be shifted simply by motion through the volume giving the phase factor e^{ipL} in momentum space. However it will also be effected by the interaction between the two particles given by the inter-particle potential $V(r)$. This will result in the scattering phase shift $e^{2i\delta(p)}$. If the potential has a short enough range, then $\delta(p)$ will be the same as in infinite volume. If we impose periodic boundary conditions, then in order to satisfy these boundary conditions the total phase shift across the volume must vanish, meaning both factors must cancel.

$$e^{2i\delta(p)} = e^{-ipL}. \tag{2.54}$$

This is the two dimensional version of what is known as "Lüscher's formula". In the formula the p will be the momentum of the various two particle scattering states in the volume L. Since these can be deduced from the energy spectrum, the formula provides a bridge between something measurable numerically on the lattice, namely the energy spectrum and the infinite volume phase shift, which contains information on resonances.

For realistic situations we will the need the four-dimensional version of the formula.
We treat the infinite volume case first. There are two massive spin 0 bosons in 3-dimensional space with vanishing total momentum $P = 0$. As before this implies that the wave-function $\psi(x, y)$, with $x, y \in \mathbb{R}^3$ is a function of the relative coordinate $r = x - y$. The Hamiltonian of the system has the

form

$$H = \frac{-1}{2\mu}\Delta + V(r). \tag{2.55}$$

Where μ is the reduced mass and Δ on the $\mathbb{R}^3$ of the relative coordinate.

The potential is assumed to be C^∞ and of finite range

$$V(r) = 0, \qquad r > R. \tag{2.56}$$

For potentials of this type all solutions of the stationary Schrödinger equation $H\psi = E\psi$ are smooth (see [22], theorem IX.26). We can expand these solutions in terms of spherical harmonics

$$\psi(r) = \sum_l \sum_{m=-l}^{l} Y_{lm}(\theta, \phi)\psi_{lm}(r), \tag{2.57}$$

and obtain the radial Schrödinger equation for the coefficients

$$\left[\frac{d^2}{dr^2} + \frac{2}{r}\frac{d}{dr} - \frac{l(l+1)}{r^2} + p^2 - 2\mu V(r)\right]\psi_{lm}(r) = 0. \tag{2.58}$$

Where p is related to the energy by $E = \frac{p^2}{2\mu}$. For a given l this radial equation has only one linearly independent solution which is well-behaved. The dependence on m comes only from a coefficient.

$$\psi_{lm}(r) = b_{lm}u_l(r; p). \tag{2.59}$$

Where we label the solution by the momentum p associated with its energy eigenvalue E. Outside the potential we have the free Schrödinger equation and $u_l(r; p)$ must take the form

$$u_l(r; p) = \alpha(p)j_l(pr) + \beta(p)n_l(pr). \tag{2.60}$$

Basic scattering theory, see [13], shows that α and β are related to the scattering phase shift through the formula

$$e^{2i\delta_l(p)} = \frac{\alpha_l(p) + i\beta_l(p)}{\alpha_l(p) - i\beta_l(p)}. \tag{2.61}$$

This concludes the infinite volume model, we now consider the finite volume case.

The particles are now located in a three dimensional box with all dimensions of equal size L. In order to satisfy the periodic boundary conditions on the box, the wave-functions must obey

$$\psi(\underline{r} + \underline{n}L) = \psi(\underline{r}), \tag{2.62}$$

$$\underline{n} \in \mathbb{Z}^3. \tag{2.63}$$

The Hamiltonian remains formally the same, but the potential is altered to

$$V_L(r) = \sum_{\underline{n}\in\mathbb{Z}^3} V(|\underline{r} + \underline{n}L|), \tag{2.64}$$

in order to respect periodicity and the presence of interactions from around the world.

The spectrum of this Hamiltonian is discrete, since a finite volume imposes a quantisation condition in momentum space. We consider only the case where the extent of the finite volume world is larger than the range of the potential, $L > 2R$. This means there is a region

$$\Omega = \left\{\underline{r} \in \mathbb{R}^3 | \quad |\underline{r} + \underline{n}L| > R \forall \quad \underline{n} \in \mathbb{Z}^3\right\}, \tag{2.65}$$

where the Schrödinger equation is no different to the infinite volume case and we have the same asymptotic form for the radial wave-function

$$\psi_{lm}(r) = b_{lm}\left\{\alpha(p)j_l(pr) + \beta(p)n_l(pr)\right\}. \tag{2.66}$$

However in this region the wave-function is also a solution to the Helmholtz equation.

$$(\Delta + p^2)\psi(r) = 0. \tag{2.67}$$

An important result is that if a solution of the Helmholtz equation has a radial component which satisfies Eq.(2.66), then it coincides with a unique eigenfunction of the Hamiltonian in Ω.

In what follows it is necessary to make the assumption that the potential does not affect high angular momenta values. This is accomplished by modifying the potential with a projector Q_Λ onto the space of wave functions with $l \leq \Lambda$, where Λ is our angular momentum cut-off.

$$H_\Lambda = \frac{-1}{2\mu}\nabla + Q_\Lambda V_L(r). \tag{2.68}$$

The mathematical necessity of this cut-off is that otherwise the analysis of the relation between the solutions of the Helmholtz equation and the energy eigenfunctions would be more difficult. The physical justification of this projection operator is that unless the energy is quite high the scattering phases $\delta_l(p)$ with large l are practically zero. Also this projection term causes virtually no change in the spectrum unless Λ is extremely small, the difference from the cut-off free spectrum vanishing exponentially in Λ.

There are two important facts about the Helmholtz equation on the torus. First of all, a solution to the Helmholtz equation satisfying

$$\sup_{0<r<\frac{L}{2}} |r^{\Lambda+1}\psi(r)| < \infty, \tag{2.69}$$

for some integer Λ is known as a solution of degree Λ. The point being that this Λ will be directly related to the angular momentum cut-off Λ.

Secondly the Helmholtz operator on the Torus has no zero modes and so its Green's function $G(r; p^2)$ is a well defined distribution. Thus every solu-

tion of the Helmholtz equation of order Λ can be expanded as

$$\psi(r) = \sum_{l=0}^{\Lambda} \sum_{m=-l}^{l} v_{lm} G_{lm}(r; p^2). \tag{2.70}$$

Where $G_{lm}(r; p^2)$ are the angular components of $G(r; p^2)$ and v_{lm} their coefficients. $G_{lm}(r; p^2)$ itself can be expanded as

$$G_{lm}(r; p^2) = \tag{2.71}$$
$$\frac{(-1)^l}{4\pi} p^{l+1} \left\{ Y_{lm}(\theta, \phi) \psi_{lm}(r) n_l(pr) + \sum_{l'=0}^{\infty} \sum_{m'=-l'}^{l'} \mathcal{M}_{lm,l'm'} Y_{l'm'}(\theta, \phi) j_{l'}(pr) \right\}.$$

The coefficients $\mathcal{M}_{lm,l'm'}$ represent the mixing of the angular momentum modes due to the finite volume. They are

$$\mathcal{M}_{lm,l'm'} = \frac{(-1)^l}{\pi^{3/2}} \sum_{j=|l-l'|}^{l+l'} \sum_{s=-j}^{j} \frac{i^j}{\kappa^{j+1}} \mathcal{Z}_{js}(1; \kappa^2) C_{lm,js,l'm'}, \tag{2.72}$$

$$\kappa = \frac{pL}{2\pi}. \tag{2.73}$$

The $C_{lm,js,l'm'}$ are just tensorial coefficients and $\mathcal{Z}_{js}(1; q^2)$ is the Zeta function on a torus, given by

$$\mathcal{Z}_{js}(1; \kappa^2) = \sum_{\underline{n} \in \mathbb{Z}^3} \frac{r^j Y_{js}(\theta, \phi)}{(\underline{n}^2 - \kappa^2)^s}, \tag{2.74}$$

commonly known as Lüscher's Zeta function.

With this technical nomenclature in place we arrive at the fundamental theorem that there is a one to one correspondence between solutions of the Helmholtz equation on a torus of degree Λ which have the asymptotic form of Eq.(2.66) and eigenfunctions of H_Λ. Namely the eigenfunctions of H_Λ are equal to these solutions of the Helmholtz equation in Ω.

The main point is that any eigenfunction of the Hamiltonian H_Λ will have

two asymptotic forms in the region Ω. One form, Eq.(2.66), coming from scattering theory and another form, Eq.(2.70), due to it being a solution to the Helmholtz equation.
If we match these two forms, by setting the expansion Eq.(2.70) for a general solution to the Helmholtz equation equal to the asymptotic form of Eq.(2.66) we obtain two equations for the coefficients v_{lm}.

$$b_{lm}\alpha_l(p) = \sum_{l'=0}^{\Lambda} \sum_{m'=-l'}^{l'} v_{l'm'} \frac{(-1)^l}{4\pi} p^{l'+1} \mathcal{M}_{l'm',lm} \tag{2.75}$$

and

$$b_{lm}\beta_l(p) = v_{lm}. \tag{2.76}$$

To solve these equations we consider the problem abstractly. Let $\mathcal{H}_\Lambda$ be the space of coefficients v_{lm}. Then $M_{lm,l'm'}$ is just an operator $M(p)$ in this space. Similarly $\alpha_l(p)$ and $\beta_l(p)$ can be considered as operators A and B through their action on the coefficients

$$[Av]_{lm} = \alpha_l(p)v_{lm}, \tag{2.77}$$

$$[Bv]_{lm} = \beta_l(p)v_{lm}. \tag{2.78}$$

One may then define a phase-shift operator through

$$e^{2i\delta} = \frac{(A + iB)}{(A - iB)}. \tag{2.79}$$

Expressed this way, the existence of a solution v_{lm} to Eq.(2.75) and Eq.(2.76) is equivalent to

$$\det[A - BM] = 0. \tag{2.80}$$

However we want this equation to involve the scattering phase shift, so we divide by the factor

$$det[(A - iB)(M - i)]. \tag{2.81}$$

This determinant never vanishes because M is hermitian and there is no value of p for which $A = iB$. Dividing Eq.(2.81) into Eq.(2.80) gives

$$\det\left[e^{2i\delta} - U\right] = 0, \tag{2.82}$$

$$U = \frac{(M(p) + i)}{(M(p) - i)}. \tag{2.83}$$

Since p is related to the energy through $E = \frac{p^2}{2\mu}$, this gives a relation between the scattering phase shift and the finite volume two particle spectrum. This is the four-dimensional version of Lüscher's formula.

For practical situations Eq.(2.82) is cumbersome and expensive. The rank of U is Λ^2+1, so the computation of this determinant becomes a problem when Λ is large. However since the Helmholtz Green's function is invariant under the cubic group O_h, the coefficients $\mathcal{M}_{lm,l'm'}$ are also cubically invariant. From the point of view of the Hilbert space $\mathcal{H}_\Lambda$ this means that the operator $M(p)$ commutes with the rotation operator and hence can be block diagonalised with each block acting on a specific representation of the cubic group.

Most commonly one sets $\Lambda < 4$, since in most cases of interest δ_l is negligible for $l \geq 4$. Also we choose cubically invariant states, that is the A_1^+ representation, since the resonance we will study shall have angular momentum $l = 0$ and will extract the spectrum related to it via cubically invariant lattice operators. This requires only the use of $U(A_1^+)$, that is the part of U which acts on A_1^+ states in $\mathcal{H}_\Lambda$ of degree ≤ 4.

$$\det\left[e^{2i\delta} - U(A_1^+)\right]. \tag{2.84}$$

However the space of cubically invariant Helmholtz functions with $\Lambda < 4$ is one-dimensional, so this is simply

$$e^{2i\delta_0} = U(A_1^+) = \frac{M_{00,00} + i}{M_{00,00} - i}. \tag{2.85}$$

From Eq.(2.73) we have $M_{00,00} = \frac{1}{\pi^{3/2} q} \mathcal{Z}(1; q^2)$ and so

$$e^{2i\delta_0(p)} = \frac{\mathcal{Z}_{00}(1; \kappa^2) + i\pi^{3/2}\kappa}{\mathcal{Z}_{00}(1; \kappa^2) - i\pi^{3/2}\kappa}. \tag{2.86}$$

It is more useful to consider Eq.(2.86) in the form

$$\delta(p) = -\phi(\kappa) + \pi n, \tag{2.87}$$

$$\tan(\phi(\kappa)) = \left(\frac{\pi^{3/2}\kappa}{Z_{00}(1; \kappa^2)} \right). \tag{2.88}$$

Eq.(2.87) is the result commonly known as the Lüscher's formula.

Of course as it stands this result only applies to quantum mechanics, to be useful it must be applicable to quantum field theory. This is done by means of a map from quantum field theory to quantum mechanics.

In quantum field theory one can decompose the four-point function into an infinite sum involving the Bethe-Salpeter Kernel $K(p_1, p_2, p_3, p_4)$ and the function $G2(k)$.

$$G_4(p_1, p_2, p_3, p_4) = K(p', p) + \sum_{n=1}^{\infty} \frac{1}{2^n} \int d^4 k_j K(p', k_1) \left[\prod_{j=1}^{n-1} G2(k_j) K(k_j, k_{j+1}) \right] K(k_n, p), \tag{2.89}$$

$$G2(k) = G\left(\frac{1}{2}P + k\right) G\left(\frac{1}{2}P - k\right). \tag{2.90}$$

where $G(k)$ is the propagator and $P = p_1 + p_2$, $p = \frac{1}{2}(p_3 - p_4)$ and $p' = \frac{1}{2}(p_1 - p2)$.

The four point function contains information on the two particle energy spectrum and thus this expansion can be seen as an expansion for the two particle energies. Analytic properties of the Bethe-Salpeter Kernel allow the contours

of integration in this expansion to be shifted so that the function $G2(k)$ takes on a non-relativistic form. Once expressed this way, the expansion is formally identical to the Born expansion for a non-relativistic theory, with the Bethe-Salpeter Kernel filling the rôle of a potential. This Born expansion can be seen as coming from an effective non-relativistic Schrödinger equation for the two-particle wave-function $\psi(r)$

$$-\frac{1}{2\mu}\nabla\psi(r) + \frac{1}{2}\int d^3r' U_E(r,r')\psi(r') = E\psi(r). \tag{2.91}$$

Where the constant E, the "Schrödinger equation energy", is related to the true physical relativistic energy by $W = 2\sqrt{m^2 + mE}$. The same analytic properties of the Bethe-Salpeter Kernel imply that, as a potential, it satisfies the conditions on a potential used in the quantum mechanical proof of Lüscher's formula, [23]. So the entire framework derived above for the non-relativistic case can simply be carried over to quantum field theory and Lüscher's formula holds in this case as well. This effective Schrödinger equation was first derived in [24].

The use of $G(k)$, instead of $G_L(k)$ in the definition of $G2(k)$ is valid in large volumes because the error is $\mathcal{O}(e^{-\frac{\sqrt{3}}{2}mL})$ as a result of the virtual polarisations discussed in Sec.2.2.1. Hence the use of Lüscher's formula in quantum field theory is valid only for volumes large enough that virtual polarisation around-the-world is a negligible effect. Another important consequence of the effective Schrödinger equation, Eq.(2.91), found in [24] is that the Born expansion for it's energies provides an asymptotic form for the two-particle spectrum which we shall use later in the numerical simulations. This form is:

$$E = \sum_{i=1}^{5} \frac{C_i}{mL^i} + \mathcal{O}(L^{-6}). \tag{2.92}$$

The form obtained in [24] is more detailed than this, but the full form will not be required for the fits to which Eq.(2.92) is applied.

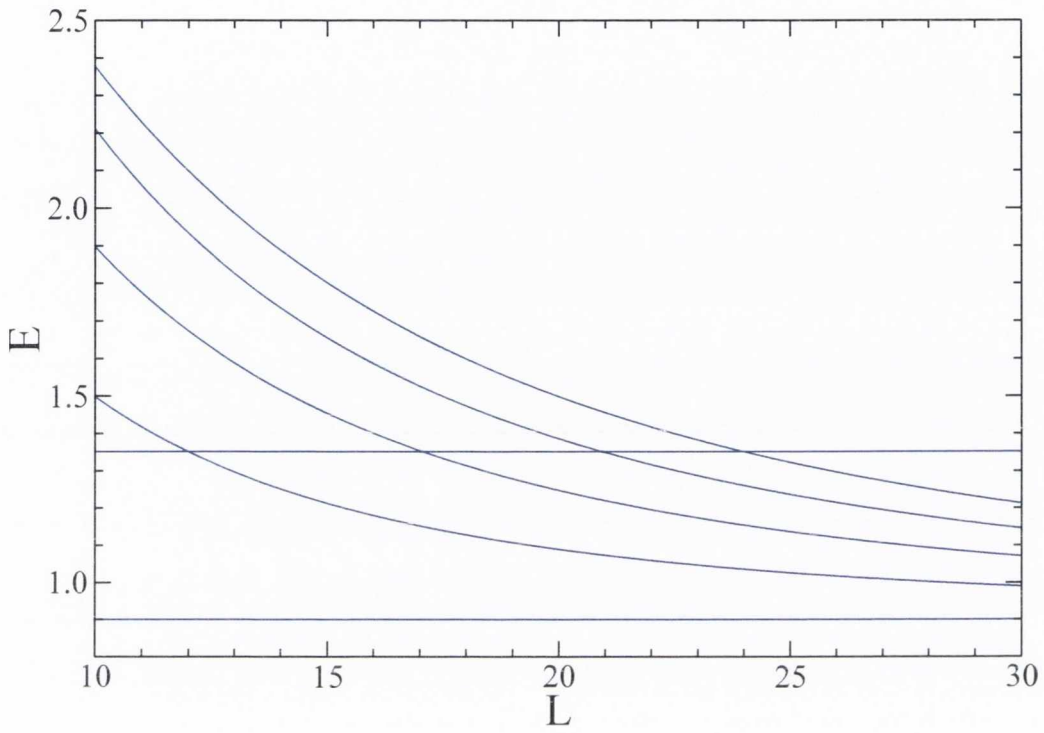

Figure 1: Example of the spectrum as a function of volume in a theory with the resonance decay width vanishing, $\Gamma = 0$. In this scenario the resonance appears as a stable state.

2.2.3 Consequences of Lüscher's formula

Not only does Lüscher's formula give a relation between the two-particle spectrum and the phase-shift, it also implies unusual behaviour in the spectrum that can be traced back to sharp changes in the phase-shift associated with resonances.

If there is a resonance in the same channel as the two-particle states, then near the resonance energy the phase shift will experience a rapid change comparable to π, as mentioned above. This behaviour in the scattering phase shift implies that the finite volume energy levels will rapidly rearrange themselves near the resonance energy.

However there is a theorem in the theory of hermitian matrices which states that eigenvalues of a matrix depending on a single continuous parameter (in our case the Hamiltonian depends on the volume[3]) cannot cross as that parameter is varied. Combined with the rearranging of the energy levels above this means there will be an abrupt change in the energy levels where they avoid each other, known as avoided level crossing. How near the energy levels are at the point of their closest approach is directly related to the decay width of the resonance. An example is provided in Fig. 1 and Fig. 2. In Fig. 1 we see the spectrum of a theory where there is no resonance. In this case we have the two particle spectrum of one species of particle and a stable one particle state of another which, up to the virtual polarisation effects of Sec.2.2.1, is independent of the volume.
However if the theory is adjusted so that stable one particle state couples to the two particle states, it becomes a resonance. In Fig. 2 we see the effect on the energy spectrum. The resonance has merged with the two particle states, however near the original mass of the resonance particle there is an avoided level crossing.

Lüscher's formula has been tested in a variety of theories such as Ising models[25], two-dimensional QED[26], the Gross-Neveau model[27] and has also been used to extract quantities in QCD itself, [28] [29] [30]. Hadronic resonances within QCD have been looked at in [31] using a generalisation of Lüscher's formula for moving frames, [32].

2.2.4 Limitations of Lüscher's formula.

Lüscher's formula is restricted to the elastic region for four fundamental reasons. Firstly, the result is actually proven in non-relativistic quantum mechanics, which is not suited to the description of inelastic scattering of the type $2 \to 4$. Secondly, all the analyticity properties of the vertex functions and the Bethe-Salpeter kernel only hold in the elastic region. Thirdly the additional physics of the inelastic scattering coefficients $\eta_l(p)$ are not taken

[3]More accurately the hermitian matrix here is the part of the Hamiltonian that couples the resonance and the stable particles.

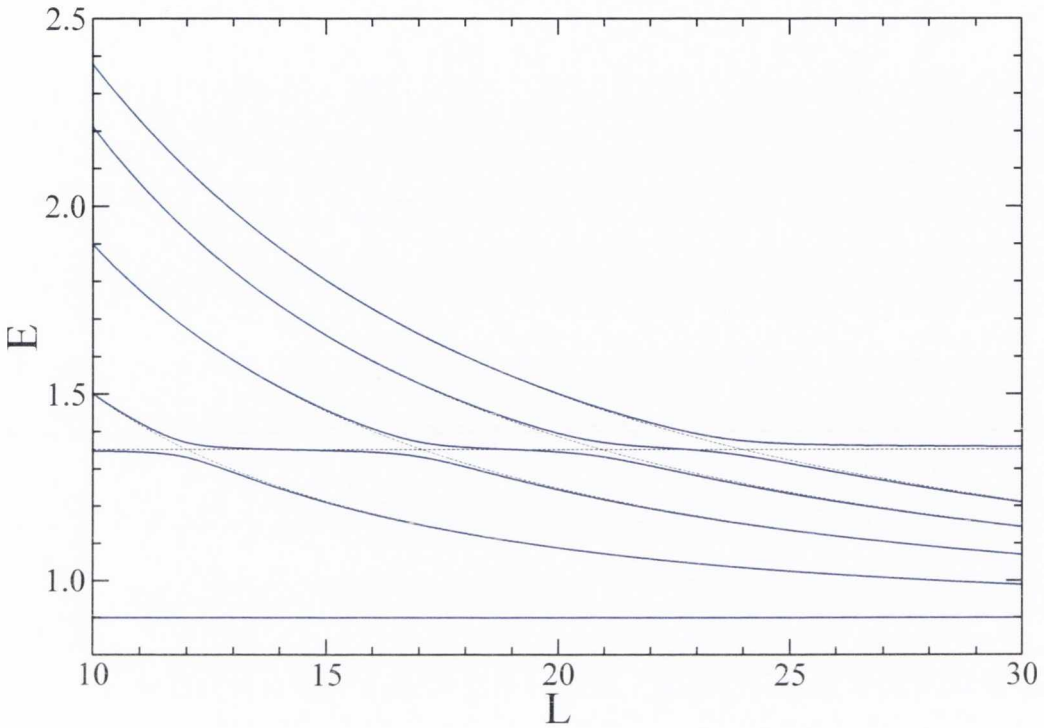

Figure 2: In this case the resonance can decay. This appears as an avoided level crossing near the mass of the resonance.

into account. Finally an extension of Lüscher's formula to the inelastic region would relate both the two particle and the four particle states to scattering data. However it is not clear how to decide if an energy eigenstate is four particle state in a finite volume, see [33] for a discussion. The restriction of Lüscher's formula to the elastic region is crucial as many resonances in QCD are found in the inelastic region. The possibility has been raised of using a Bethe-Salpeter wavefunction to derive Lüscher's formula in an alternative, albeit less rigorous, manner. An exposition of this Bethe-Salpeter wavefunction approach can be found in [34]. This approach has already been used in numerical calculations, [28], however it has also lead to a possible extension of Lüscher's formula into the inelastic region,[35]. There has also been a

generalisation of Lüscher's formula to a simplified inelastic case, [36], where one still has $2 \to 2$ scattering, but with two species of particles.

2.3 Histogram Method

The second method for obtaining resonance parameters from the lattice is the Histogram method. This method focuses on how the volume dependence of the spectrum $E_n(L)$ differs from its form in the case where the two particles do not scatter off each other, or $\delta(p) = 0$. The motivation for the method is the avoided level crossing shown in Fig. 2. At the mass of the resonance, a plateau occurs in the two particle spectrum, unlike the $\delta(p) = 0$ energy levels. Hence at momenta close to the resonance mass there are far more energy levels present across all volumes than in the free case. The idea is that the difference between the amount of energy levels present at a given momentum in the two cases $\delta(p) = 0$ and $\delta(p) \neq 0$ can be quantitatively linked to the scattering phase shift.

First the range of volumes and momenta is limited to the fixed region

$$[p_{min}, p_{max}] \times [L_{min}, L_{max}], \tag{2.93}$$

where p_{min}, p_{max} are usually chosen to encompass the entire elastic region $p_{min} = 0$, $p_{max} = \sqrt{3}m$. The limit $L_{max} \to \infty$ will be taken in the end and the choice of L_{min} will be discussed below.

This region is then partitioned into boxes of equal width ΔL and height Δp. We then define a histogram, which counts the amount of energy levels present in a given momentum range $[p_i, p_{i+1}]$, where $i = 1, \cdots, N = \frac{p_{max} - p_{min}}{\Delta p}$ across all volumes. Specifically the Histogram, $W(p_i)$, is given by:

$$W(p_i) = \sum_{n=1}^{N} \sum_{j=0}^{M} f_n(L_j), \tag{2.94}$$

$$f_n(L_j) = \begin{cases} 1, & p_n(L_j) \in [p_i, p_{i+1}] \\ 0, & p_n(L_j) \notin [p_i, p_{i+1}] \end{cases} \tag{2.95}$$

$$L_j = L_{min} + j\Delta L \qquad M = \frac{L_{max} - L_{min}}{\Delta L}. \tag{2.96}$$

In the limit of vanishing ΔL and Δp, it can be shown that that

$$\sum_{j=0}^{M} f_n\left(L_j\right) = \frac{1}{p_n^{'}(L)}, \tag{2.97}$$

and so in this limit the histogram is:

$$W(p_i) = C \sum_{n=1}^{N} \frac{1}{p_n^{'}(L)}. \tag{2.98}$$

In the elastic region, we already know that Lüscher's formula Eq.(2.87) holds. When differentiated with respect to L this formula gives:

$$\frac{1}{p_n^{'}(L)} = \frac{L}{p} + \frac{2\pi\delta^{'}(p)}{p\phi^{'}(\kappa)}. \tag{2.99}$$

It is at this point that the choice of L_{min} enters. For small values of L, the virtual polarisation effects of Sec.2.2.1 may make the use of Lüscher's formula invalid, hence L_{min} is chosen to be some volume at which these effects are highly suppressed.
If we substitute Eq.(2.99) into Eq.(2.98) we obtain the following expression for the histogram

$$W(p_i) = C \sum_{n=1}^{N} \frac{L_n(p)}{p} + \frac{2\pi\delta^{'}(p)}{p\phi^{'}(\kappa_n(p))}. \tag{2.100}$$

In Eq.(2.100) we use the expressions $L_n(p)$ and $\phi^{'}(\kappa_n(p))$. These invert the functional relations between the variables κ, L and the momentum p, which allows the histogram to be viewed purely as a function of momentum. The relations can be obtained by using Lüscher's formula and the definition of κ

$$L_n(p) = \frac{2\pi}{p}\phi^{-1}\left(\pi n - \delta(p)\right), \tag{2.101}$$

$$\kappa = \frac{pL}{2\pi}. \tag{2.102}$$

In this form the histogram is not particularly useful. It requires one to know the explicit values for the function $\phi(\kappa)$, which would make it no more than an rewriting of Lüscher's formula. However if we expand the expression Eq.(2.101) for the volume about the case where there is no scattering $\delta = 0$, we obtain

$$L_n(p) = \frac{2\pi}{p}\phi^{-1}(\pi n) - \frac{2\pi}{p}\delta(p)\frac{1}{\phi'(\phi^{-1}(\pi n))} + \mathcal{O}(\delta^2). \tag{2.103}$$

This can be simplified by recognising that $\phi^{-1}(\pi n)$ are simply the values of κ_n in a theory without scattering, which we will label $\overline{\kappa}_n$. This gives

$$L_n(p) = \frac{2\pi}{p}\overline{\kappa}_n - \frac{2\pi}{p}\delta(p)\frac{1}{\phi'(\overline{\kappa}_n)} + \mathcal{O}(\delta^2). \tag{2.104}$$

If Eq.(2.104) is substituted into Eq.(2.100), then we see that the histogram is given by

$$C^{-1}W(p_i) = \sum_{n=1}^{N}\frac{2\pi}{p^2}\overline{\kappa}_n - \sum_{n=1}^{N}\frac{2\pi}{p}\frac{1}{\phi'(\overline{\kappa}_n)}\left(\frac{\delta(p)}{p} - \delta'(p)\right) + \mathcal{O}(\delta^2). \tag{2.105}$$

The first term is exactly the histogram which would be constructed in a theory where the resonance is a stable particle and there is no scattering, $\delta(p) = 0$, which we will call the free background. Subtracting off this free background $C_0^{-1}W_0(p)$, where C_0 is its normalisation constant, we have

$$C^{-1}W(p_i) - C_0^{-1}W_0(p) = -\sum_{n=1}^{N}\frac{2\pi}{p}\frac{1}{\phi'(\overline{\kappa}_n)}\left(\frac{\delta(p)}{p} - \delta'(p)\right) + \mathcal{O}(\delta^2). \tag{2.106}$$

Now, if we take $L_{\max}$ quite large, then the number of energy levels which appear in the elastic region is quite large. For the fast majority of these energy levels $\delta(p) << \pi n$ and so the $\mathcal{O}(\delta^2)$ terms are negligible compared

with the first two terms. Hence in the large volume limit

$$C^{-1}W(p_i) - C_0^{-1}W_0(p) \approx -\left[\sum_{n=1}^{N} \frac{2\pi}{\phi'(\overline{\kappa}_n)}\right] \frac{1}{p}\left(\frac{\delta(p)}{p} - \delta'(p)\right). \tag{2.107}$$

The final observation is that

$$\sum_{n=1}^{N} \frac{2\pi}{\phi'(\overline{\kappa}_n)}, \tag{2.108}$$

is independent of the the phase shift $\delta(p)$ and the momentum p and hence is just a constant that can be absorbed into the normalisation constant of the histogram and so for large L_{max} we have

$$C^{-1}W(p_i) - C_0^{-1}W_0(p) \approx \frac{1}{p}\left(\frac{\delta(p)}{p} - \delta'(p)\right). \tag{2.109}$$

Eq.(2.109) shows that the total histogram, giving the relative density of energy levels between the free and interacting cases, is directly related to the scattering phase shift. The advantage over Lüscher's formula is that detailed knowledge of the function $\phi(\kappa)$ is not required to obtain the scattering phase shift, the histogram is directly related to $\delta(p)$ itself.

Unlike Lüscher's method, the histogram method has not been tested in realistic lattice simulations. In [12] it is tested against synthetic data obtain from applying Lüscher's formula in reverse to obtain a model two particle spectrum from experimental measurements of $\delta(p)$. In [37] it is tested in the case of non-relativistic quantum mechanics.
In a warm-up to a direct test of the method in comparison with Lüscher's method in a nonperturbative numerical simulation of a quantum field theory, we first test the method in a perturbative setting. This allows us to see how the method performs in the realistic case of relativistic quantum field theory, but without the extra complications of Monte-Carlo errors on the spectrum. Also, in perturbation theory the value for the resonance width can be computed directly in Minkowski spacetime, the calculation amounting to nothing

more than a standard tree-level Feynman diagram. We proceed now with this calculation.

3 Perturbative Calculations

In this section the linear sigma model is treated to first order as a test of the histogram method discussed in the previous section.

3.1 The model

For the perturbative calculation we consider a model which is similar to the one we will use in the numerical tests of the histogram method. That model will be the the $O(4)$ linear sigma model with an explicit symmetry breaking term.

$$\mathcal{L} = \frac{1}{2}\partial_\mu\phi_i\partial_\mu\phi_i + \lambda(\phi_i^2 - \nu^2)^2 - m_\pi^2\nu\phi_4 \ . \tag{3.1}$$

The reason for the explicit symmetry breaking term $m_\pi^2\nu\phi_4$ is that this model displays spontaneous symmetry breaking which will result in massless Goldstone bosons. However as Lüscher's formula only works in the case of massive field theories, an explicit symmetry breaking term is included in order to give these potential Goldstone bosons a mass.

For the perturbative calculations we use the following Lagrangian.

$$\begin{aligned}\mathcal{L} = &\frac{1}{2}\partial_\mu\tilde{\pi}_j\partial_\mu\tilde{\pi}_j + \frac{1}{2}\partial_\mu\sigma\partial_\mu\sigma + \lambda\sigma^4 + m_\sigma^2\sigma^2 + 4\nu\lambda\sigma^3 \\ &+\frac{1}{2}m_\pi^2\tilde{\pi}_j\tilde{\pi}_j + \frac{m_\pi^2}{2\nu}\sigma\tilde{\pi}_j\tilde{\pi}_j \ .\end{aligned} \tag{3.2}$$

Eq.(3.2) is inspired by the actual Lagrangian used in the simulations, namely Eq.(3.1). It has similar physics to the true Lagrangian as the particles it describes will carry an $SO(3)$ Isospin charge, I. The pions are an Isospin triplet, $I = 1$ and the sigma is an Isospin singlet, $I = 0$. Provided that $m_\sigma > 2m_\pi$, the σ particle will be unstable and will only appear as a resonance in the $I = 0$ channel. In the numerical simulations the Lagrangian Eq.(3.1) will also give rise to singlet and triplet states, however m_σ will actually be a function of the parameters λ and ν. The major difference between this perturbative Lagrangian and the one used in the simulations is that the resonance coupling to the pions does not depend on the momentum of the pions.

The first step in applying the Histogram method is obtaining the two-pion energy spectrum as a function of the volume. In infinite volume these states would form a continuum which would appear as a branch cut in some correlation function with the appropriate quantum numbers. In finite volume however, due to the discretisation of momentum, the spectrum of these states is discrete and they appear as isolated poles in the correlator. Hence we can find the spectrum by locating the poles of the correlation function in momentum space.

A good choice for the correlation function is the $\sigma\sigma$ two-point function. This is because it has the right quantum numbers, $I = 0$, $l = 0$ and in the elastic region covered by Lüscher's formula, $2m_\pi < E < 4m_\pi$, the only isospin singlet states are two-pion states. It is the scattering phase shift of these states, $\delta_0^0(p)$ that contains information on the σ resonance.

The $\sigma\sigma$ two point function is given by

$$G(\Omega) = \frac{1}{\Omega^2 + (m_\sigma^0)^2 - \Pi_L(\Omega)}. \tag{3.3}$$

Where m_σ^0 is the bare mass and $\Pi_L(\Omega)$ is the finite-volume self-energy. In order to find the poles and hence the two particle spectrum, we must solve the pole equation

$$\Omega^2 + (m_\sigma^0)^2 - \Pi_L(\Omega) = 0. \tag{3.4}$$

This will be done by computing the self-energy to first order in the coupling, which shall be denoted $\Pi^{(2)}(\Omega)_L$, and solving the approximate equation

$$\Omega^2 + (m_\sigma^0)^2 - \Pi_L^{(2)}(\Omega) = 0. \tag{3.5}$$

3.2 Renormalisation

If computed naively the Eq.(3.5) will produce a divergent integral. This integral needs to be renormalised by replacing the bare mass with the physical

mass. In infinite volume this would be accomplished via the renormalisation condition:

$$\Omega^2 + (m_\sigma^0)^2 - \Re e\Pi^{(2)}(\Omega) = 0, \tag{3.6}$$

with the physical mass being the solution, $\Omega = iM_R$, of Eq.(3.6).

The reason that $\Re e\Pi^{(2)}(\Omega)$ is used is that in infinite volume the σ is once again unstable, so its self-energy picks up an imaginary part through the optical theorem. For unstable particles one renormalises their mass using only the real part of the self-energy, in analogy with stable particles.

In finite volume however the σ is stable and hence there is no imaginary part to the propagator. Furthermore, the σ is no longer an isolated pole on the unphysical sheet, instead it will have merged with the two pion poles. Hence in finite volume m_σ^0 is a bare Lagrangian parameter with no obvious physical counterpart. This makes it unclear what value of Ω should be chosen as the point to impose the renormalisation conditions. For this reason we will simply use the infinite volume condition, Eq.(3.6), to choose the physical value of m_σ^2, i.e we take the physical mass as the solution to Eq.(3.6) at $\Omega = im_\sigma$. This is simply a renormalisation scheme, one which is consistent with the infinite volume limit, and does not affect the results. So the physical value m_σ^2 is related to the bare one via:

$$-(m_\sigma)^2 + (m_\sigma^0)^2 - \Re e(\Pi^{(2)}(im_\sigma)) = 0, \tag{3.7}$$

$$(m_\sigma^0)^2 = (m_\sigma)^2 + \Re e(\Pi^{(2)}(im_\sigma)). \tag{3.8}$$

Substituting this expression for the bare mass into the original pole equation (3.5) yields the result:

$$\Omega^2 + (m_\sigma)^2 - \Pi_L^{(2)}(\Omega)_R = 0. \tag{3.9}$$

Where $\Pi_L^{(2)}(\Omega)_R$, the renormalised finite volume self-energy, is $\Pi_L^{(2)}(\Omega) - \Re e\Pi^{(2)}(\Omega)$, the difference between the infinite volume and finite volume self-energy. We retain $\Re e\Pi^{(2)}(\Omega)$ for all arguments not just im_σ since the values

in the whole elastic region are close enough to $\Re e\Pi^{(2)}(im_\sigma)$ for this to be valid.

3.3 Finite volume Feynman rules

For the linear sigma model in finite volume the Feynman rules relevant to this computation are

$$-\delta_{ij}g, \tag{3.10}$$

for the vertices, where $g = \frac{m_\pi^2}{2\nu}$ and

$$\frac{1}{p^2 + m_\pi^2}, \tag{3.11}$$

for the pion propagator.
The only new features in finite volume is that the momenta in the pion propagators must take the form

$$p = (\omega, \underline{p}), \qquad \underline{p} = \frac{2\pi}{L}\underline{n}, \qquad \underline{n} \in \mathbb{Z}^3, \tag{3.12}$$

and all loop integrals are replaced by sums

$$\int \frac{d^4k}{(2\pi)^4} \to \int \frac{d\omega}{2\pi} \frac{1}{L^3} \sum_{\underline{n}\in\mathbb{Z}^3}. \tag{3.13}$$

In the computations, we will use g^2 for the coupling and m_π, m_σ for the masses rather than their expressions in terms of h and ν. $E_{\underline{n}}$ will denote the free two pion energies $E_{\underline{n}} = 2\sqrt{m^2 + p^2}$, with p quantised as in Eq.(3.12). We also measure all physical quantities in units of the vacuum expectation value, that is units with $\nu = 1$.

3.4 Computing the self-energy

$\Pi_L^{(2)}(\Omega)$ is given by the diagram

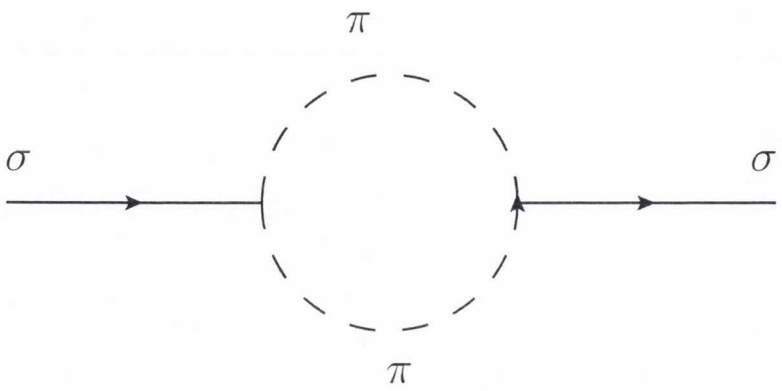

By the finite volume Feynman rules this is

$$\Pi_L^{(2)}(\Omega) = \frac{3g^2}{2L^3} \sum_{\underline{n} \in \mathbb{Z}^3} \int d\omega \frac{1}{\omega^2 + \underline{k}^2 + m_\pi^2} \frac{1}{(\omega + \Omega)^2 + \underline{k}^2 + m_\pi^2}, \tag{3.14}$$

with a factor of 3 coming from the three pions in the theory and $\frac{1}{2}$ from the symmetry factor of the diagram. We obtain $\Pi_L^{(2)}(\Omega)_R$ by subtracting off the infinite volume self-energy

$$\begin{aligned} \Pi_L^{(2)}(\Omega)_R = \frac{3g^2}{2L^3} \sum_{\underline{n} \in \mathbb{Z}^3} \int d\omega \frac{1}{\omega^2 + \underline{k}^2 + m_\pi^2} \frac{1}{(\omega + \Omega)^2 + \underline{k}^2 + m_\pi^2} \\ -\frac{3g^2}{2} \Re e \left(\int d^4k \frac{1}{\omega^2 + \underline{k}^2 + m_\pi^2} \frac{1}{(\omega + \Omega)^2 + \underline{k}^2 + m_\pi^2} \right). \end{aligned} \tag{3.15}$$

The standard procedure would be to simplify both of these expressions by using Feynman parameters to combine the denominators. However this will not get us far as the Euclidean energy Ω is above the decay threshold for the energies we are interested in, and so there may be singularities in the domain of the Feynman parameter integration, see [38, 39]. Also, even though the expression as it stands is meant to be renormalised and thus is finite, this is not manifest due to the ultraviolet divergence in the finite volume sum[4].
To get around both of these problems we perform a Taylor expansion of the renormalised self energy about the point $\Omega = 0$, which is below the decay

[4]Ultimately this divergence is cancelled by the infinite volume integral.

threshold

$$\Pi_L^{(2)}(\Omega)_R = \Pi_L^{(2)}(0)_R + \Omega^2 \frac{d}{d\Omega^2}\Pi_L^{(2)}(0)_R + \Pi_L^{(2)}(\Omega)_R^{TR}. \tag{3.16}$$

This is done for two reasons. Firstly it will be possible to calculate the first two terms and show that they are negligible, leaving the final Taylor remainder term where the ultraviolet convergence will be explicit. Secondly at $\Omega = 0$ the infinite volume integral will be purely real, which will allow the finite volume and infinite volume expressions to be combined in the first two Taylor terms.

Focusing first on the zeroth order term we have

$$\Pi_L^{(2)}(0)_R = \frac{3g^2}{2L^3}\sum_{\underline{n}\in\mathbb{Z}^3}\int d\omega \frac{1}{(\omega^2 + \underline{k}^2 + m_\pi^2)^2} - \frac{3g^2}{2}\int d^4k \frac{1}{(\omega^2 + \underline{k}^2 + m_\pi^2)^2}. \tag{3.17}$$

The sum can be replaced with an integral as follows

$$\frac{1}{L^3}\sum_{\underline{n}\in\mathbb{Z}^3}\int d\omega = \int d^4k \left[\sum_{\underline{n}\in\mathbb{Z}^3}\delta^4\left(\underline{k} - \frac{2\pi\underline{n}}{L}\right)\right]. \tag{3.18}$$

Resulting in

$$\begin{aligned}\Pi_L^{(2)}(0)_R = 3g^2 &\int d^4k \left[\sum_{\underline{n}\in\mathbb{Z}^3}\delta^4\left(\underline{k} - \frac{2\pi\underline{n}}{L}\right)\right]\frac{1}{(\omega^2 + \underline{k}^2 + m_\pi^2)^2} \\ &- 3g^2\int d^4k \frac{1}{(\omega^2 + \underline{k}^2 + m_\pi^2)^2}.\end{aligned} \tag{3.19}$$

Using the distributional version of Poisson's summation formula, [40]

$$\left[\sum_{\underline{n}\in\mathbb{Z}^3}\delta^4\left(\underline{k} - \underline{n}\right)\right] = \sum_{\underline{n}\in\mathbb{Z}^3} e^{2\pi i \underline{n}\cdot\underline{k}}. \tag{3.20}$$

This simplifies the integral to

$$\Pi_L^{(2)}(0)_R = \frac{3g^2}{2}\sum_{\underline{n}\in\mathbb{Z}^3}\int d^4k \frac{1}{(\omega^2+\underline{k}^2+m_\pi^2)^2}e^{iL\underline{n}\cdot\underline{k}} - \frac{3g^2}{2}\int d^4k \frac{1}{(\omega^2+\underline{k}^2+m_\pi^2)^2}. \tag{3.21}$$

However the $\underline{n}=0$ term is identical to infinite volume term, hence they cancel to give

$$\Pi_L^{(2)}(0)_R = \frac{3g^2}{2}\sum_{\underline{n}\in\mathbb{Z}^3,\underline{n}\neq 0}\int d^4k \frac{1}{(\omega^2+\underline{k}^2+m_\pi^2)^2}e^{iL\underline{n}\cdot\underline{k}}. \tag{3.22}$$

Expanding the integral in spherical coordinates for the spatial momentum we obtain:

$$\Pi_L^{(2)}(0)_R = \frac{3g^2}{2}\sum_{\underline{n}\in\mathbb{Z}^3,\underline{n}\neq 0}\int_{-\infty}^{\infty}d\omega\int_0^\infty dk\int_0^\pi d\theta\int_0^{2\pi}d\phi \frac{\sin(\theta)k^2}{|n|(\omega^2+\underline{k}^2+m_\pi^2)^2}e^{iL|n|k\cos(\theta)}. \tag{3.23}$$

where $|n|=\sqrt{n_1^2+n_2^2+n_3^2}$.
The integration of the angular variables can be performed quite easily, giving

$$\Pi_L^{(2)}(0)_R = \frac{6\pi g^2}{L}\sum_{\underline{n}\in\mathbb{Z}^3,\underline{n}\neq 0}\int_{-\infty}^{\infty}d\omega\int_0^\infty dk\frac{\sin(|n|kL)k}{(\omega^2+\underline{k}^2+m_\pi^2)^2}, \tag{3.24}$$

The ω integral can be calculated via Cauchy's residue theorem, using a contour in the upper half ω plane. Performing this contour integral and picking up the poles gives the final integral

$$\Pi_L^{(2)}(0)_R = \frac{3\pi^2 g^2}{L}\sum_{\underline{n}\in\mathbb{Z}^3,\underline{n}\neq 0}\int_0^\infty dk\frac{\sin(|n|kL)k}{|n|(\underline{k}^2+m_\pi^2)^{3/2}}. \tag{3.25}$$

However the integral Eq.(3.25) is one of the definitions of the zeroth modified Bessel function of the second kind. Hence the zeroth order term is given by

$$\Pi_L^{(2)}(0)_R = 3\pi^2 g^2\sum_{\underline{n}\in\mathbb{Z}^3,\underline{n}\neq 0} K_0\left(L|n|m_\pi\right). \tag{3.26}$$

Since the modified Bessel functions have a singularity at the origin, the presence of a $n = 0$ term would have produced the singular factor $K_0(0)$. Hence the infinite volume integral renormalises the finite volume Feynman diagrams by removing the singularities of the modified Bessel functions.

For the first order term the integral, after the subtraction of the infinite volume term, is:

$$\frac{d}{d\Omega^2}\Pi_L^{(2)}(0)_R = \frac{3g^2}{2}\sum_{\underline{n}\in\mathbb{Z}^3,\underline{n}\neq 0}\int d^4k \frac{-1}{(\omega^2+\underline{k}^2+m_\pi^2)^3}e^{iL\underline{n}\cdot\underline{k}}, \tag{3.27}$$

with the extra power in the denominator coming from the Ω^2 derivative. Once again, integrating the angular variables can be performed easily giving

$$\frac{d}{d\Omega^2}\Pi_L^{(2)}(0)_R = \frac{6\pi g^2}{L}\sum_{\underline{n}\in\mathbb{Z}^3,\underline{n}\neq 0}\int_{-\infty}^{\infty}d\omega\int_0^\infty dk \frac{-\sin(|n|kL)k}{|n|(\omega^2+\underline{k}^2+m_\pi^2)^3}. \tag{3.28}$$

The ω integral just involves the same contour integration as the zeroth order term and so:

$$\Pi_L^{(2)}(0)_R = \frac{-9\pi^2 g^2}{4L}\sum_{\underline{n}\in\mathbb{Z}^3,\underline{n}\neq 0}\int_0^\infty dk \frac{\sin(|n|kL)k}{|n|(\underline{k}^2+m_\pi^2)^{5/2}}. \tag{3.29}$$

The integral Eq.(3.29) involves the definition of the first modified Bessel function of the second kind. The first order term is then

$$\Omega^2\frac{d}{d\Omega^2}\Pi_L^{(2)}(0)_R = -\Omega^2\frac{3\pi^2 g^2 L}{4m_\pi}\sum_{\underline{n}\in\mathbb{Z}^3,\underline{n}\neq 0}|n|K_1(Lnm_\pi). \tag{3.30}$$

Again the infinite volume integral has removed the singular factor $K_1(0)$.

Due to the extremely fast rate of decay of the modified Bessel functions for large arguments, these terms are essentially negligible (see Fig. 3) and hence we will concentrate solely on the Taylor remainder term $\Pi_L^{(2)}(\Omega)_R^{TR}$.

We are now left only with the Taylor remainder. This term can be divided

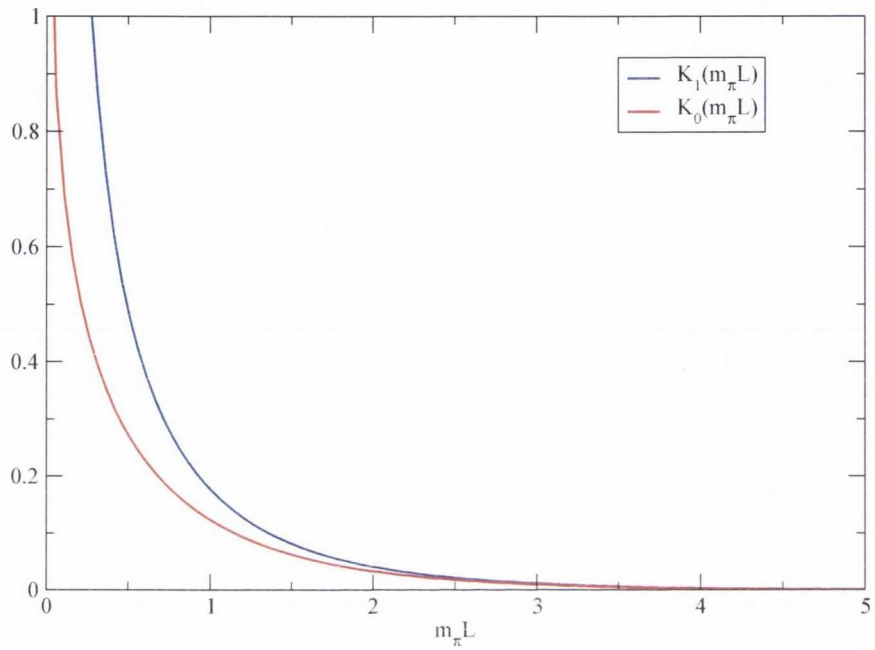

Figure 3: **Behaviour of the first two modified Bessel functions.** One can see that at even small L these terms are insignificant.

into its infinite volume and finite volume components:

$$\Pi_L^{(2)}(\Omega)_R^{TR} = \Pi_L^{(2)}(\Omega)^{TR} - \Re e(\Pi^{(2)}(\Omega)^{TR}). \tag{3.31}$$

The first to deal with is the twice subtracted finite volume self-energy. To calculate this it is simpler the evaluate the ω integral in the original expression for the Feynman diagram, Eq.(3.14), and then perform the Taylor subtraction. Performing the ω integral gives:

$$\Pi_L^{(2)}(\Omega) = \frac{3g^2}{L} \sum_{\underline{n} \in \mathbb{Z}^3} \frac{1}{E_n} \frac{1}{\Omega^2 + E_n^2}. \tag{3.32}$$

Of course Eq.(3.32) is divergent, but we are only using it as a formal step in Taylor subtraction. The Taylor subtraction can then be performed using the formula

$$D = \frac{1}{A+B} = \frac{1}{A} - \frac{B}{A^2} + D\left(\frac{B^2}{A^2}\right), \tag{3.33}$$

on the term

$$\frac{1}{\Omega^2 + 4E_n^2}, \tag{3.34}$$

with $A = E_n^2$ and $B = \Omega^2$. Since the first two terms in Eq.(3.33) give the first two Taylor terms, the Taylor remainder is given by the final term:

$$\Pi_L^{(2)}(\Omega)^{TR} = \Omega^4 \frac{3g^2}{2L^3} \sum_{\underline{n} \in \mathbb{Z}^3} \frac{1}{E_{\underline{n}}} \frac{1}{E_{\underline{n}}^4} \frac{1}{\Omega^2 + E_{\underline{n}}^2}. \tag{3.35}$$

The infinite volume part is just the twice subtracted infinite volume integral. Performing the ω integral first and then performing the subtraction, just as for the finite volume energy, gives

$$\Pi^{(2)}(\Omega)^{TR} = \Re e \left(\int \frac{d^3p}{(2\pi)^3} \frac{1}{E_p} \frac{1}{\Omega^2 + E_p^2} \frac{1}{E_p^4} \right), \tag{3.36}$$

$$E_p = 2\sqrt{\underline{p}^2 + m_\pi^2}. \tag{3.37}$$

This double subtraction lowers the degree of divergence from $D = 0$ to $D = -2$, so the integral is convergent. It can be evaluated quite easily using standard integration techniques, however an simpler estimate on its value is given by treating $E_p \approx 2p$ and shifting the lower limit of integration to m_π^2

$$\Pi^{(2)}(\Omega)^{TR} \approx \Re e \left(\int_{m_\pi^2}^{\infty} dp \frac{p^2}{2p} \frac{1}{\Omega^2} \frac{1}{16p^4} \right). \approx \frac{1}{m_\pi^2 \Omega^2} \tag{3.38}$$

For values of Ω corresponding to energies in the elastic region this term will be negligible, so it can be ignored.

Since we have shown that all other terms are negligible, due to dying off

with the volume or at energies above the two-pion threshold, the self-energy to this order in the elastic region is

$$\Pi_L^{(2)}(\Omega)_R \approx \Omega^4 \frac{3g^2}{2L^3} \sum_{\underline{n}\in\mathbb{Z}^3} \frac{1}{E_{\underline{n}}} \frac{1}{E_{\underline{n}}^4} \frac{1}{\Omega^2 + E_{\underline{n}}^2}. \tag{3.39}$$

3.5 The two particle spectrum

Now that we have a simple expression for the self-energy we can use it in the pole equation, Eq.(3.9)

$$\Omega^2 + (m_\sigma)^2 - \Omega^4 \frac{3g^2}{2L^3} \sum_{\underline{n}\in\mathbb{Z}^3} \frac{1}{E_{\underline{n}}} \frac{1}{E_{\underline{n}}^4} \frac{1}{\Omega^2 + E_{\underline{n}}^2} = 0. \tag{3.40}$$

We will change variables to the Minkowski energy $E = i\Omega$, as the spectrum

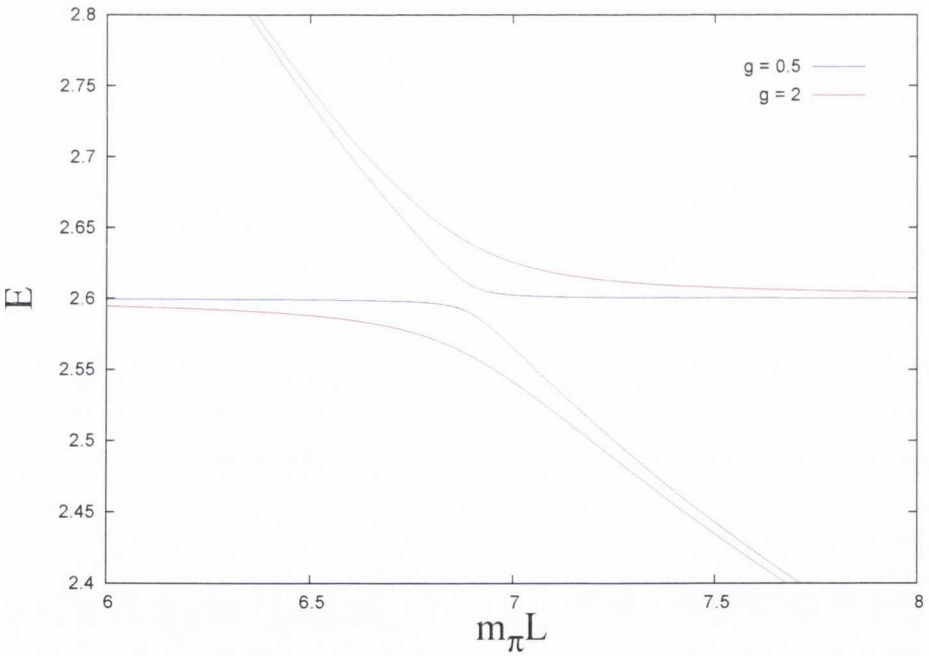

Figure 4: **Energy Levels for different couplings** $m_\sigma = 2.6$, $m_\pi = 1$.

will given by poles at real values of this variable.

$$E^2 - (m_\sigma)^2 - E^4 \frac{3g^2}{2L^3} \sum_{\underline{n} \in \mathbb{Z}^3} \frac{1}{E_{\underline{n}}} \frac{1}{E_{\underline{n}}^4} \frac{1}{E^2 - E_{\underline{n}}^2} = 0. \tag{3.41}$$

This expression defines a meromorphic function of E, with poles located at $E = E_{\underline{n}}$, a pole for each term in the sum. We will solve the equation by looking at the solutions near the $n^2 = 1$ poles. This is because one of the solutions near the $n^2 = 0$ pole will correspond to a state of two pions at rest, which will not contain information on the resonance. The other pole will be located beneath the two particle threshold and is in fact completely spurious. Other values of n^2 correspond to energies well above the resonance mass we shall choose, except at very large volumes, so we ignore them.
Near the $n^2 = 1$ poles the E^4 factor in the numerator is approximately $E_{\underline{n}}^4$, with $|n| = 1$. There are six $n^2 = 1$ poles in total so the equation for the energy levels is

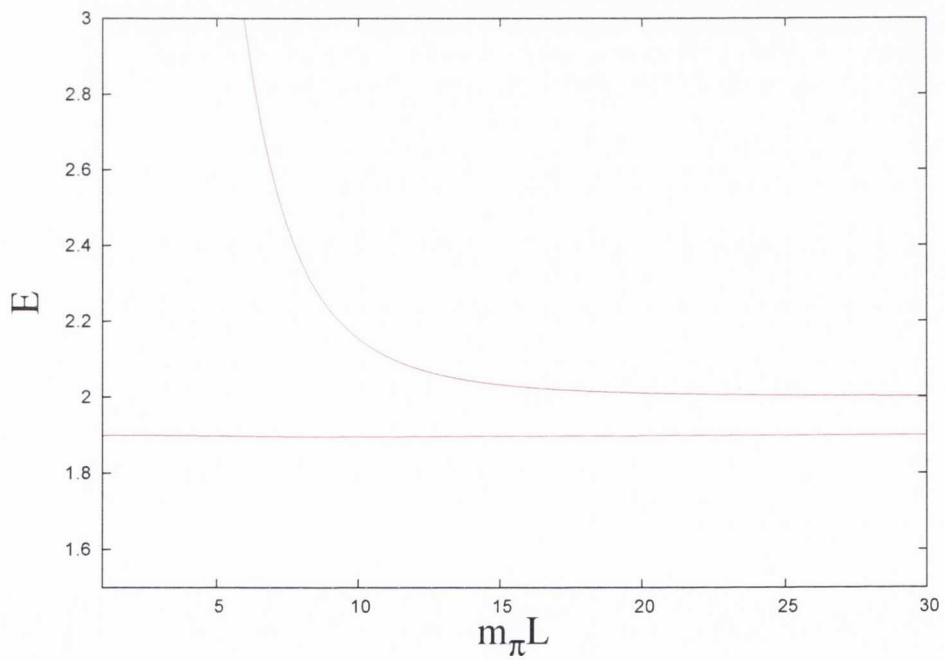

Figure 5: **Sigma beneath two particle threshold** $m_\sigma = 1.9$, $m_\pi = 1$ in units of the vacuum expectation value.

$$E^2 - (m_\sigma)^2 - \frac{9g^2}{L^3}\frac{1}{E_{\underline{n}}}\frac{1}{E^2 - 4E_{\underline{n}}^2} = 0. \tag{3.42}$$

This is a bi-quadratic equation which can be solved quite easily with two solutions near the pole given by,

$$E(L)^2 = \frac{1}{2}\left\{(E_{\underline{n}}^2 + m_\sigma^2) \pm \sqrt{(E_{\underline{n}}^2 - m_\sigma^2)^2 + \frac{36g^2}{L^3 E_{\underline{n}}}}\right\}. \tag{3.43}$$

The solutions are two energy levels given as a functions of L. In Fig. 4 the energy levels for two different values of the coupling can be seen. One can see the features discussed in Sec.2.2.3, namely the avoided level crossing, with the gap between the energy levels increasing with g. From the original Lagrangian, Eq.(3.2), it is clear that the width of the resonance is proportional to g^2, hence this corresponds to the expected effect of the gap between the levels being related to the width Γ. It should also be noted that Eq.(3.43) is similar to perturbative estimates of the spectrum found in [10] and [41].

If we bring the mass of the sigma beneath the two particle threshold, we obtain the spectrum of Fig. 5. As expected we see no avoided level crossing, with the sigma appearing as a stable state with no dependence on L and the two particle state having the $\mathcal{O}(\frac{1}{L})$ dependence of a free two particle state. To apply the histogram method of [12] we require the free energy levels. Fig(6) shows the free and interacting levels necessary for the construction of the histogram in the case $g = 0.5$. We will detail the construction of the histogram in the next section, in the context of numerical simulations, for now we will simply say that the method produces the histogram of Fig. 7 when applied to the data of Fig. 6. It should be noted that this histogram is unusually regular, since it is extracted from a perturbative calculation. The histograms obtained numerically will not be this regular. Fitting this

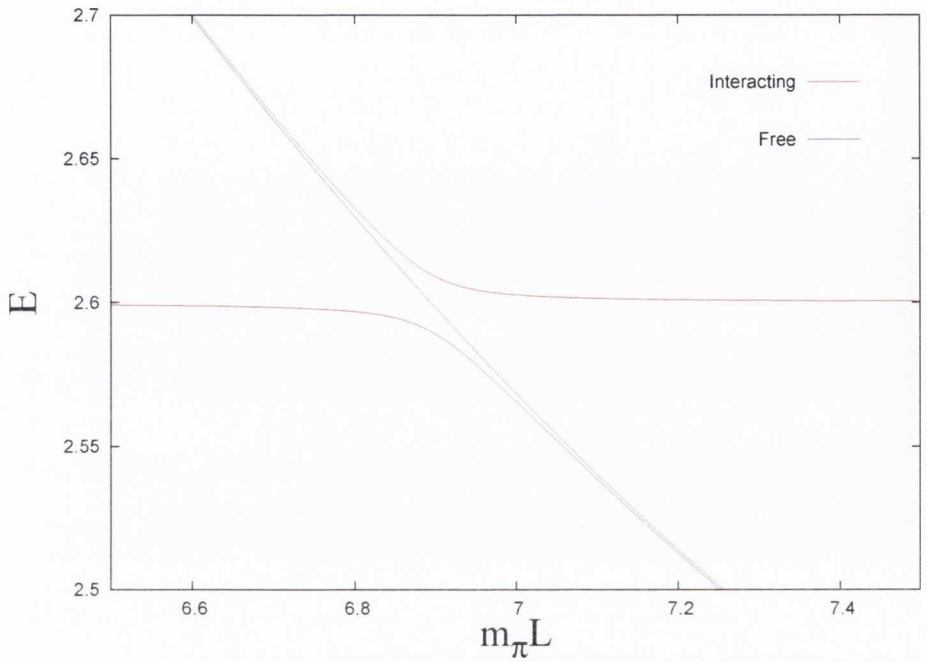

Figure 6: **Free and Interacting levels** $g = 0.5$, $m_\sigma = 2.6$, $m_\pi = 1$

histogram to the formula:

$$\frac{1}{C}W(p) - \frac{1}{C_0}W_0(p) \approx \frac{1}{[E(p)^2 - M_\sigma^2]^2 + M_\sigma^2\ \Gamma^2}\ . \tag{3.44}$$

which is obtained from Eq.(2.109) via substitution of Eq.(2.30) we obtain as the width

$$\Gamma_\sigma^{Histogram} = 0.0343(2). \tag{3.45}$$

Applying Lüscher's method we obtain the phase shift depicted in Fig. 8. This gives us the scattering phase shift, displaying the clear arc-tangent structure it should possess near a resonance. The construction of the phase shift using Lüscher's method will be detailed in the Sec.4.4, however we will just note that this phase shift was obtained using the more accurate estimation of $\phi(\kappa)$ that will be detailed there. This can be fitted to

$$\delta(p) - \frac{\pi}{2} \approx \arctan\left(\frac{4p^2 + 4M_\pi^2 - M_R^2}{M_R\Gamma_\sigma}\right), \tag{3.46}$$

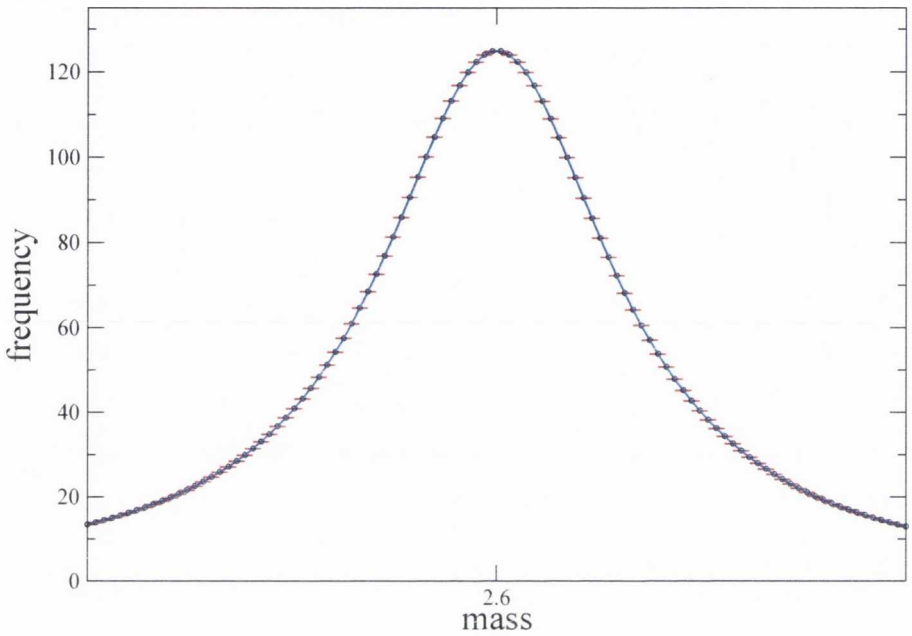

Figure 7: **The histogram** The peak occurs at the resonance mass.

from Eq. 2.31, giving the width:

$$\Gamma_{\sigma}^{Lüscher} = 0.0344(3). \tag{3.47}$$

Already we can see that Lüscher's method and the histogram method agree quite well, reproducing the same width, only with slightly different errors. For both methods the errors are generated via a estimate on the size of the $\mathcal{O}(g^4)$ corrections to the spectrum.

3.6 Comparison with Minkowski case

The advantage of working with a model in perturbation theory is that the results can be checked against the exact result coming from a calculation of

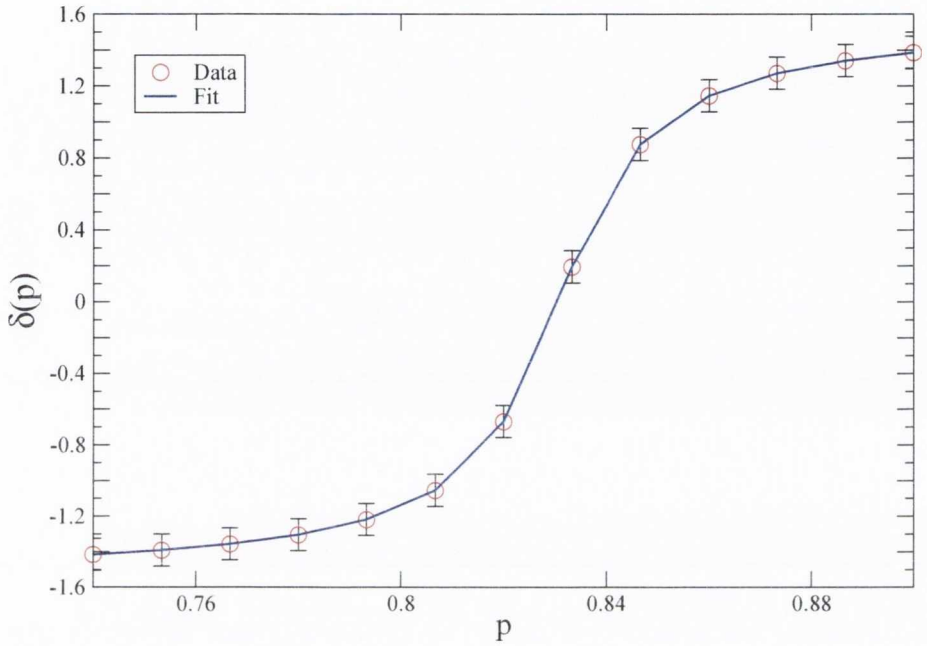

Figure 8: **The scattering phase shift** from the perturbative energy levels.

the three-point function in Minkowski spacetime. The Minkowski calculation is quite routine, involving the evaluation of only a single Feynman diagram.

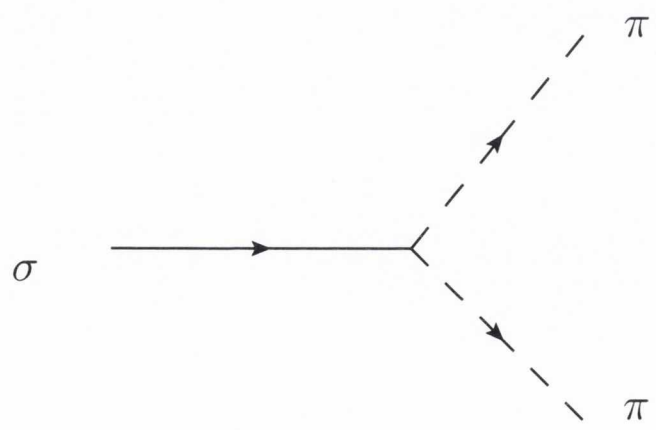

Since there are no internal lines, the amplitude for this process is simply $-6g$, with a factor of 2 coming from the pions being bosons.
The width of the sigma in its rest frame can be obtained from the standard formula, [1]

$$\Gamma = \frac{1}{2m_\sigma}\int \frac{d^3p_1}{(2\pi)^3(2E_p)}\int \frac{d^3p_2}{(2\pi)^3(2E_p)} 36g^2(2\pi)^4\delta^3(p_1+p_2)\delta(E_1+E_2-m_\sigma), \tag{3.48}$$

which is just a typical phase-space integral giving:

$$\Gamma_\sigma^{Minkowski} = \frac{9g^2}{8\pi m_\sigma}\sqrt{1-\left(\frac{2m_\pi}{m_\sigma}\right)^2}, \tag{3.49}$$

which, using the same parameters as those producing the Lüscher and Histogram estimates, gives a value for the decay width of

$$\Gamma_\sigma^{Minkowski} = 0.0344. \tag{3.50}$$

The agreement between Eq.(3.50) and the two expressions Eq.(3.45) and Eq.(3.47) is quite good and so it would appear that the histogram method provides a good determination of the resonance width in a perturbative setting. It should be noted that the Histogram estimate of Eq. 3.45 did not require detailed knowledge of the function $\phi(\kappa)$ of Lüscher's method, which demonstrates that this method can capture the physical parameters of the resonance without this function.
We will now move onto the numerical simulations and test the relative strengths and weaknesses of Lüscher's method and the Histogram method.

4 Numerical Simulations

We treat here the histogram method and Lüscher's method in a numerical context. The ultimate intended application for either of these techniques is the analysis of resonances in QCD. However we wish to compare and contrast these two methods as unambiguously as possible. For this reason we choose the linear sigma model as our field theory. This theory possesses a resonance from the outset which corresponds directly to terms which appear in the Lagrangian, hence there will not be issues relating to the background part of the scattering cross section $\delta_{bg}(p)$. Also it will be possible in this theory to obtain small relative errors on the two-particle spectrum, something which would be quite difficult in QCD. We will set up the model itself first, then give an account of how the spectrum is obtained. After that we describe the application of Lüscher's method and the Histogram method. Finally we compare and contrast them. Some elements of the results given in this section have been reported before in [42], [43].

4.1 The model

As mentioned, we wish to study resonances and the techniques for extracting resonance parameters from the lattice. However we do not wish to include the added complications of QCD itself. Instead we will study resonances in a simpler theory which allow us to use the methods and see their strengths and weaknesses without these additional complications.
The model we use is the is the $O(4)$ linear sigma model in the broken phase. This model has been used previously as a test of Lüscher's method, [44]. The Lagrangian is given by

$$\mathcal{L} = \frac{1}{2}\partial_\mu \phi^T \partial_\mu \phi + \lambda(\phi^T\phi - \nu^2)^2 - m_{\pi,0}^2 \nu \phi_4 \ . \tag{4.1}$$

In the broken phase the $O(4)$ symmetry will be broken down to an $O(3)$ symmetry. Since the dimension of $O(N)$ is $\frac{N(N-1)}{2}$, there will be $N-1 = dim(O(N)) - dim(O(N-1))$ Goldstone bosons associated with broken phase, in our case this gives three Goldstone bosons.

However an explicit symmetry breaking $m_{\pi,0}^2 \nu \phi_4$ is included in Eq.(4.1). This is because Lüscher's method relies explicitly on massive states. The spontaneous symmetry breaking alone will produce three massless Goldstone bosons, so we introduce the explicit breaking term to lift the masses of these Goldstone bosons. In the broken phase, with this Lagrangian we will have three stable massive particles and one unstable particle, the resonance σ. We do not use the unbroken phase as this simply consists of four stable particles. We shall rewrite this Lagrangian to tie it more directly to the physics. We introduce new fields σ and ρ_i, with the constraint that $\rho_i \rho_i = 1$.

$$\phi_i = (\nu + \sigma)\rho_i \ , \qquad \text{with } i = 1, 2, 3, 4 \ ; \tag{4.2}$$

We expand the potential around the classical minimum of the fields $\phi^T \phi = \nu^2$. This is typical for a broken phase as the Lagrangian fields will no longer be directly associated with the particle spectrum. Using the identity $\rho_i \partial \rho_i = 0$ we obtain the Lagrangian as

$$\begin{aligned} \mathcal{L} = \frac{1}{2}\nu^2 \partial_\mu \rho_i \partial_\mu \rho_i + \frac{1}{2}\sigma^2 \partial_\mu \rho_i \partial_\mu \rho_i + \frac{1}{2}\partial_\mu \sigma \partial_\mu \sigma + \nu \sigma \partial_\mu \rho_i \partial_\mu \rho_i \\ + \lambda \sigma^4 + 4\nu^2 \lambda \sigma^2 + 4\nu \lambda \sigma^3 - m_{\pi,0}^2 \nu^2 \rho_4 - m_{\pi,0}^2 \nu \sigma \rho_4 \ . \end{aligned} \tag{4.3}$$

The σ field is related to the massive ϕ_4 in the original Lagrangian and the ρ_i are related to what would be the Goldstone bosons if it were not for the explicit symmetry breaking term.

This theory will describe three massive particles transforming as triplet of the internal $SO(3)$ symmetry group, as well as a massive particle in the singlet representation of this group.

At the moment we cannot directly interpret the physical content of the Lagrangian Eq.(4.3), due to the presence of linear terms and it is not obvious that the explicit breaking term has given the pions a mass. It will turn out that the σ field is related to the massive ϕ_4 term in the original Lagrangian, but also to the physical σ resonance. The ρ_i are then related to the three massive pions. This relation between the ρ_i and the stable massive pion

states is not easy to see. To demonstrate the relation, we will introduce the pion fields as being related to $SU(2)$ fields; this is similar to the treatment of the non-linear sigma model in [9].
We introduce an $SU(2)$-valued field based on the ρ_j fields as follows

$$U = \rho_4 + i\sigma_j \rho_j \ , \tag{4.4}$$

with $j = 1, 2, 3$ and σ_j are the Pauli matrices.
In the non-linear sigma model, the pions are typically related to the fundamental $SU(2)$ fields via the relation

$$U = e^{\frac{i}{f}\pi_j \sigma_j} = \cos\left(\frac{|\vec{\pi}|}{f}\right) + i\sigma_j \frac{\pi_j}{|\vec{\pi}|} \sin\left(\frac{|\vec{\pi}|}{f}\right) \ , \tag{4.5}$$

where ν plays the rôle of the pion decay constant.
Using Eq.(4.4) and Eq.(4.5) we may say naively that the relation between the ρ_j fields and the pions is given by:

$$\rho_4 = \cos\left(\frac{|\vec{\pi}|}{\nu}\right) \ , \tag{4.6}$$

$$\rho_j = \frac{\pi_j}{|\vec{\pi}|} \sin\left(\frac{|\vec{\pi}|}{\nu}\right) \ . \tag{4.7}$$

We may replace the ρ fields in the Lagrangian by the use of a few identities. First of all we take the expression $\frac{1}{2}\,\mathrm{Tr}(U + U^\dagger)$. For the ρ fields this gives:

$$\frac{1}{4}\,\mathrm{Tr}(U + U^\dagger) = \rho_4. \tag{4.8}$$

For the pion fields it is:

$$\frac{1}{4}\,\mathrm{Tr}(U + U^\dagger) = \cos\left(\frac{|\vec{\pi}|}{\nu}\right). \tag{4.9}$$

So we have

$$\rho_4 = \cos\left(\frac{|\vec{\pi}|}{\nu}\right) \tag{4.10}$$

We also use the expression $\frac{1}{2}\,\mathrm{Tr}(\partial_\mu U \partial_\mu U^\dagger)$. For the ρ fields this is

$$\frac{1}{2}\,\mathrm{Tr}(\partial_\mu U \partial_\mu U^\dagger) = \sum_{i=1}^{4} \partial_\mu \rho_i \partial_\mu \rho_i, \tag{4.11}$$

For the pion fields this gives

$$\frac{1}{2}\,\mathrm{Tr}(\partial_\mu U \partial_\mu U^\dagger) = \frac{1}{\nu^2} \sum_{i=1}^{3} \partial_\mu \pi_i \partial_\mu \pi_i, \tag{4.12}$$

and so we have:

$$\sum_{i=1}^{4} \partial_\mu \rho_i \partial_\mu \rho_i = \frac{1}{\nu^2} \sum_{i=1}^{3} \partial_\mu \pi_i \partial_\mu \pi_i. \tag{4.13}$$

Eq.(4.10) and Eq.(4.13) can then be substituted into the original Lagrangian, Eq.(4.3). Expanding the $\cos\left(\frac{|\vec{\pi}|}{\nu}\right)$ which has replaced the ρ_4 field, we obtain as our Lagrangian:

$$\begin{aligned}\mathcal{L} = \frac{1}{2}\partial_\mu \pi_j \partial_\mu \pi_j + \frac{1}{2\nu^2}\sigma^2 \partial_\mu \pi_j \partial_\mu \pi_j + \frac{1}{2}\partial_\mu \sigma \partial_\mu \sigma + \\ \frac{1}{\nu}\sigma \partial_\mu \pi_j \partial_\mu \pi_j + \lambda\sigma^4 + 4\nu^2\lambda\sigma^2 + 4\nu\lambda\sigma^3 + \\ \frac{1}{2}m_{\pi,0}^2 \pi_j \pi_j + \frac{m_{\pi,0}^2}{2\nu}\sigma \pi_j \pi_j \ + ...\end{aligned} \tag{4.14}$$

Where the higher order terms include higher order couplings between the pions and the σ resonance, as well as pion self-interaction terms.
We can see that the σ field has mass

$$m_\sigma = 2\nu\sqrt{2\lambda} \tag{4.15}$$

and due to terms such as the three-point interaction $\nu\sigma\partial\rho_i\partial\rho_i$ the sigma particle is unstable. We can also see that the parameter $m_{\pi,0}$ that we introduced functions as the bare pion mass. So our explicit breaking term has given the Goldstone bosons a mass.

Two things should be noted about the three-point interaction term. First of all it both depends on ν, so the sigma resonance should be more unstable with decreasing values of ν. However we will not make direct use of this. It also contains a derivative. In momentum space this will give an extra p^2 term to the Feynman diagrams. So we expect the interaction between the pions and the sigma resonance to be stronger when the pions have larger relative momentum. The decay rate of the sigma resonance will also depend on λ, since the σ field self-coupling terms will affect the interactions between the σ-particle and the pions.

For certain values of the parameters the $O(4)$ symmetry will be restored and the theory will enter the unbroken phase. Since we do not want this to occur we must avoid the region of the λ, ν parameter space in which the symmetry is unbroken. For any fixed value of λ the symmetry is restored when ν is small enough. The point of this phase transition $\nu_*(\lambda)$ increases with increasing λ. In particular

$$\lim_{\lambda \to \infty} \nu_*(\lambda) \approx 0.78 \tag{4.16}$$

Hence we will always keep ν above 0.78, specifically we use $\nu = 1$ or 1.05, to guarantee that the symmetry remains broken.

A derivation of Eq.(4.16) is contained in Ref [44], although there, due to different parameters being used, it appears as $\kappa_c \approx 0.304$.

4.2 Extracting the spectrum

With the model in place and a link established between its Lagrangian parameters and the physical parameters of the theory, we proceed to the numerical simulation of the theory. The theory is placed on a $64 \times L^3$ lattice, where L, the spatial extent of the lattice, will vary as required by both methods. The lattice action used was:

$$\mathcal{S} = a^4 \sum_x \left(\frac{1}{2}\phi^T(x) \left(-\Delta\phi\right)(x) + \lambda \left(\phi^T(x)\phi(x) - \nu^2\right)^2 - m_{\pi,0}^2 \nu \phi_4(x) \right), \tag{4.17}$$

where the Laplacian is as defined in Eq.(1.16).

The Monte-Carlo simulations themselves were performed by Dr. Pietro Giudice on the Lonsdale computer cluster at Trinity College Dublin. The cluster consists of 1232 Opteron processor cores with a clock speed of 2.3 Ghz. For each choice of the parameters $m_{\pi,0}, \nu, \lambda$, the computational time was around one hundred hours for each specific choice of the volume L. This consisted of running the same set of parameters on ten different processor cores, each with a different random seed. On each core the simulation took ten hours. This time was held fixed for each volume by making a different number of measurements for each volume. For instance in our first set of parameters below, with $\lambda = 1.4, m_{\pi,0} = 0.36$, 225000 measurements were performed for the $L = 8$ case and 22000 for the $L = 19$ case.

The sample field configurations for the Monte-Carlo estimate of the path integral are obtained differently for the ϕ_4 field and the ϕ_j fields, $j = 1, 2, 3$. For the ϕ_4 field, the configurations are obtained by the Metropolis algorithm. For the ϕ_j fields they are obtained from an over-relaxation algorithm.

In order to apply either the Histogram or Lüscher's method knowledge is needed of the mass of the pion. For the Histogram method the mass is necessary in order to fit the histogram, however in Lüscher's method it is even more fundamental as it is required in the dispersion relations. In both methods it is also a way of measuring if the virtual polarisation effects of Sec.2.2.1 are negligible. To obtain m_π we expand the fields in terms of a par-

tial Fourier transform (PFT). We Fourier transform the spatial coordinates, but leave the temporal coordinate untransformed.

$$\tilde{\phi}_i(\vec{n},t) = \frac{1}{V}\sum_x \phi_i(\vec{x},t)e^{-i\vec{x}\vec{p}}\ , \qquad p_i = \frac{2\pi}{L}n_i\ , \tag{4.18}$$

where n_i varies over the lattice $n_i = 0, \cdots, L_i - 1$ and $V = L^3$. Using these fields we can extract the mass of the pion from the $\vec{n} = \vec{0}$ field. This field has zero-momentum and hence will give the mass of the pion most directly. We use the standard method of extracting the mass from the exponential decay of the correlator

$$C_i(t) = \langle \tilde{\phi}_i(\vec{n},t)\tilde{\phi}_i(-\vec{n},0)\rangle\ . \tag{4.19}$$

for $i = 1, 2, 3$. The masses of all three pion fields should be the same within errors, due to the remaining $O(3)$ symmetry of the theory. We will refer to the bare mass in the Lagrangian as $m_{\pi,0}$ and the physical mass of the pion, as obtain from the zero-momentum correlator, as m_π.

In order to measure the two pion spectrum, the most fundamental data for both methods, we need a correlator with the correct quantum numbers. Obviously there are several classes of two pion states, with varying linear momentum, angular momentum and isospin. We pick our correlator according to the following requirements:

1. Both methods require states of zero total linear momentum.

2. Both methods will involve the scattering phase shift $\delta_I^l(p)$, from which the resonance parameters will be obtained. Since the sigma resonance has $l = 0$ and $I = 0$ it will only be seen in that channel. Hence we need two pion states of $l = 0$ and $I = 0$ to obtain $\delta_0^0(p)$. One the lattice we will achieve this by using operators in the A_1^+ representation of the cubic group.

We will use N such operators, where N will be varied depending on the simulation parameters. More operators will be necessary for parameters corresponding to wider resonances.

A set of $N-1$ operators obeying these conditions is given by

$$O_{\vec{n}}(t) = \sum_{i=1}^{3} \tilde{\phi}_i(\vec{n}, t)\tilde{\phi}_i(-\vec{n}, t) \ ; \tag{4.20}$$

as well as a single operator given by the $\vec{p} = 0$ PFT of the ϕ_4 field

$$O_N(t) = \tilde{\phi}_4(\vec{0}, t)\tilde{\phi}_4(-\vec{0}, 0). \tag{4.21}$$

Obtaining energy levels from a set of correlators such as these is somewhat more complicated. To do so we use the method of [21]. First the matrix $C_{ij}(t) = \langle O_i O_j \rangle$ is constructed. Each $\langle O_i O_j \rangle$ is the Monte-Carlo estimate of the correlations of the O_i and O_j fields.
One then solves the generalised eigenvalue problem

$$C(t)\psi = \lambda(t, t_*)C(t_*)\psi \ , \tag{4.22}$$

where t_* must be small. We choose $t_* = 0$ for reasons of numerical stability. In [21] it is shown that the generalised eigenvalues behave as follows:

$$\lambda_\alpha(t, t_*) = e^{-(t-t_*)E_\alpha} \ , \tag{4.23}$$

with $\alpha = 1, \cdots, N$ labelling the eigenvalues. E_α is then then the energy of some state with the quantum numbers of these operators. The two particle energy levels E_α can be labelled by $\underline{n} = (n_1, n_2, n_3)$ the components of the relative momentum between them.

4.3 Choosing parameters

To test the two methods we consider four different choices of parameters. For the first three cases we fix $\nu = 1$ in order to ensure that we are in the broken phase. The basic idea is to look at a narrow, medium and broad resonance and finally the inelastic region.
These parameters were chosen after tuning over the course of several sim-

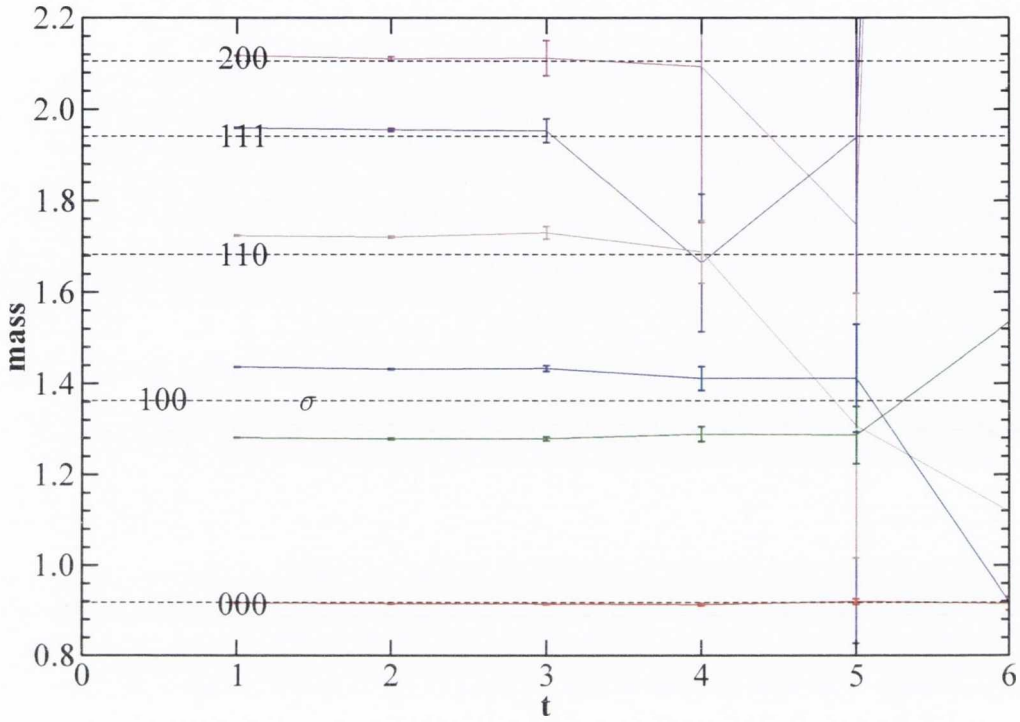

Figure 9: Effective mass versus time as determined by the diagonalisation of the correlation matrix C_{ij}. The dashed constant lines describe the free two-particle spectrum. Simulation parameters: $\nu = 1.0$, $\lambda = 1.4$, $m_\pi^0 = 0.36$, volume=$12^3 \times 64$.

ulations. As mentioned previously the resonance width will depend on the relative momentum of the pions. For large relative momentum the resonance will be broad. If we keep the picture of resonances as bound states which become unstable when some interaction is turned on, we look at the energy levels which would be obtained if the interactions between the sigma field and pion fields were switched off. For the pion energy levels this is just given by the formula

$$E_{2\pi} = 2\sqrt{m_\pi^2 + p^2}. \tag{4.24}$$

For the sigma particle, the spectrum of interest just consists of a single sigma particle at rest, the mass of which is estimated by the effective mass extracted

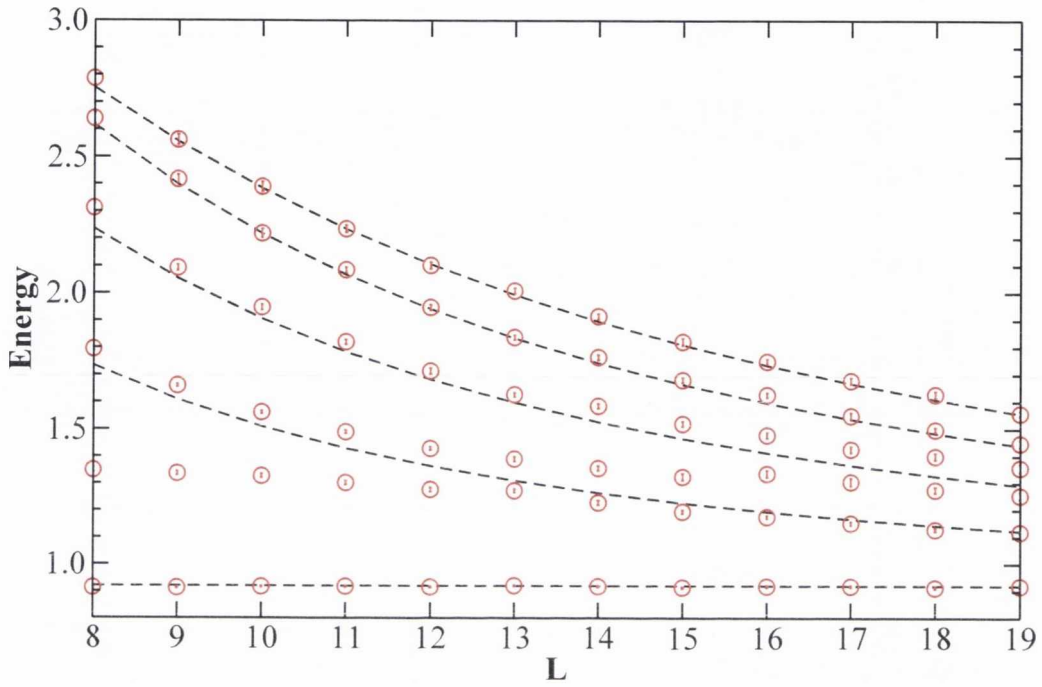

Figure 10: Spectrum of the theory for different values of the volume for the following simulation parameters: $\nu = 1.0$, $\lambda = 1.4$, $m_\pi^0 = 0.36$. The dashed lines describe the free two-particle spectrum.

from the $i = 4$ correlator in Eq.(4.21). λ and m_π are tuned so that the sigma mass intersects a chosen two pion energy level at a certain volume. If a two pion energy level with large relative momentum is chosen, then when the interaction is switched on, the sigma will couple to that two pion state and due to the high relative momentum it will become broad resonance. There are two ways the two pion energy level can have high relative momentum, if the parameters (n_1, n_2, n_3) are large or if the volume is small, since

$$\underline{p} = \frac{2\pi}{L}\underline{n} \qquad \underline{n} = (n_1, n_2, n_3). \tag{4.25}$$

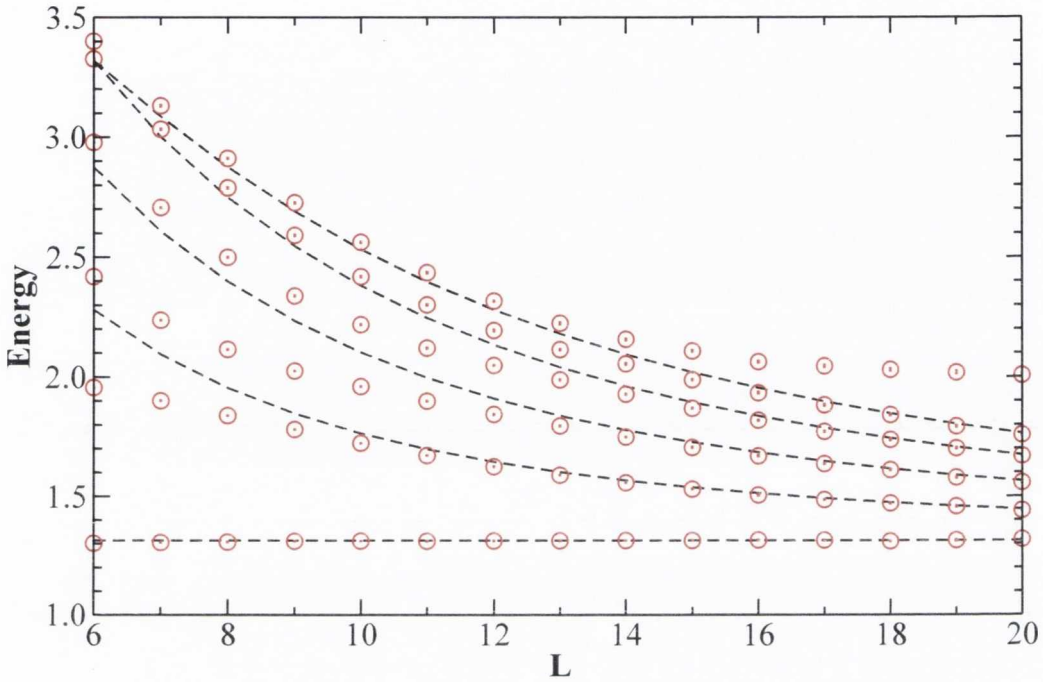

Figure 11: Spectrum of the theory for different values of the volume for the following simulation parameters: $\nu = 1.0$, $\lambda = 4.0$, $m_\pi^0 = 0.56$.

The first set of parameters, giving a narrow resonance, are $\lambda = 1.4, m_{\pi,0} = 0.36$. These give an intersection between the sigma mass and the $(1,0,0)$ energy level at $L = 12$, corresponding to a relative momentum of $p \approx 0.524$. The physical mass of the pion obtain from the PFT method mentioned above is $m_\pi = 0.460(2)$. The mass of the pion was found to stabilise near $L = 7$, indicating that the virtual polarisation effects are negligible at this volume. Hence, for this first set of parameters we take a volume range of $L \in [8, 19]$.

An example of the use of the diagonalised correlation matrix, used to obtain the two particle spectrum, is depicted in Fig. 9. Here we see the behaviour of the effective masses obtained from each of the eigenvalues $\lambda_\alpha(t)$ on the

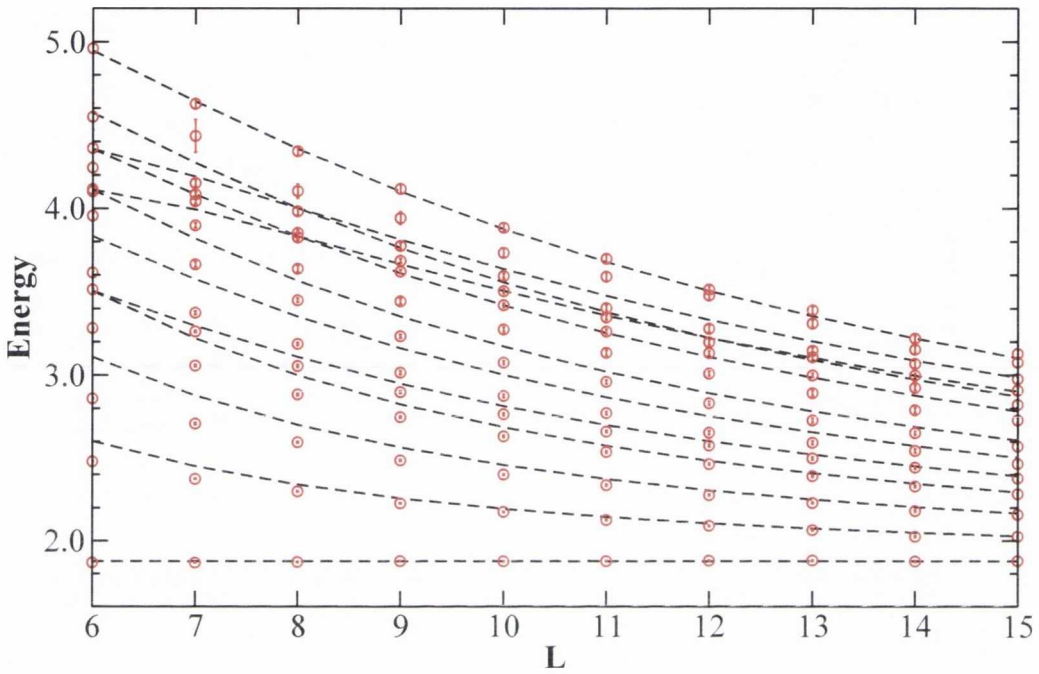

Figure 12: Spectrum of the theory with simulation parameters: $\nu = 1.0$, $\lambda = 200.0$, $m_\pi^0 = 0.86$.

lattice of volume $L = 12$. Due to the diagonalisation method we can see an obvious plateau for each effective mass, m_{eff}. We take as the Energy of a given two particle state, the value of m_{eff} at some chosen value of t where the plateau has already occurred for all energy levels and volumes. In the case of these parameters this point is $t = 2$.

Repeating this for several volumes builds up a profile of the dependence of the two-pion spectrum as a function of volume. This volume dependence of the spectrum is depicted in Fig. 10. Shown with dashed lines are the corresponding free energy levels, which are necessary for the construction of the histograms. The relative error on the energy levels is in the range 0.5% - 1.0%.

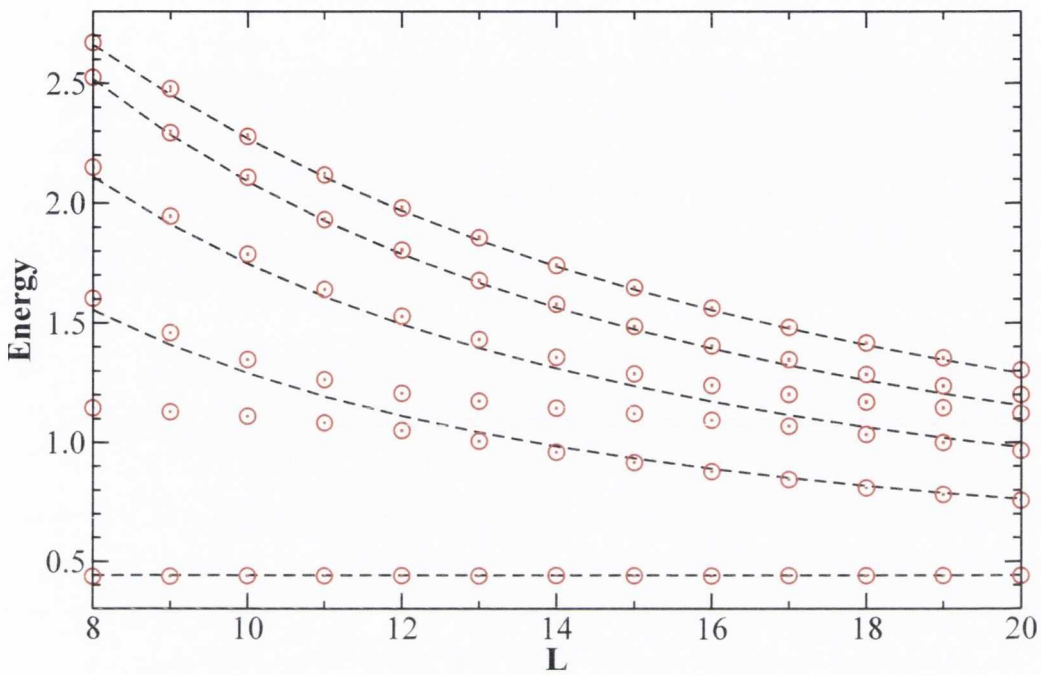

Figure 13: Spectrum of the theory for different values of the volume for the following simulation parameters, describing an inelastic scattering: $\nu = 1.05$, $\lambda = 0.85$, $m_\pi^0 = 0.17$.

$\lambda = 4, m_{\pi,0} = 0.56$ is the next set of parameters giving an intersection between the sigma mass and the $(1,0,0)$ energy level at $L = 8$, corresponding to a relative momentum of $p \approx 0.785$. The volume range is $L \in [6, 20]$ obtained from the stabilisation of the single pion mass. The onset of the effective mass plateau for the two-pion states is $t = 1$. The physical pion mass works out to be $m_\pi = 0.657(3)$. The two pion spectrum is shown in Fig. 11. The relative errors on the energy levels are 0.05% - 0.2%.

The final choice of elastic region parameters are $\lambda = 200, m_{\pi,0} = 0.86$, giving a physical pion mass of $m_\pi = 0.938(3)$. This produces an intersection between the sigma mass and the $(2,0,0)$ energy level at $L = 10$, corresponding

to a relative momentum of $p \approx 1.257$. This is the broad resonance. The volume range is $L \in [6, 15]$ and the effective mass plateau for the two-particle states begins at $t = 1$. The reason for the large value $\lambda = 200$ is that the resonance width depends only weakly on λ, so it must be raised to a high value in order to increase the resonance width. Also λ is a bare parameter and so large values of λ do not necessarily imply large values of its physical counterpart λ^{ph}. The spectrum is depicted in Fig. 12 with relative (statistical) errors 0.15% - 0.4%.

These are the main sets of parameters we focus on. However, as both Lüscher's method and the Histogram method are justified only in the elastic region, we take a set of parameters which produce a resonance in the inelastic region in order to test their limitations. These parameters are $\nu = 1.05$, $\lambda = 0.85$, $m_\pi^0 = 0.17$, the only set of parameters with $\nu \neq 1$. The reason for this can be seen from the original Lagrangian where Eq.(4.15) shows us that the mass of the sigma particle depends on the square of ν, hence altering ν will increase the resonance mass more appreciably. The volume range is $L \in [8, 20]$ and the two particle effective mass plateau begins at $t = 2$.
These parameters give a physical pion mass of $m_\pi = 0.2213(5)$. However the parameters also cause an intersection between the sigma mass and the $(1, 0, 0)$ energy level at $L = 11$. This corresponds to a relative momentum of $p \approx 0.326$. A two pion energy level with such relative momenta has energy $E \approx 1.225 > 4m_\pi$, hence the resonance will be in the inelastic region. The spectrum for this set of inelastic parameters is shown in Fig. 13. Here the relative errors are 0.08% - 0.4%.

4.4 Numerical application of Lüscher's Method

We now have the two-particle spectra. Using these spectra and Lüscher's formula, the scattering phase shift may be constructed. The use of Lüscher's formula consists of five basic steps:

1. Using the Monte Carlo data, obtain the two particle energy spectrum $E_n(L)$ as a function of the volume;
2. Using dispersion relations obtain a momentum, $p_n(L)$, from the energy spectrum;
3. Eq.(2.87) will map the values $p_n(L)$ to values of $\delta(p_n(L))$;
4. If this procedure is repeated for several energy levels and volumes, a profile of $\delta(p)$ is produced;
5. This profile can then be fitted against the Breit-Wigner form for $\delta(p)$ in the vicinity of a resonance as given in Eq.(2.31). This fit should give the resonance mass M_σ and width Γ_σ.

The first step has already been discussed above. To use Lüscher's formula however we need to convert this information on the energy spectrum into information on the momentum spectrum. This is because $\phi(\kappa)$ which appears in Lüscher's formula depends on momentum through:

$$\kappa = \frac{pL}{2\pi}. \tag{4.26}$$

The most obvious way to convert from Energy to momentum is through the use of the dispersion relations. Here we encounter a choice, it is possible to use the continuum dispersion relations:

$$E = 2\sqrt{m_\pi^2 + p^2}, \tag{4.27}$$

or the lattice dispersion relations

$$2\sinh\left(\frac{E}{2}\right) = 2\sqrt{m_\pi^2 + \sum_{i=1}^{3}\left(2\sin\left(\frac{p_i}{2}\right)\right)^2}. \tag{4.28}$$

In the course of our simulations both sets of dispersion relations were used. The most obvious advantage of using the lattice dispersion relations is that they will suppress the effects of lattice artefacts. However they will also have an effect on the phase shift profile constructed through Lüscher's formula. The two dispersion relations will be compared and contrasted below.
Either way, using the dispersion relations gives the momentum spectrum $p_n(L)$ as a function of the volume. These can now be used to construct the scattering phase-shift. Let us quote Lüscher's formula with the momentum dependence made explicit:

$$\delta(p) = -\phi(p) + \pi n, \tag{4.29}$$

$$\tan(\phi(\kappa)) = \frac{\pi^{3/2}\kappa}{Z_{00}(1;\kappa^2)}. \tag{4.30}$$

It can be seen that without a method to evaluate the function $\phi(p)$, Lüscher's formula cannot be applied.
As mentioned in Sec.2.2.2, $Z_{00}(s;\kappa^2)$ is a generalised zeta function as can be seen from its definition:

$$\mathcal{Z}_{00}(s;\kappa^2) = \sum_{\underline{n}\in\mathbb{Z}^3} \frac{1}{(\underline{n}^2 - \kappa^2)^s}. \tag{4.31}$$

However this series expansion only converges for $\Re e(s) \geq \frac{3}{2}$, where as Lüscher's formula requires $s = 1$. Instead of Eq.(4.31) the following integral representation is used:

$$\begin{aligned}\mathcal{Z}_{00}(s;\kappa^2) = &\sum_{|\underline{n}|\leq\lambda} \frac{1}{(\underline{n}^2 - \kappa^2)^s} \\ &+ \frac{(2\pi)^3}{\Gamma(s)} \left\{ \frac{1}{(4\pi)^2(s-\frac{3}{2})} + \int_0^1 dt t^{s-1} \left[e^{t\kappa^2}\mathcal{K}^\lambda(t) - \frac{1}{(4\pi)^2 t^{3/2}} \right] \right. \\ &\left. + \int_1^\infty dt e^{t\kappa^2}\mathcal{K}^\lambda(t) \right\}.\end{aligned} \tag{4.32}$$

Where

$$\mathcal{K}^{\lambda}(t) = \mathcal{K}(t) - \frac{1}{(2\pi)^3} \sum_{|\underline{n}| \leq \lambda} e^{-t\underline{n}^2}. \tag{4.33}$$

$\mathcal{K}(t)$ can be defined in one of two ways:

$$\mathcal{K}(t) = \frac{1}{(2\pi)^3} \sum_{\underline{n}} e^{-t\underline{n}^2}, \tag{4.34}$$

$$\mathcal{K}(t) = \frac{1}{(4\pi t)^{3/2}} \sum_{\underline{n}} e^{-\frac{1}{t}(\pi^2 \underline{n}^2)}. \tag{4.35}$$

The relation between the Zeta-function $\mathcal{Z}_{00}(s;\kappa^2)$ and $\mathcal{K}(t)$ is due the fact that $\mathcal{K}(t)$ is the heat kernel of the Laplacian on a torus, which enters the toroidal Helmholtz equation that produces $\mathcal{Z}_{00}(s;\kappa^2)$.

The expansion Eq.(4.32) converges for $\Re e(s) > \frac{1}{2}$, which includes the point of interest $s = 1$. The first integral in Eq.(4.32) can be evaluated more easily using the following $t \to 0$ asymptotic behaviour of the kernel $\mathcal{K}^{\lambda}(t)$:

$$e^{tq^2}\mathcal{K}^{\lambda}(t) = \frac{1}{(4\pi)^2 t^{3/2}} + O(t^{-1/2}). \tag{4.36}$$

The constant λ is chosen to make the sum in the expansion of $\mathcal{K}^{\lambda}(t)$ converge faster, ideally $\lambda > \Re e(\kappa^2)$. The choice between the different expansions Eq.(4.34) and Eq.(4.35) for $\mathcal{K}(t)$ depend on the value of t. Eq.(4.34) is used when $t \geq 1$ and Eq.(4.35) otherwise. The integral expression Eq.(4.32) can then be computed numerically to evaluate the function $\phi(p)$
Some properties of $\phi(\kappa)$ should be noted. First of all it's Taylor expansion consists solely of even terms:

$$\phi(p) = \sum_{n=1}^{\infty} a_n p^{2n}. \tag{4.37}$$

Secondly, due to the fact that $\mathcal{Z}_{00}(1;\kappa^2)$ has poles at integer values of p, the relation Eq.(4.30) implies that $\phi(\underline{n})$, $\underline{n} \in \mathbb{Z}$, is some integer multiple of π.

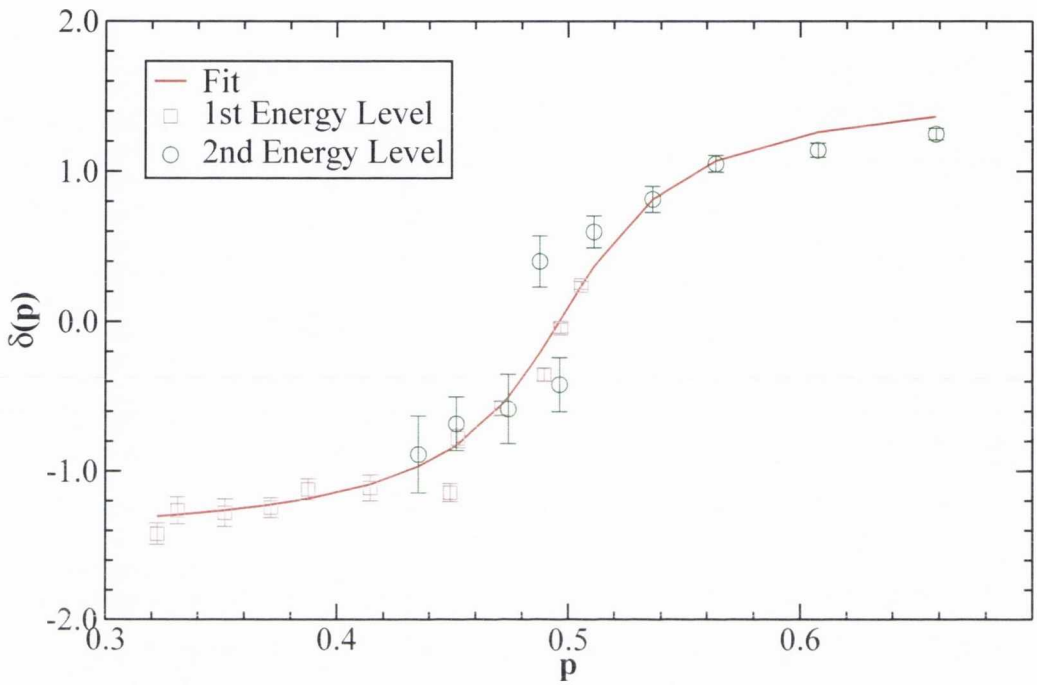

Figure 14: $\delta(p)$ using Lattice dispersion relations for: $\nu = 1.0$, $\lambda = 1.4$, $m_\pi^0 = 0.36$.

This combined with the fact that it has an even Taylor expansion leads to the standard approximation of $\phi(\underline{n})$ as $\phi(\underline{n}) \approx \pi n^2$, which is then extended to all real numbers as $\phi(\kappa) \approx \pi\kappa^2$. Evaluating $\phi(\kappa)$ numerically shows that this is indeed an accurate approximation for integer values of κ. However for other real numbers in the range $0.1 < \kappa \leq 8.0$, the evaluation reveals that

$$0.8704 \leq \frac{\phi(\kappa)}{\pi\kappa^2} \leq 1.1353. \tag{4.38}$$

For this reason we fitted $\phi(\kappa)$ to the numerical values obtained from Eq.(4.32) in the range $\kappa \in [0.1, 1.5]$ using a non-linear Levenberg-Marquardt fit [46].

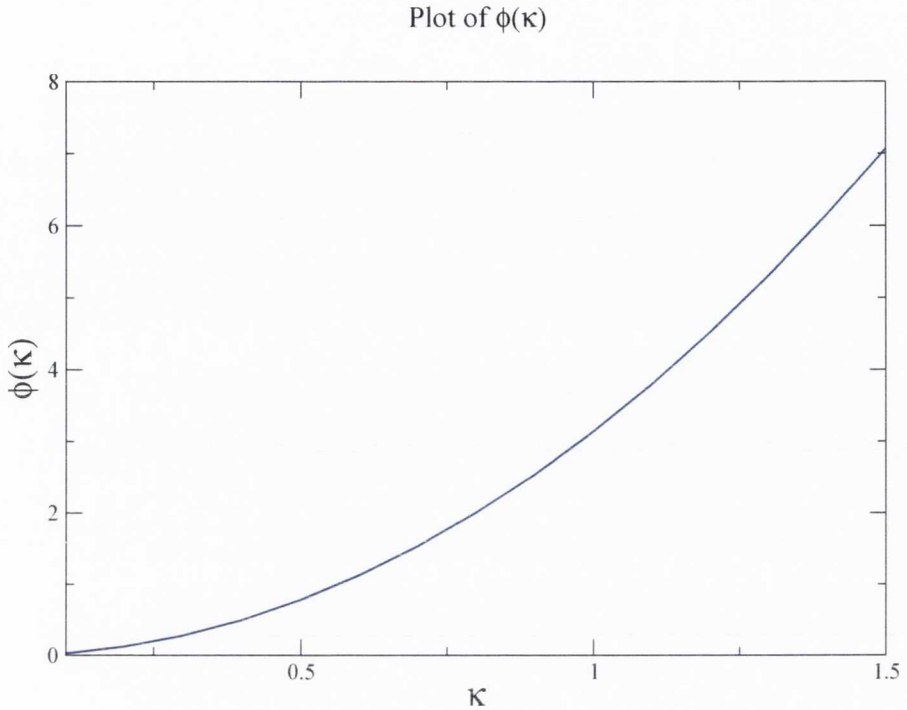

Figure 15: Plot of function $\phi(\kappa)$

This gives the approximation of $\phi(\kappa)$ as

$$\begin{aligned}\phi(\kappa) \approx (-0.09937)\kappa^8 + (0.47809)\kappa^6 + \\ (-0.62064)\kappa^4 + (3.38974)\kappa^2 \ .\end{aligned} \tag{4.39}$$

The error between this approximation and the true value of $\phi(\kappa)$ is quite small, the deviation being

$$|\phi(\kappa) - \phi_{approx}(\kappa)| \leq 0.00002, \qquad \kappa \in [0.1, 1.5] \tag{4.40}$$

In this formula $\phi_{approx}(\kappa)$ is the approximation of Eq.(4.39). We will use $\phi(\kappa)$ to refer to both in the rest of the text, where the meaning can be inferred

from context.
Both approximations of $\phi(\kappa)$ were used in applying Lüscher's formula, they will be compared and contrasted below. It should also be noted that both approximations are inaccurate when considering $\kappa < 0.1$, however such small values of κ do not occur in the three cases considered here. It should also be noted that Eq.(4.39) does not have the same coefficients as the Taylor expansion of $\phi(\kappa)$ and indeed at very small values of κ one uses an expression involving inverse powers of κ coming from the summation of the Taylor series. Additionally our approximation is for the region $\kappa \in [0.1, 1.5]$ only and is worse than the traditional $\pi\kappa^2$ approximation outside this interval. $\phi(\kappa)$ is plotted in Fig. 15.
Applying the approximation Eq.(4.39) of $\phi(\kappa)$ to Lüscher's formula we obtain the value of the scattering phase shift at $p_n(L)$ as:

$$\delta(p_n(L)) = (0.09937)\left(\frac{pL}{2\pi}\right)^8 + (-0.47809)\left(\frac{pL}{2\pi}\right)^6 + (0.62064)\left(\frac{pL}{2\pi}\right)^4 + (-3.38974)\left(\frac{pL}{2\pi}\right)^2 + \pi n. \tag{4.41}$$

where n is the energy level from which $p_n(L)$ was obtained. One simply applies this formula for all volumes and energy levels included in the simulation and a profile of $\delta(p)$ is slowly built up.

An example of such a phase shift profile for the parameters $\lambda = 1.4, m_{\pi,0} = 0.36, m_\pi = 0.460(2)$ is displayed in Fig. 14.
It can be seen from Fig. 14 that the scattering phase shift displays the arctangent profile that is typical in the vicinity of a resonance. With the scattering phase shift obtained one then simply fits the scattering phase shift to the Breit-Wigner formula:

$$\delta(p) - \frac{\pi}{2} \approx \arctan\left(\frac{4p^2 + 4M_\pi^2 - M_\sigma^2}{M_\sigma \Gamma_\sigma}\right) . \tag{4.42}$$

Of course the scattering phase shift is given by $\delta(p) = \delta_{bg}(p) + \delta_{res}(p)$, where $\delta_{bg}(p)$ is the scattering phase shift due to non-resonant scattering, the back-

ground phase shift. $\delta_{res}(p)$ has the form Eq.(4.42) and is the resonance part of the scattering phase-shift, so in applying Eq.(4.42) it is assumed that $\delta_{bg}(p) \approx 0$. The split between $\delta_{bg}(p)$ and $\delta_{res}(p)$ is somewhat naive, we simply define $\delta_{res}(p)$ to be the component of the phase shift coming purely from an isolated resonance. This is valid in our model as the resonance dominates the scattering as inspection of the numerical results displayed in Fig. 14 show a rapid increase in the phase shift by a factor of π, typical of an isolated resonance as explained in Sec.2.1.

After performing a nonlinear fit of the data to Eq. 4.42 the results for the continuum and lattice dispersion relations are obtained using both approximations for $\phi(p)$. The lattice and continuum dispersion results are given in table 1 and 2 respectively for each of the three simulation parameters.

Results: Lattice Dispersion Relations		
Parameters	$\phi(\kappa)$	$\pi\kappa^2$
$\nu = 1.0,\ \lambda = 1.4$	$M_\sigma = 1.35(2)$ $\Gamma_\sigma = 0.115(8)$	$M_\sigma = 1.36(4)$ $\Gamma_\sigma = 0.17(2)$
$\nu = 1.0,\ \lambda = 4$	$M_\sigma = 2.03(2)$ $\Gamma_\sigma = 0.35(2)$	$M_\sigma = 2.2(2)$ $\Gamma_\sigma = 0.42(5)$
$\nu = 1.0,\ \lambda = 200$	$M_\sigma = 3.1(7)$ $\Gamma_\sigma = 1.2(5)$	$M_\sigma = 3(1)$ $\Gamma_\sigma = 2(1)$

Table 1: Resonance mass and decay width using two different approximations for $\phi(\kappa)$, with lattice dispersion relations.

There are two major sources of error in these results. First the propagation of error coming from the determination of the energy levels. Although the energy levels are determined quite precisely, the error is noticeably large when propagated to the phase shift. The second source of error comes from fitting the data to the functional form given in Eq.(4.42). The fit was a Levenberg-Marquardt fit, [46].
One thing to be noted is that the continuum dispersion relations give greater errors on both the mass and the width of the resonance, although the effect

Results: Continuum Dispersion Relations		
Parameters	$\phi(\kappa)$	$\pi\kappa^2$
$\nu = 1.0,\ \lambda = 1.4$	$M_\sigma = 1.32(8)$ $\Gamma_\sigma = 0.117(9)$	$M_\sigma = 1.4(1)$ $\Gamma_\sigma = 0.16(5)$
$\nu = 1.0,\ \lambda = 4$	$M_\sigma = 2.1(4)$ $\Gamma_\sigma = 0.39(4)$	$M_\sigma = 2.2(4)$ $\Gamma_\sigma = 0.42(5)$
$\nu = 1.0,\ \lambda = 200$	$M_\sigma = 3(1)$ $\Gamma_\sigma = 1.2(7)$	$M_\sigma = 3(1)$ $\Gamma_\sigma = 2(2)$

Table 2: Resonance mass and decay width using two different approximations for $\phi(\kappa)$, with continuum dispersion relations.

is stronger for the mass. The reason for this can be seen from Fig. 16. When the lattice dispersion relations are used the third energy level is mapped to the inelastic region and hence can not be used with Lüscher's formula. Using the continuum dispersion relations the third energy is included causing a slight distortion in the arctangent profile, as well as being completely spurious. This suggests the lattice dispersion are useful beyond the obvious effect of suppressing discretisation errors.

The use of the two different approximations of $\phi(\kappa)$ can be seen to affect the resonance width most strongly. This is because an inaccurate approximation of $\phi(\kappa)$ will distort the mapping from p to $\delta(p)$, in particular it will affect the arc-tangent profile associated with a resonance. A variation in Γ will not produce much of a variation in the slope of the arc-tangent profile of $\delta(p)$, hence unless the slope is resolved to high precision there will be a large error in Γ. This is the major advantage of using a good approximation of $\phi(p)$.

It can also be noticed that in all three cases larger errors are obtained the broader the resonance is. This is also caused by a lack of resolution in the slope of the phase-shift. In Fig. 17 it can be seen that for a broad resonance the slope is quite flat, hence a large variation in Γ again produces very little change in the profile of $\delta(p)$. In order to accurately measure the parameters of a broad resonance the slope of $\delta(p)$ would have to be determined quite ac-

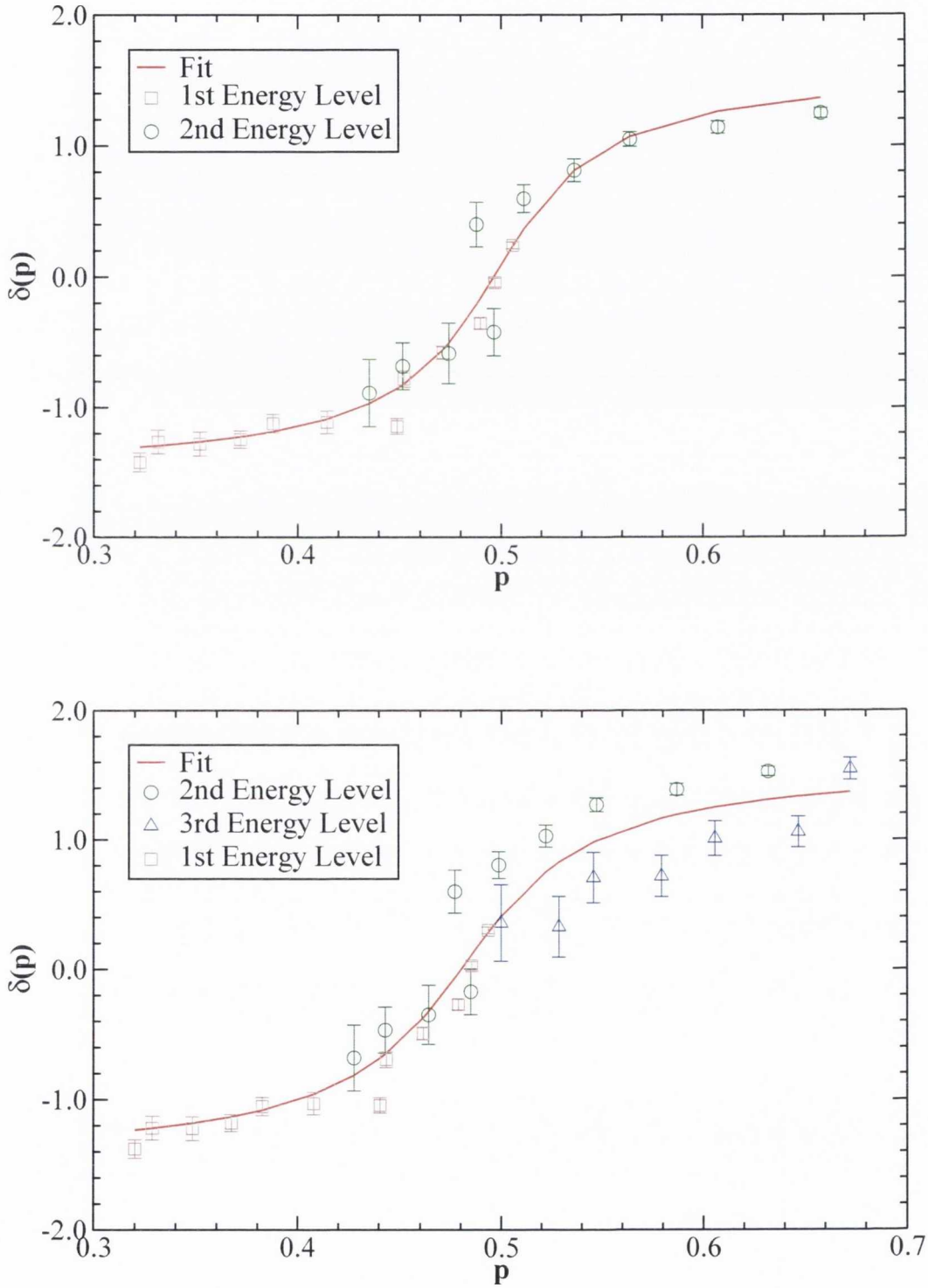

Figure 16: (Top) $\delta(p)$ using Lattice dispersion relations at: $\nu = 1.0$, $\lambda = 1.4$, $m_\pi^0 = 0.36$. (Bottom) Same parameters, but with continuum dispersion relations. Both done with accurate approximation to $\phi(p)$. In the continuum case $\frac{\chi^2}{\nu} = 0.8124$ and in the lattice case $\frac{\chi^2}{\nu} = 0.9768$

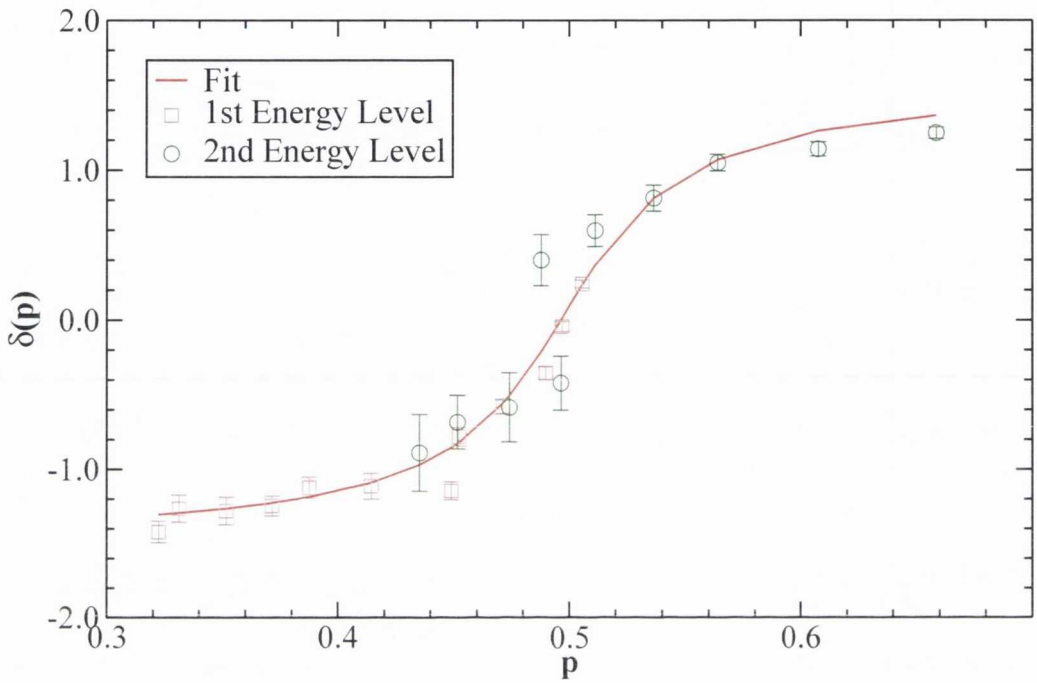

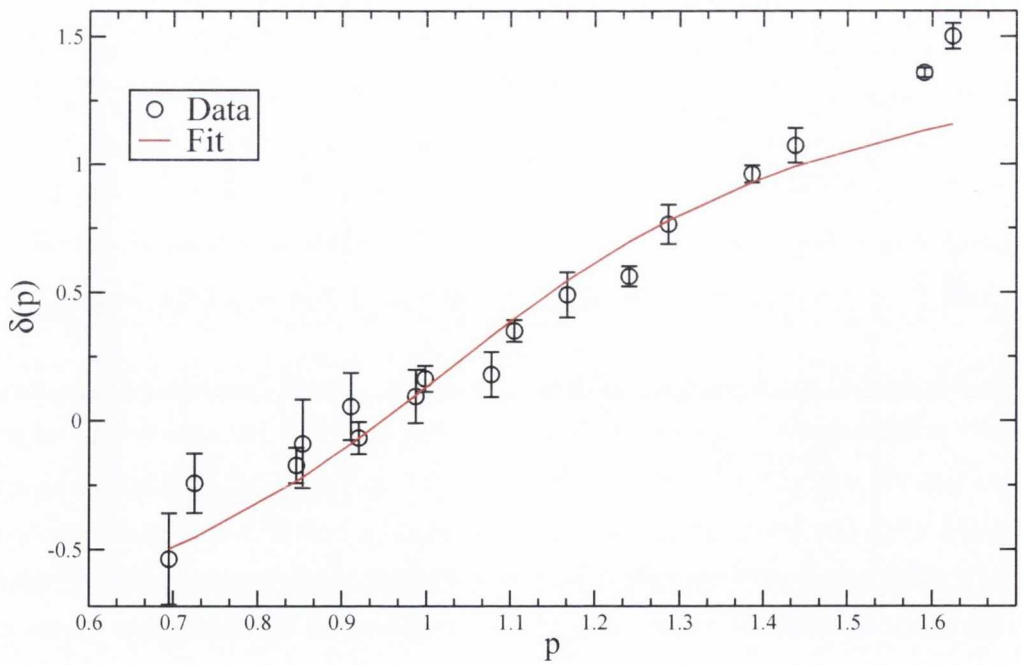

Figure 17: Phase shift for narrow and broad resonances.

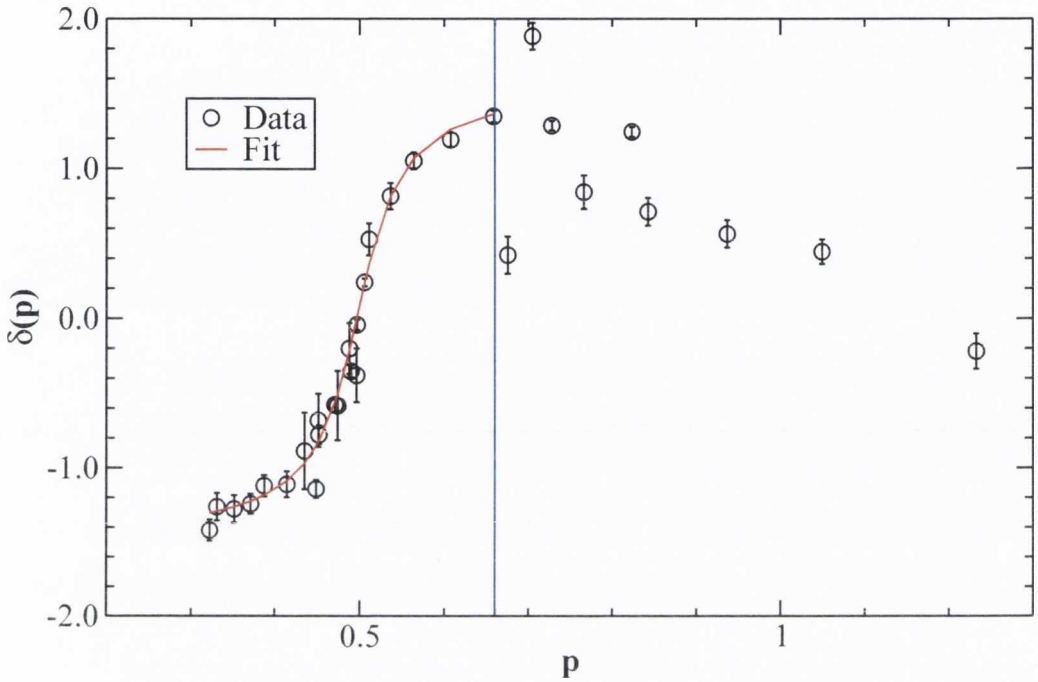

Figure 18: Inelastic data with Lüscher's formula. For the case of $\nu = 1.0$, $\lambda = 1.4$, $m_{\pi,0} = 0.36$. (Onset of inelastic region marked).

curately. This would require a very good approximation of $\phi(\kappa)$, but also a very accurate measurement of the energy levels, since the error on the phase shift data must be small enough to tightly constrain the slope.

We will take the results using the lattice dispersion relations and the approximation Eq.(4.39) of $\phi(\kappa)$ as the outcome of Lüscher's method when making a comparison with the Histogram method.

Finally we discuss the major limitation of Lüscher's method, the inelastic region. First of all we consider the the case of the narrowest resonance when the parameters are $\nu = 1.0$, $\lambda = 1.4$, $m_{\pi,0} = 0.36$, which is displayed in the

Fig. 18. In the elastic region (to the left of the line), the results already discussed are obtained. However to right of the line is data obtain by using Lüscher's formula on momenta in the inelastic region. The breakdown of the formula is indicated by the existence of a point which, by exceeding π, breaks unitarity. In general applying Lüscher's formula in the inelastic region produces these scatter plot type profiles for $\delta(p)$. Fortunately for the three sets of parameters considered above the resonance exists in the elastic region, so this breakdown of the formula is not a concern.

However for the final set of parameters $\nu = 1.05$, $\lambda = 0.85$, $m_\pi = 0.17, m_\pi = 0.2213(5)$, where the intersection between the sigma particles mass and the two pion energy level $(1, 0, 0)$ occurs in the inelastic region, the breakdown of the formula means that no meaningful data about the resonance can be obtained as the results are uninterpretable.

This is a major restriction of Lüscher's method because, as mentioned in Sec.2.2.4, the resonances in QCD mostly occur in the inelastic region. With such a barrier in place and the lack of an inelastic generalisation of the formula (which may be difficult to obtain, for the reasons mentioned in Sec.2.2.4), the applicability of the method to the realistic case of QCD is limited.

4.5 Numerical application of the Histogram Method

As mentioned in Sec.2.3, the Histogram method constructs a distribution containing information on the relative density of the energy levels between the free theory, where the sigma and the pions do not interact, and the interacting case. The formula once again is:

$$\frac{1}{C}W(p) - \frac{1}{C_0}W_0(p) \approx \frac{1}{p}\left(\frac{\delta(p)}{p} - \delta'(p)\right) . \tag{4.43}$$

where C and C_0 are the normalisation constants for the interacting and free distributions respectively. The formula becomes more accurate as the number of energy levels considered increases, with exact equality holding in the $N \to \infty$ limit, where N is the number of energy levels. However, the convergence is quite rapid so in fact in the case of $N = 6$, considered below, N is large enough to justify use of the formula.

If we assume that the scattering phase shift obeys $\delta(p) \approx \delta_{res}(p)$, just as is assumed with Lüscher's method above, then this formula can be recast in the much more useful form of:

$$\frac{1}{C}W(p) - \frac{1}{C_0}W_0(p) \approx \frac{1}{[E(p)^2 - M_\sigma^2]^2 + M_\sigma^2\,\Gamma^2} . \tag{4.44}$$

Hence if we build this Histogram we should be able to recover information on the resonance. As mentioned, in [12] the method was only tested on synthetic data. Here instead the method is tested on genuine Monte-Carlo data, the same data used with Lüscher's formula.

First of all, it should be said that the distribution as a function of energy $W(E)$ is used, instead of the suggested $W(p)$. The reason for this is so that the distribution can be constructed directly from the energy levels. The relation between the two distributions is:

$$W(p) = W(E)\left(\frac{\partial E}{\partial p}\right) , \tag{4.45}$$

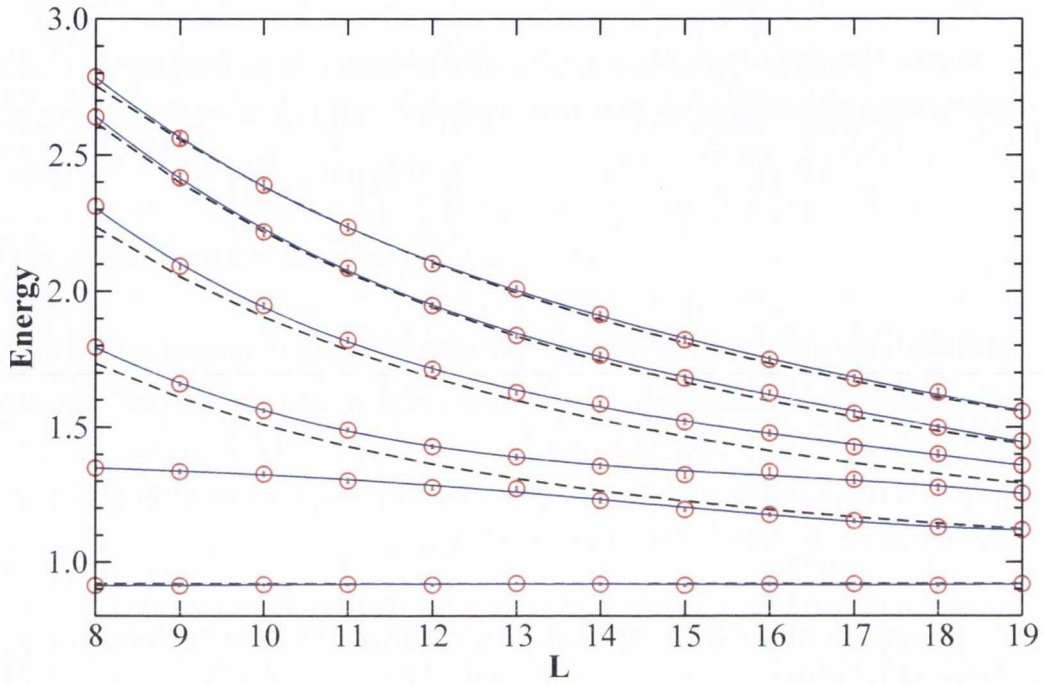

Figure 19: Spectrum for $\nu = 1.0$, $\lambda = 1.4$, $m_\pi = 0.36$. The fit to Eq.(4.46) is indicated in blue.

The multiplicative term $\frac{\partial E}{\partial p}$ does not modify the Breit-Wigner shape near the resonance, so this does not affect the results.

Let us consider the parameters $\nu = 1.0$, $\lambda = 1.4$, $m_{\pi,0} = 0.36$ as the model case and discuss the others only in terms of their major differences from this case. The method requires us to partition some chosen interval of the E, L-plane into boxes of some chosen width ΔL and height ΔE. An energy level is considered to be in one of these intervals $[E_i, E_j]$, if at some volume L_k we have $E_n(L_k) \in [E_i, E_j]$. The value of $W(E_i)$ is then the number of energy levels in the range $[E_i, E_j]$ across all volumes. An energy level located in one energy range at n different volumes is counted n times.

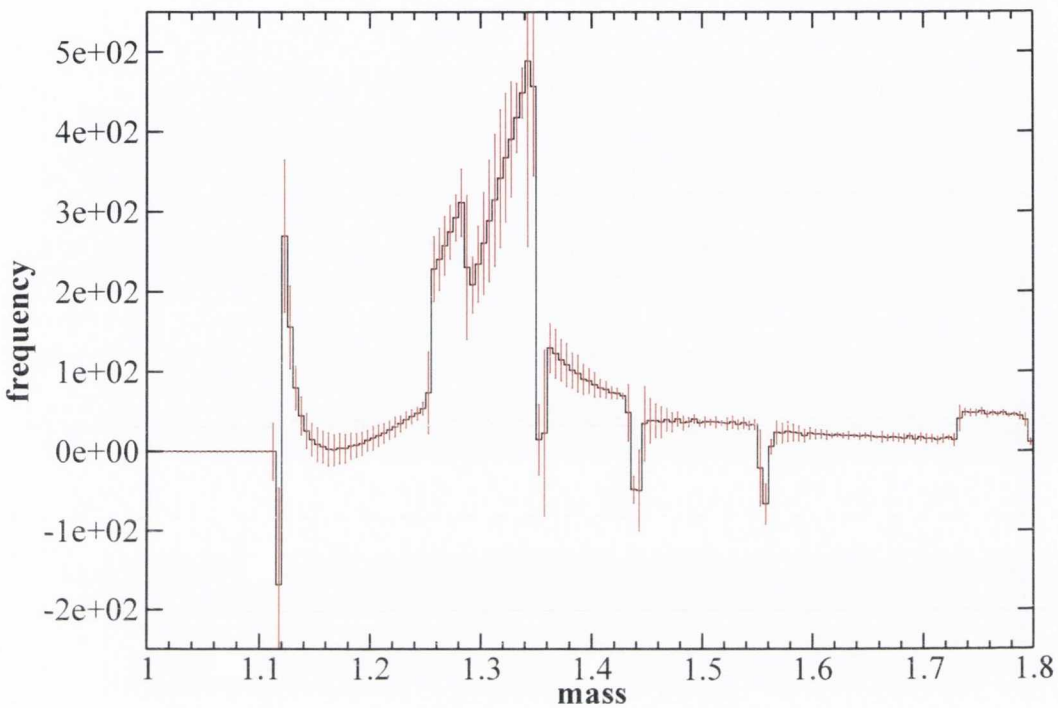

Figure 20: The histogram $\tilde{W} = W - W_0$ obtained from the spectrum in Fig.19.

Since the Monte-Carlo simulations only obtain the energy levels at specific integer values of L it is almost always the case that the value of $E_n(L_i)$ is not known. To get around this problem the function E_L is extrapolated to all values of L by using the asymptotic form of the scattering state energies obtained [24]. Specifically the Energy levels have the form:

$$E = \sum_{i=1}^{5} \frac{C_i}{mL^i} + \mathcal{O}(L^{-6}). \tag{4.46}$$

As already given in Eq.(2.92). The fit on the spectrum, for the $\nu = 1.0$, $\lambda = 1.4$, $m_{\pi,0} = 0.36$ parameters, can be seen in Fig. 19. Fig. 19 also shows the free-particle spectrum which will be used to construct $W_0(p)$. This is

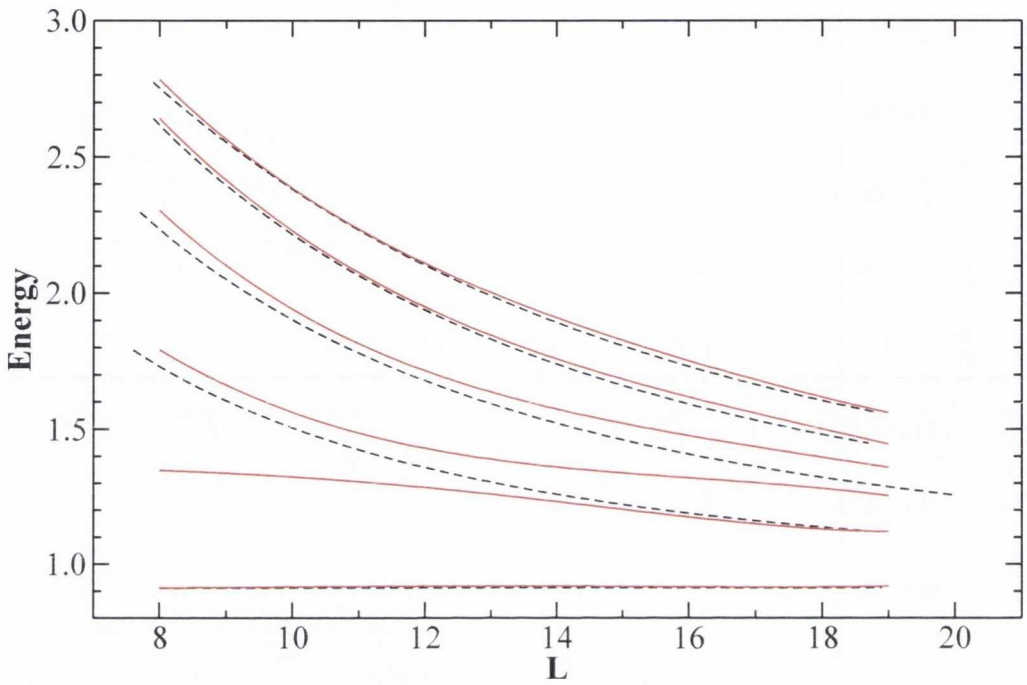

Figure 21: Energy levels of Fig.19 with the free spectrum continued.

obtained from the standard free lattice two particle spectrum:

$$E = 4 \sinh^{-1} \left[\frac{1}{2} \sqrt{(m_\pi^2 + \tilde{p}^2} \right] \ , \tag{4.47}$$

In order to produce results as accurate as possible we choose $\Delta L = 0.001$ in lattice units and the range of L to be from the smallest volume considered to the largest, i.e. $L \in [8, 19]$. The energy bin width is taken to be $\Delta E = 0.005$, again so as to have an accurate determination of the distribution.

The histogram obtained for these set of parameters is shown in Fig. 20 The main errors in the histogram are as follows:

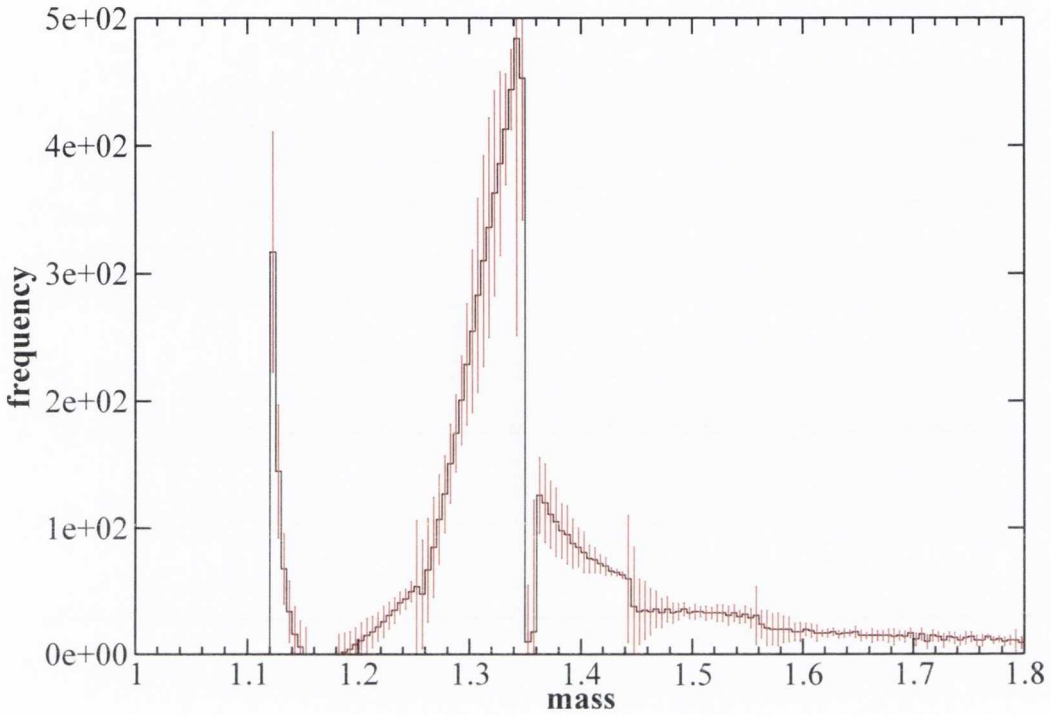

Figure 22: Histogram $\tilde{W}$ obtained from the continued free spectrum in Fig.21

1. Statistical Errors in $W(p)$ coming from the Monte Carlo determination of the energy levels

2. Errors in $W(p)$ due to the fit to Eq.(2.66).

3. Statistical Errors in $W_0(p)$ coming from the Monte-Carlo determination of the single pion mass.

As it appears in Fig. 20, the histogram can not be said to have an obvious Breit-Wigner form. This is due to the sharp "spikes" in the histogram, to whose origin we now turn.
An investigation of the location of the spikes shows that they occur at any value of energy where the six energy levels $E_n(L)$ intersect the the extremities of the volume at $L = 8$ and $L = 19$. This is because near the extremities of

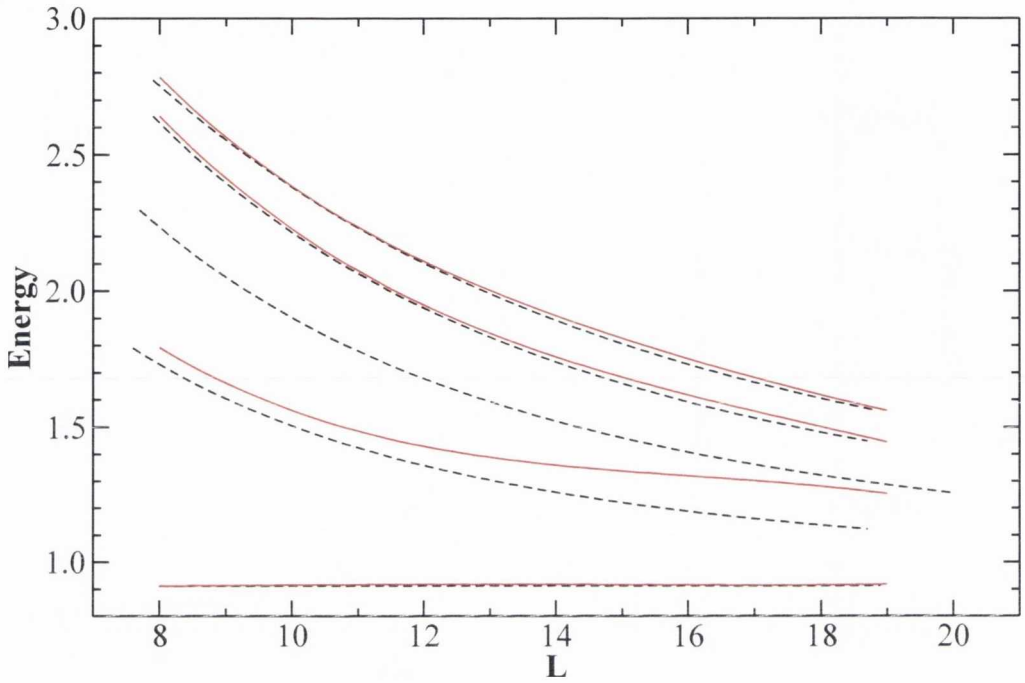

Figure 23: Energy levels of Fig. 21 where we have deleted the two levels that do not possess the appropriate free background.

the volume the interacting energy levels terminate with no free energy levels in the corresponding energy range. In Fig. 19 the second lowest energy level shows the effect. The free energy level needs to be continued beyond the volume range in order to line up with the interacting energy level. In other words, at the volume extremities the interacting energy levels are missing the free background that needs to be subtracted. Due to this, we continue the free energy levels as far as required. This is an easy task as they are given by Eq.(4.47) and so we easily obtain the modified spectrum Fig. 21. We then perform the subtraction again and obtain the histogram shown in Fig. 22 However it can be seen from Fig. 22 that there are still discontinuities in the histogram, particularly one still persists at $E \approx 1.35$. This is due

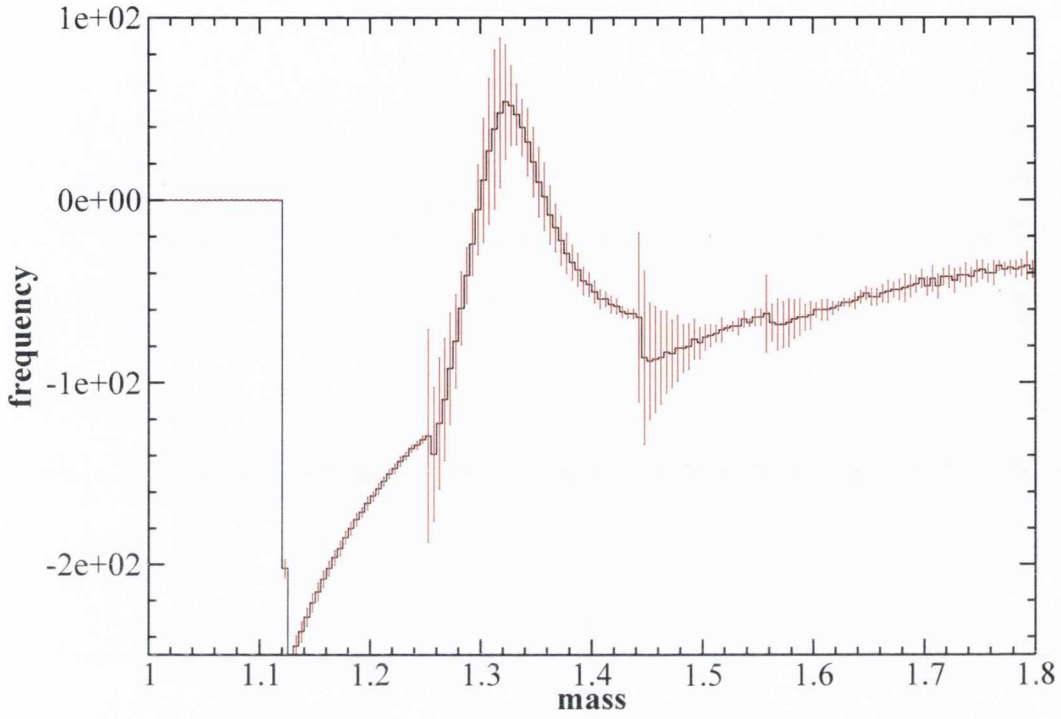

Figure 24: The correct histogram $\tilde{W}$ obtained from the altered spectrum in Fig.23.

the another intersection of the energy levels with the boundaries, specifically $E_2(8)$ and $E_4(19)$. For these energy levels, particularly $E_2(8)$ the free energy levels would have to be extrapolated particularly far in order to remove the discontinuities. In fact in order to obtain the necessary free background it would probably be necessary to increase the number of energy levels. In order to avoid this we simply remove these two energy levels from the analysis and concentrate on building the histogram only from spectrum depicted in Fig. 23. Here we have extrapolated the free energy levels as necessary and excluded the energy levels which would require a cumbersome amount of extrapolation. This will be the general procedure for all three sets of parameters. The histogram obtain from these energy levels is shown in Fig. 24. It can be seen that the histogram now displays the characteristic Breit-Wigner profile. We fit the histogram with the formula Eq.(4.44), using a sliding win-

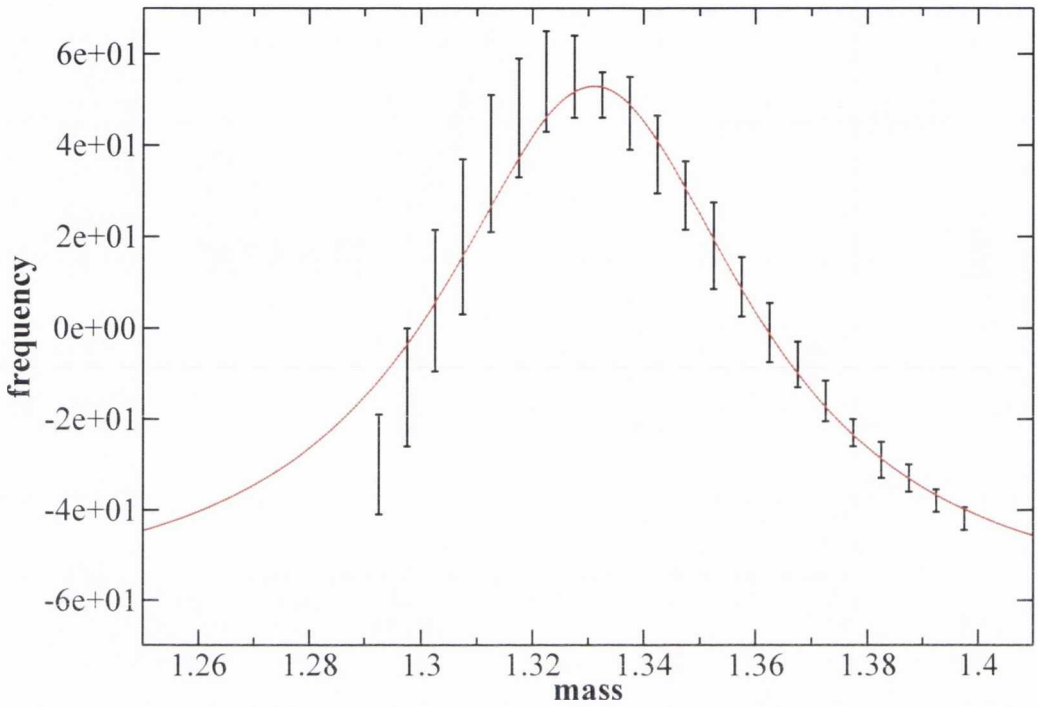

Figure 25: Data from Fig.24 that we fitted to determine the resonance parameters with the final curve fitting.

dow procedure around the peak as depicted in Fig. 25. The results for the resonance parameters are $M_\sigma = 1.330(5)$ and $\Gamma_\sigma = 0.10(5)$, in good agreement with the results of Lüscher's method.

For the second set of parameters $\lambda = 4.0$, $m_\pi^0 = 0.56$ the procedure is much the same. The histogram obtained from extending the free energy levels can be seen in Fig. 26. It should be noted that here the volume runs from $L = 6$ to $L = 20$.

Again there are noticeable discontinuities at the energies $E \approx 1.95$ which corresponds to an intersection with the boundary $L = 6$ and at $E \approx 2.00$ related to an intersection with $L = 20$. Again we simply exclude the two

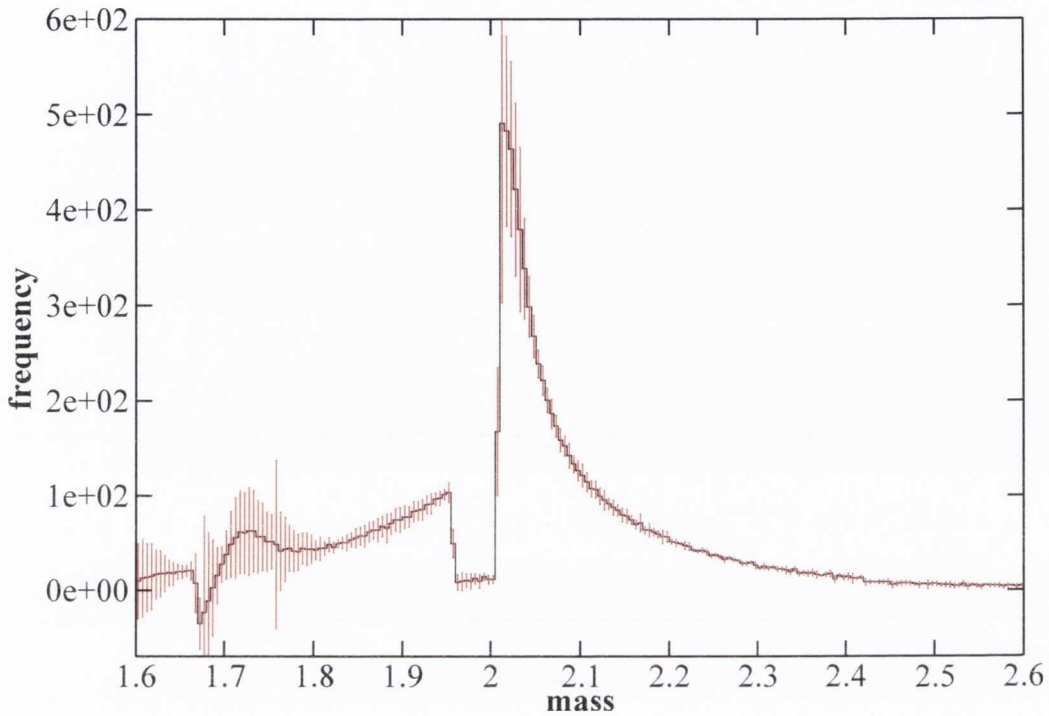

Figure 26: The histogram after continuing the free energy levels for the simulation parameters: $\lambda = 4.0$, $m_\pi^0 = 0.56$.

energy levels ($n = 2, 4$ as before) that are missing their free backgrounds, to obtain the histogram shown in the left of Fig. 27. Once more the fit is performed on the data around the peak (bottom of Fig. 27). The resonance parameters obtained are as follows: $M_\sigma = 2.01(2)$, $\Gamma_\sigma = 0.35(10)$.

For the final set of parameters $\lambda = 200, m_{\pi,0} = 0.86$, those corresponding to a broad resonance, it was necessary to increase the number of energy levels to $N = 13$. This is because the resonance intersects with higher energy two pion states and so to resolve it we must include these extra energy levels. Also the resonance occurs at high enough energies that free energy levels beyond $n = 6$ form part of the necessary background for the $n \leq 6$ interacting

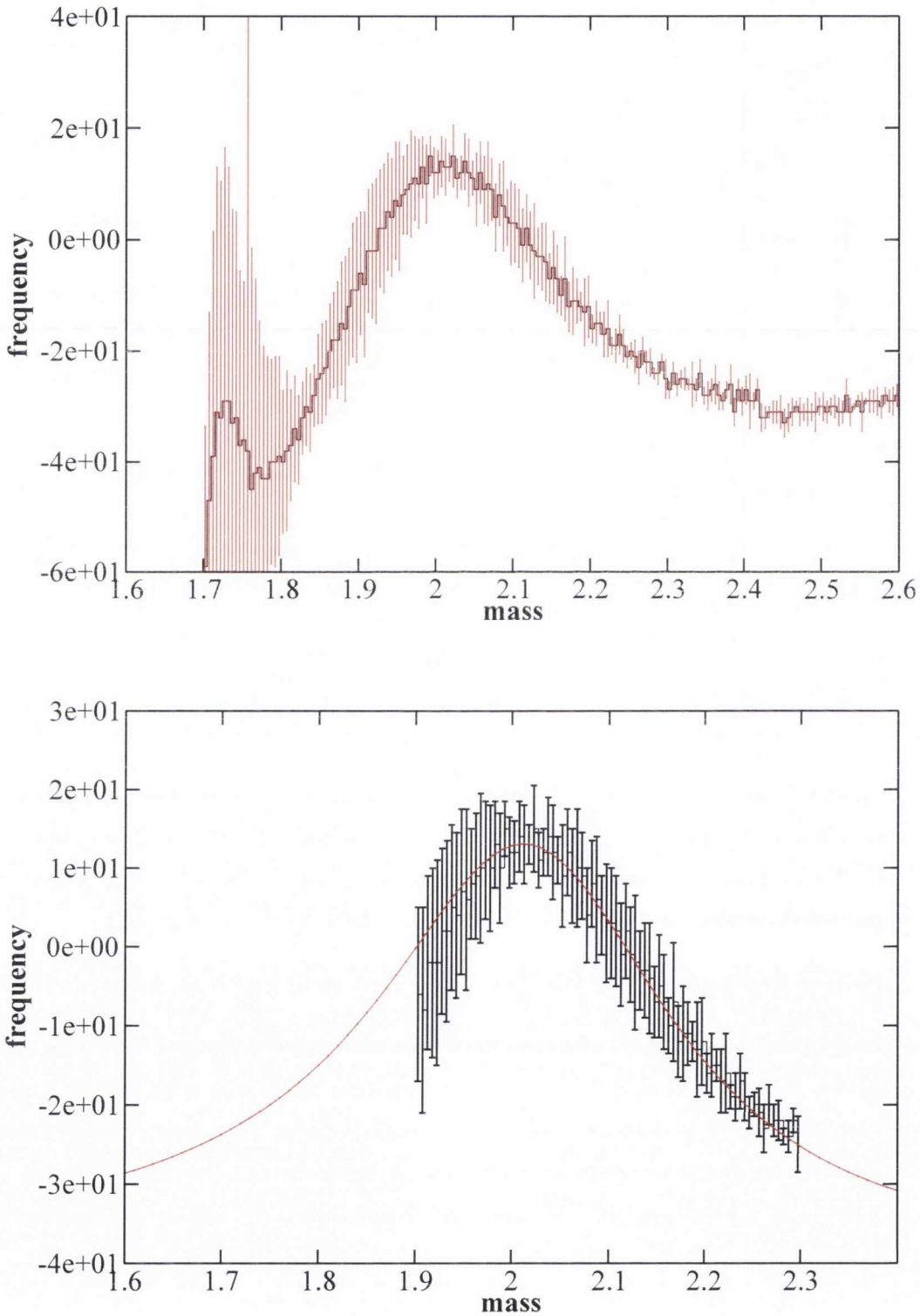

Figure 27: (Top) The histogram $\tilde{W}$ after using the correct background and excluding the two levels that are without a corresponding background. (Bottom) Data we fitted to determine the resonance parameters with the final curve fitting.

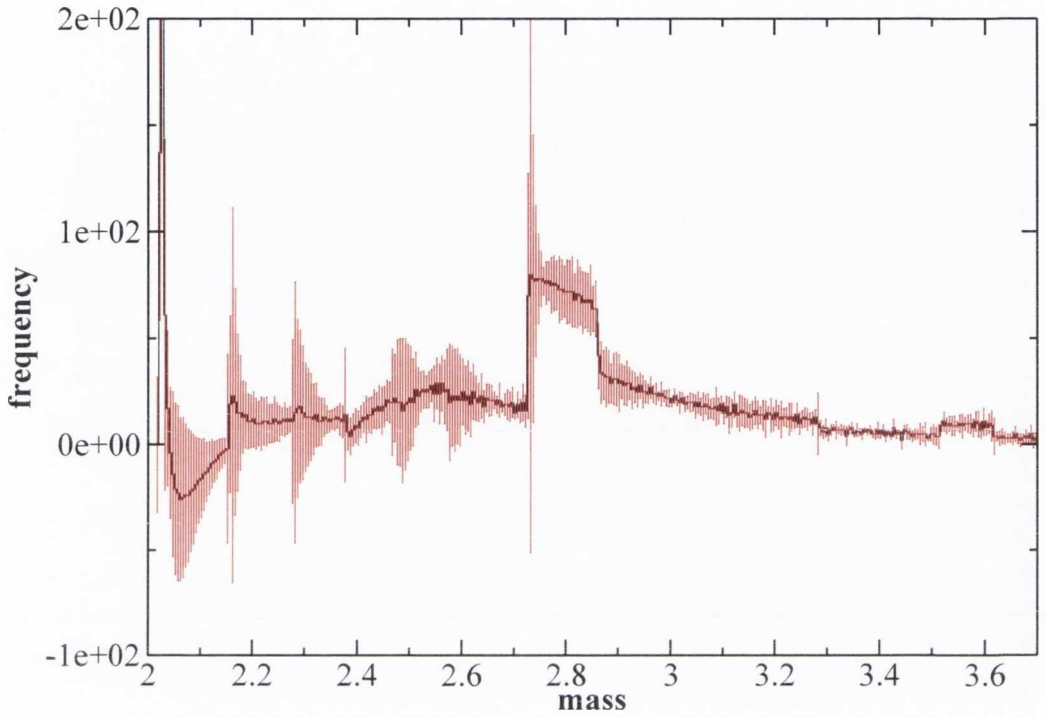

Figure 28: The broad resonance histogram obtained by continuing the free spectrum

energy levels. For these parameters the volume L takes values from $L = 6$ to $L = 15$

Applying the same procedure as before the histogram shown in Fig. 28. We see that the histogram has a peak at $E \approx 2.8$, which is close to the values given by Lüscher's formula. However there are discontinuities which must be removed in order to construct the correct Breit-Wigner shape. This is achieved by excluding the interacting energy levels without a free background, as before. The resulting histogram is depicted in Fig. 29.

Unfortunately the histogram of Fig. 29 is flat, within errors. A Breit-Wigner profile cannot be resolved and so meaningful values of the resonance parame-

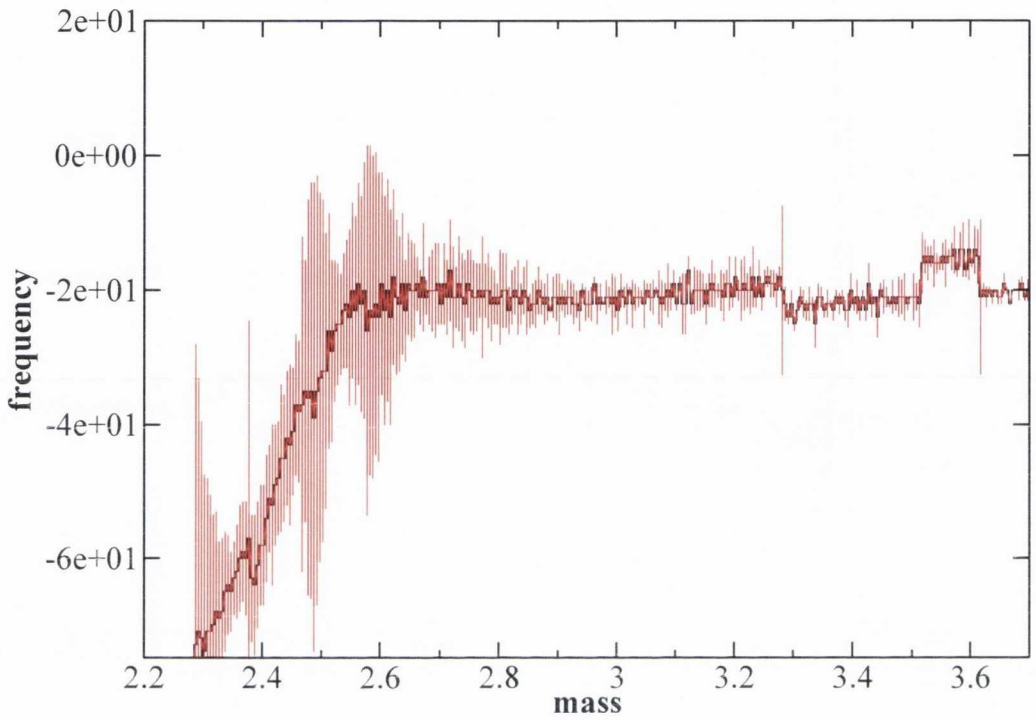

Figure 29: The broad resonance histogram after the removal of the levels without a background.

ters cannot be extracted. However the fact that the histogram shows a peak near $E \approx 2.8$ indicates that perhaps the histogram does capture some aspects of the resonance, even if they do not survive our modifications. The most obvious method of improving the histogram would involve either or both of the following steps.

1. Decrease the errors on the determination of the spectrum. As mentioned above the histogram is flat *within the errors*. A more accurate determination of the spectrum would lead to a more finely resolved histogram, one in which the Breit-Wigner might possibly emerge.

2. Increase the number of energy levels. Since information on the resonance is contained within the energy levels including more may lead to

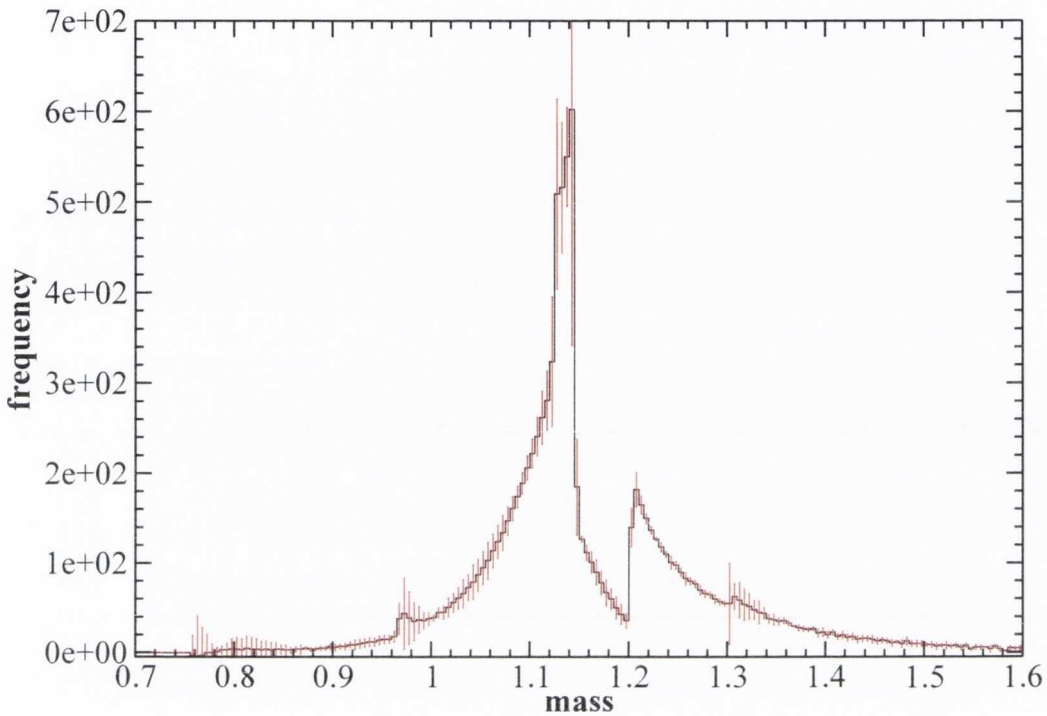

Figure 30: The inelastic region histogram with the initial range of volumes

a histogram with a more obvious Breit-Wigner profile. However it was found that no improvement occurred in the Histogram when $N = 16$ was taken.

Finally, with a view to the comparison of the two methods in the next section, a histogram is constructed in the inelastic region, with parameters $\nu = 1.05$, $\lambda = 0.85$, $m_\pi^0 = 0.17$. The range of volumes is $L \in [8, 20]$ and the number of energy levels is $N = 6$ This case will be useful to study, not only because the resonance occurs in the inelastic region, but it also shows up further difficulties with constructing the histograms that have not shown up in the previous cases, but which could occur even in the elastic case.

The basic histogram constructed using an extension of the free energy levels

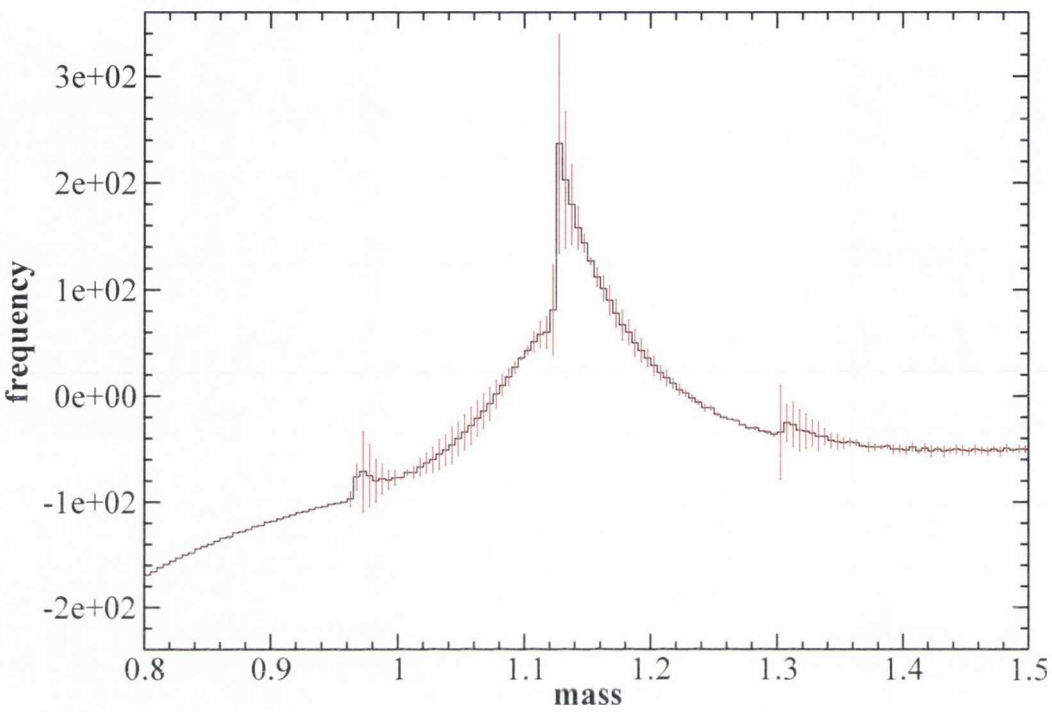

Figure 31: The inelastic region histogram with the altered range of volumes.

and removing the energy levels without a background is shown in Fig. 30. However a jump at $E \approx 1.13$ is still visible, which has a different origin to the discontinuities mentioned before. Looking at the inelastic spectrum in Fig. 13, it can be seen that the fourth energy level, corresponding to relative momenta $(1, 1, 1)$ between the pions, is highly displaced from any free energy level. This is particularly noticeable in the range of volumes $L \in [18, 20]$. This is due to the strong effect of the interactions on the volume dependence of this energy level. To solve this we change our range of volumes to $L \in [8, 18]$ in order to remove the regions were the $(1, 1, 1)$-energy level deviates too strongly from the free energy levels. The problem may also have been solved by increasing the number of energy levels so that free energy levels in the same energy range as the $(1, 1, 1)$-level are included. However it

is difficult to know how high N must be raised in order for this to be a valid solution. Raising the number of energy levels to $N = 10$ did not solve the problem.

With this new range of volumes we repeat the procedure and obtain the histogram in Fig. 31. This histogram has a clear Breit-Wigner profile and so we preform the same fitting procedure as in the elastic case, giving us the resonance parameters $M_\sigma = 1.11(3)$ and $\Gamma_\sigma = 0.11(3)$. Of course the fitting formula, Eq.(4.43), can only be justified in the elastic region. We will comment on this and the comparison of this method with Lüscher's in the Sec.(4.6).

4.6 Discussion and comparison of methods

With the resonance examined with both Lüscher's Method and the Histogram method, we turn now to a comparison of the two methods. First of all, we summarise the results obtained so far in table 3. The results for Lüscher's method are those taken using the approximation Eq.(4.39) for $\phi(\kappa)$ and with the lattice dispersion relations. On the most basic level the data reveals

Results		
Parameters	Lüscher's Method	Histogram Method
$\nu = 1.0,\ \lambda = 1.4$	$M_\sigma = 1.35(2)$ $\Gamma_\sigma = 0.115(8)$	$M_\sigma = 1.33(5)$ $\Gamma_\sigma = 0.10(5)$
$\nu = 1.0,\ \lambda = 4$	$M_\sigma = 2.03(2)$ $\Gamma_\sigma = 0.35(2)$	$M_\sigma = 2.01(2)$ $\Gamma_\sigma = 0.35(10)$
$\nu = 1.0,\ \lambda = 200$	$M_\sigma = 3.1(7)$ $\Gamma_\sigma = 1.2(5)$	$M_\sigma = N/A$ $\Gamma_\sigma = N/A$

Table 3: A comparison between the Lüscher's method and the Histogram Method.

that the two methods give consistent results. Where there is data for the Histogram method it agrees with the results from Lüscher's method within errors, which demonstrates that the Histogram method continues to capture resonance parameters despite the absence of $\phi(\kappa)$, although the Histogram method has larger errors. Another trend is that the errors become greater the broader the resonance for both methods. This is interesting as there is no significant increase in the relative error of the two pion energy levels on which both methods are based. This implies that this increase in error isn't purely a result of the Monte-Carlo error. Let us examine it for both methods.

In Lüscher's method the increase in the error is directly related to a flattening out of the phase shift as can be seen in comparing the two plots in Fig. 17. As already mentioned, when the slope of the phase shift is so flat, large variations in Γ produce very little variation in $\delta(p)$. Hence an evaluation of the width of a broad resonance will have larger errors due to this effect even if the simulations are performed with the same accuracy as a narrow

resonance.
For the Histogram method the resonance manifests as a Breit-Wigner profile in the histogram. The width of this Breit-Wigner profile is directly related to the resonance width. When the resonance is very broad, the profile is very flat and higher precision will be needed to resolve the structure of the histogram in which resonance information is contained.

So for both methods broad resonances cause difficulties because they are associated with some feature becoming less marked in the output data (slope of $\delta(p)$, width of histogram), which causes a reduced sensitivity to the resonance parameters. In both cases the solution to the problem is either increasing the amount of data, namely the energy levels, or a more likely solution, increasing the precision with which the energy levels are measured. High precision data will prevent the relevant features in either method from being lost in the noise.
This problem with broad resonances affects the Histogram method more strongly. Lüscher's method was capable of producing resonance parameters in the broadest case, where as nothing was obtained from the Histogram method. This suggests that the characteristic structure of the Histogram method, namely the width of the histogram, is more sensitive to errors in the original spectral data than the phase shift of Lüscher's method. However it should be noted that the histogram in the broad case did initially display a possible peak at $m_\sigma \approx 2.8$ which could be in agreement with the results from Lüscher's method. This peak was removed when the interacting energy levels without a free background were removed. Hence it is possible that the Histogram method is not significantly poorer than Lüscher's method for broad resonances, but rather that it suffers due to the ambiguity of its construction, which we now discuss.

The major practical advantage of Lüscher's method is that it is straight forward to apply. One simply needs data on the two particle spectrum and information on the phase shift follows through the application of the formula Eq.(4.29). Since $\phi(\kappa)$ in Lüscher's formula Eq.(4.29) is a well defined func-

tion which is independent of the theory being considered, it only needs to be calculated once. However the Histogram method, by contrast, involves several ambiguities:

1. The choice of Energy and Volume range, i.e. the subset $[E_{min}, E_{max}] \times [L_{min}, L_{max}]$ of the E, L plane we choose to use.

2. The resolution of both axis used in constructing the histogram, namely ΔE and ΔL

3. The amount of energy levels to include in the analysis. Of course the choice of the number of energy levels is also present in Lüscher's method, however in the Histogram method it is difficult to fix a choice since a higher number may become necessary in order to have the correct free background.

4. Of the energy levels included in the analysis one must choose how many to disregard because they don't possess a free background.

An incorrect choice for any these may result in an unusable histogram. The histogram method also requires the energy levels to be interpolated to all values through the use of a polynomial fit. However this is not a major problem since the use of such polynomials is theoretically justified and the errors on the fit are much smaller than other errors in the simulation. In fact as the polynomial fit is a numerical fit of a function known analytically, to some degree, this can be seen as the Histogram Method's analogue of the numerical evaluation of $\phi(\kappa)$. Hence overall, because of its smaller errors and its unambiguous application, Lüscher's method would seem to be the better method for resonances in the elastic region. However we now discuss two possible advantages of the Histogram method.

The first is purely a visual one. The Histogram literally peaks at the mass of the resonance and so one can read of the mass of the resonance without detailed fitting. This may be an advantage in cases where the precision is too low for either method to resolve the resonance parameters numerically in

a valid way and would provide an indication as to the mass of the resonance. The second advantage is of less obvious merit, but is interesting. For Lüscher's method the results from the inelastic region are uninterpretable, however for the histogram method it was still possible to construct a reasonable histogram, with a clear peak and width, as shown in Fig. 31. The disadvantage is that the meaning of this histogram is not clear. Outside the elastic region, due to the breakdown of Lüscher's formula, there is nothing to connect the histogram to the scattering phase shift and hence the resonance. This probably excludes a determination of the resonance width using the histogram method in the inelastic region, but it is possible that it may still give some indication of the mass. As mentioned in Sec.2.2.3, avoided level crossing is a feature of the eigenvalues of any hermitian matrix. If the resonance is narrow this avoided level crossing will possess a marked plateau, leading to an over abundance of interacting energy levels in the energy range containing m_σ. The plateau will occur simply through a combination of the mixing of the resonance with the stable states (which in the inelastic region will include four-particle states) and the avoided level crossing. This will lead to peak in the histogram at this value, independent of the validity of Lüscher's formula. So the Histogram method may be useful for basic visual estimates of the mass of a narrow inelastic resonance.

One final weakness of the two methods as they are applied here is the substitution of the Breit-Wigner form for the scattering cross section Eq.(4.42). Both methods link the two-particle spectrum to the phase shift $\delta(p)$. To go from $\delta(p)$ to resonance parameters requires an assumption of the functional form of $\delta(p)$. Using Eq.(4.42) assumes that the scattering phase shift is pure Breit-Wigner or that the resonance dominates the two particle scattering. The assumption of a negligible scattering background is valid for our model, as we see by inspection since the phase shift has a pure Breit Wigner profile. However in more general settings, such as QCD, there is no way to know the strength of the non-resonant background, since the physical particles are not clearly related to the Lagrangian fields. One possible way around this is to use a form for the phase shift $\delta(p)$ suggested by perturbation theory (this is

done in [47] for example by using one-loop results from chiral perturbation theory given in [48])or some other method and fit the results to this form.

5 Correlator method

A third and final method has also been tested on this same set of data. This method was proposed in [49] and shall be labelled the correlator method in what follows. The Correlator method aims to treat resonances on a similar footing to stable states in a lattice setting by extracting resonance parameters directly from some asymptotic estimate on the correlator. For stable states this is the well known exponential decay at large time. For resonances this method uses a more complicated asymptotic form at small times.

5.1 Asymptotic form of the correlator at small times

The Euclidean correlator $D(t,x)$ for some local quantum field $\mathcal{A}$ is defined as in the Sec.1.1, as

$$D(t,\mathbf{x}) = \int \mathcal{D}\phi \mathcal{A}(t,\mathbf{x})\mathcal{A}(0,0)e^{-S(\phi)} = \left(\Omega, \mathcal{A}(t,x)\mathcal{A}^{\dagger}(0,0)\Omega\right). \tag{5.1}$$

The Fourier transform of the correlator $D(i\omega,\mathbf{k})$, given by

$$D(t,\mathbf{x}) = \frac{1}{TL^3}\sum_{\omega}\sum_{\mathbf{k}} D(i\omega,\mathbf{k})e^{-i\omega t - i\mathbf{k}\mathbf{x}}, \tag{5.2}$$

can, by the completeness relation, be expressed as an integral over the Källén-Lehmann spectral function

$$D(i\omega,\mathbf{k}) = \int_{-\infty}^{\infty} \frac{d\omega'}{\omega' - i\omega}\rho_L(\omega,\mathbf{k}). \tag{5.3}$$

Applying the properties of ρ_L derived from discrete symmetries in [50], namely

$$\rho_L(\omega,k) \geq 0 \qquad \rho_L(-\omega,-k) = \mp\rho_L(\omega,k) = \mp\rho_L(\omega,-k), \tag{5.4}$$

the Fourier transform can be expressed as:

$$D(i\omega,\mathbf{k}) = \int_{0}^{\infty} \frac{d\omega'^2}{\omega'^2 + \omega^2}\rho_L(\omega'). \tag{5.5}$$

Of course the spectral function vanishes at values of $\omega^{'}$ less than the minimum mass in the channel. In our case we will be looking at the two pion states as before, so this value is $\omega_{min} = 2m_\pi$ and hence the integral can be rewritten as:

$$D(i\omega, \mathbf{k}) = \int_{2m_\pi}^{\infty} \frac{2\omega' d\omega'}{\omega'^2 + \omega^2} \rho_L(\omega'). \tag{5.6}$$

The basic idea of the method can now be explained. The infinite volume spectral function ρ has resonance poles on the second Riemann sheet. If the resonance is very narrow, Γ small, then these poles will come quite close to the branch cut and hence have an effect on the physical sheet "through the branch cut". However away from the branch cut the difference $\rho_L - \rho$ vanishes exponentially via the regular summation theorem [24], so at large volumes the effects of these resonance poles will show up in ρ_L and hence ultimately in the correlator itself.

We drop the dependence on k since it will not matter in what follows and does not occur in our correlators. If we let $T \to \infty$, then we obtain from Eq.(5.6) and Eq.(5.1):

$$D(t) = \int_{2m_\pi}^{\infty} d\omega e^{-\omega t} \rho_L(\omega). \tag{5.7}$$

Now at large volumes ρ_L can be replaced by ρ in the domain of integration.

$$D(t) = \int_{2m_\pi}^{\infty} d\omega e^{-\omega t} \rho(\omega). \tag{5.8}$$

In our case we will be dealing with a channel with angular momentum $l = 0$. In this case the spectral function has the form:

$$\rho(\omega) \approx (\omega - 2m_\pi)^{1/2}, \tag{5.9}$$

in the elastic region when there is no resonance. If there is a resonance then it takes the form:

$$\rho(\omega) = \frac{(\omega - 2m_\pi)^{1/2}}{(\omega - \omega_R)(\omega - \omega_R^*)} Q(\omega). \tag{5.10}$$

If we shift integration variables in Eq.(5.8) to $E = \omega - 2m_\pi$, where the resonance is found at $E_R = (m_\sigma - 2m_{pi}) - i\frac{\Gamma}{2}$ and substitute Eq.(5.10) we obtain:

$$D(t) = e^{-2m_\pi t} \int_{2m_\pi}^{\infty} d\omega e^{-\omega t} \frac{E^{1/2}}{(E - E_R)(E - E_R^*)} Q(E + 2m_\pi). \tag{5.11}$$

If the resonance is narrow enough then the singularities of $Q(E + 2m_\pi)$ will be far enough away from the elastic threshold that its Taylor expansion will converge in the region of the complex plane containing the resonance poles. Of course it is not possible to know *a priori* how narrow the resonance must be, so we applied the method to our data for the narrowest resonance. Expanding $Q(\omega)$ as $\sum_{k=0}^{\infty} q_k E^k$, the correlator is:

$$D(t) = e^{-2m_\pi t} \sum_{k=0}^{\infty} F^k(t, E_R), \tag{5.12}$$

$$F^k(t, E_R) = \int_0^{\infty} \frac{dE E^{k+1/2} e^{-Et}}{(E - (m_\sigma - 2m_\pi))^2 + \frac{\Gamma^2}{4}}. \tag{5.13}$$

All of the F^k with $k \geq 2$ can be expressed using F^0 and F^1 and so their contributions can be gathered together to give the following form for the correlator:

$$D(t) = \mathrm{e}^{-\omega_{\mathrm{min}} t} \left\{ c_0 F^{(0)}(t, E_R) + c_1 F^{(1)}(t, E_R) + \sum_{k=0}^{\infty} \frac{x_k}{t^{l+k+3/2}} \right\}. \tag{5.14}$$

The x_k parametrise the component of the scattering cross-section which is not due to the resonance, namely $\delta_{bg}(p)$. In our model we expect these numbers to be small as the resonance dominates the scattering. This approximation of the correlator should be valid in the region where $t \approx \frac{1}{\Gamma}$. In order to perform

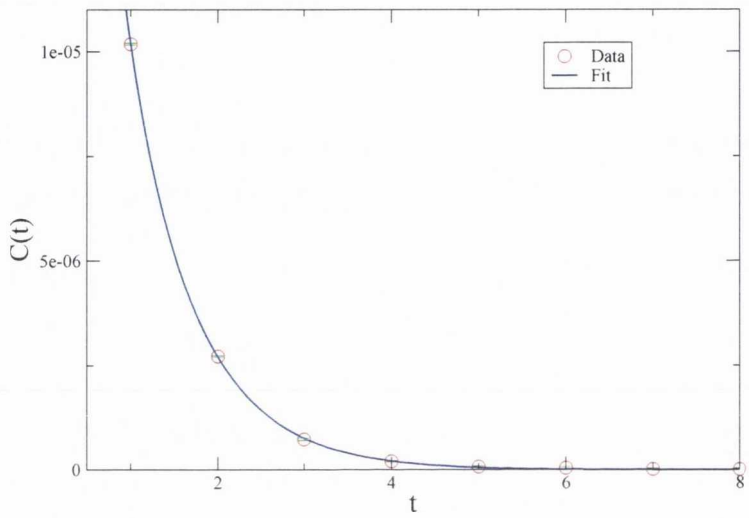

Figure 32: **Fit to sigma correlator** $\nu = 1.0$, $\lambda = 1.4$, $m_\pi^0 = 0.36$

this fit to the appropriate correlator, which in our case is the sigma correlator (the only local field with the correct quantum numbers), it is necessary to have a workable expression for the x_k, this is provided in [49]:

$$F^{(0)}(t, E_R) = -\frac{2}{\Gamma} \operatorname{Im} \chi(t, E_R),$$
$$F^{(1)}(t, E_R) = \operatorname{Re} \chi(t, E_R) - \frac{2E_0}{\Gamma} \operatorname{Im} \chi(t, E_R), \tag{5.15}$$

with the function $\chi(t, E_R)$ computable either via its integral representation:

$$\chi(t, E_R) = \int_0^\infty \frac{dE\, E^{1/2} \mathrm{e}^{-Et}}{E - E_R}, \tag{5.16}$$

or, more usefully, through the following expansion:

$$\chi(t, E_R) = -\pi \sqrt{-E_R}\, \mathrm{e}^{-E_R t} + \sqrt{\frac{\pi}{t}} \left\{ 1 + \sum_{i=0}^{\infty} \frac{(-2E_R t)^{i+1}}{(2i+1)!!} \right\}. \tag{5.17}$$

Hence fitting the sigma correlator directly to the form Eq.(5.14), should provide a direct determination of the resonance parameters in a manner similar to how stable particle masses are obtained. The Lüscher and Histogram methods get around the Maiani-Testa theorem via the indirect route of computing the two particle spectrum across several volumes. This method avoids the theorem by returning to the only n-point function on which it has no effect, the two-point function, requiring only a computation at a single large volume, in order that the difference $|\rho_L - \rho|$ be small.

5.2 The Fit

This method was not studied in as detailed a manner as the previous methods, however some results were obtained for the narrowest case. The medium and broad case do not produce meaningful results, it would seem, however this is to be expected as the method depends on assumptions related to a narrow resonance. An example of a fit to the sigma correlator for the parameters $\nu = 1.0$, $\lambda = 1.4$, $m_\pi^0 = 0.36$ is shown in Fig. 32.

Once $\chi(t, E_R)$ is well enough approximated, i.e. around $i = 2$ in Eq.(5.17), the fit produces good results. Including the x_k in Eq.(5.14) has no major effect on the results beyond $k = 2$, taking values of $k < 2$ was found to give very poor results. Fig. 32 is taken with $i = 1$, $k = 2$, giving resonance parameters of $M_\sigma = 1.5(2)$ and $\Gamma_\sigma = 0.11(3)$. The fitting window was taken as $t \in [1, 9]$. The fitting window does have a noticeable effect on the fit. In particular, a wider fit reduces the errors, but if the window is taken too wide unrealistic parameters are obtained. This is to be expected as the method relies on an asymptotic form at small times. All other parameters were found

to be small in magnitude as would be expected, specifically:

$$\begin{aligned} M_\sigma &= 1.32(5), \\ \Gamma_\sigma &= 0.107(7), \\ c_0 &= -0.00122(4), \\ c_1 &= 0.00023(8), \\ x_0 &= 0.078(1), \\ x_1 &= 0.158(5). \end{aligned}$$

With the fit having a value of $\frac{\chi^2}{\nu} = 0.8362$ for the reduced chi-squared value. Much was not investigated for this method, particularly a more precise estimate of the errors via the Bayesian analysis of [51] suggested in [49].

The main advantage of this method is that it requires only a fit to the correlator in a single, large, volume. The disadvantage is the presence of extra parameters, in our case c_0, c_1, x_0 and x_1, which make the fit less unique. Also the method appears to be restricted to narrow resonances. However, overall the results are consistent with the two preceding methods. One possible advantage to this method is that it is only restricted to the elastic region via the estimate on the spectral function in Eq.(5.10). It may be possible to derive a similar estimate of the spectral function in the inelastic region and apply the method there. Also the method avoids a computation of the two particle spectrum, which may be prohibitively expensive numerically in a more complex theory.

6 Conclusions

In this work, we have investigated and contrasted two major methods of determining resonance parameters, both in a perturbative and nonperturbative setting. Both of these methods are similar in that they use the two particle scattering spectrum as input data.

The first of the methods uses the well known Lüscher's formula. Given the input data of the scattering spectrum, the method requires an approximation of a known function, $\phi(\kappa)$, as well as an ansatz for the scattering phase shift. The advantage of the method is that once these two requirements are met the method is relatively straight forward to apply and, at least in the model tested here, capable of extracting resonance parameters across a wide range of resonance widths. Some disadvantages are that errors were found to increase with increasing resonance width and the additional errors coming from the approximation of $\phi(\kappa)$, although these are usually quite small and can be controlled.

The second method was the histogram method, which has been shown to give consistent results in both the perturbative and nonperturbative settings. In the perturbative setting the method reproduces the decay width found from the Minkowski space calculation. In the nonperturbative setting it agrees with the results of Lüscher's method. Together these show that the removal of $\phi(\kappa)$ has not affected the measurement of resonance parameters. The advantages of the method are that it does not require an estimate on $\phi(\kappa)$ and that, as it is tied to the avoided level crossing, may be capable of visually indicating the presence of a resonance, even if the errors are too large to determine the parameters. The disadvantages come from the ambiguity in its construction, making it difficult to apply and the larger errors for broad resonances.

Overall, for the ease of application and the smaller errors, Lüscher's method appears to be the better of the two. Both methods however suffer from com-

mon drawbacks. First of all they are rather indirect as, in separate ways, they recover the resonance from its influence on the two particle states. Secondly both methods are much better at handling narrow resonances than broad resonances, since some characteristic feature, necessary for a good fit, becomes less explicit and hence the fit isn't as well constrained. In using either methods, the spectrum must be very well determined in order to prevent a propagation of errors which will "wash out" this fundamental structure.

The most serious drawback however is that both methods are confined to the elastic region, which severely restricts their use in understanding physically relevant resonances. To extend these methods to the inelastic region would require a significant theoretical advancement in the understanding of finite volume field theory. To obtain a useful expression for the inelastic region a proof directly from quantum field theory would be required. In addition to this, a better understanding of the analytic properties of the n-point functions, $n < 6$, and the Bethe-Salpeter kernel would be required, as these are not as well understood in the elastic region. However it should be mentioned that a histogram can still be constructed in the inelastic region and in the case of the model here had the expected Breit-Wigner type structure. However the method lacks a proof which would connected this Breit-Wigner profile to an explicit expression containing the scattering phase shift.

For these reasons a third method was investigated which uses some appropriately chosen correlator, just as for stable particles. This means the method is more direct and similar to methods for stable particles, which allows it to avoid the problem of determination of the two particles spectrum in more complex theories. The initial results seem to be consistent with other methods, although there are more fitting parameters and the method is restricted to narrow resonances. The method also has the possibility of being extended to the inelastic region.

In conclusion, Lüscher's method and the Histogram method appear to be complementary in the case of elastic resonances below a certain width. For

broad resonances it would appear to be better to use Lüscher's method, unless the spectrum has been determined quite accurately. The main challenge for studying resonances on the lattice however remains the inelastic region which would require either new methods, such as analysis of Bethe-Salpeter wavefunctions, or a non-trivial extension of current methods.

References

[1] Weinberg, S. *The Quantum Theory of Fields: Volume I.* Cambridge University Press. (1995).

[2] Nakamura, K. et al. (Particle Data Group), "Review of Particle Physics" *J. Phys. G* **37**, 075021 (2010).

[3] Montvay, I. and Münster G., *Quantum Fields on the Lattice*, Cambridge Monographs on Mathematical Physics. Cambridge University Press. (1997).

[4] Fröhlich, J. "Schwinger functions and their generating functionals, I." *Helv. Phys. Acta* **47**, p.265 (1974).

[5] Glimm, J. and Jaffe, A. *Quantum Physics: A Functional Integral Point of View.* Springer-Verlag, New York. (1987).

[6] Nielsen, H.B., Ninomiya, M. "Absence of neutrinos on a lattice I: Proof by homotopy theory" *Nucl. Phys. B* **185**, 20. (1981).

[7] Friedan, D. "A proof of the Nielsen-Ninomiya theorem", *Comm. Math. Phys.* **85**, p.481. (1982).

[8] Lüscher, M. "Signatures of unstable particles in finite volumes", *Nucl. Phys. B* **364**, p.237 (1991).

[9] DeGrand, T. "Resonance masses from Monte Carlo simulations", *Phys. Rev. D* **43**, p.2296 (1991).

[10] Wiese, U.J., "Identification of resonance parameters from the finite volume energy spectrum" *Nucl. Phys. Proc. Suppl.* **9** p.609 (1989).

[11] Michael, C. "Particle decay in lattice gauge theory", *Nucl. Phys. B* **327**, p.515 (1989).

[12] Bernard, V.M., Lage, M., Meißner U.G. and Rusetsky, A. "Resonance properties from the finite-volume energy spectrum", *J. High Energy Phys.* **8(2008)**, p.24 (2008).

[13] Taylor, J. *Scattering Theory: The Quantum Theory of Nonrelativistic Collisions*, Dover Edition, Dover Publications. (2006).

[14] Reed, M. and Simon, B. *Methods of Modern Mathematical Physics*, Vol. III, New York: Academic Press. (1979).

[15] L. Maiani and M. Testa, "Final state interactions from euclidean correlation functions" *Phys. Lett. B*, **245**, p. 585 (1990).

[16] Watson, K.M. "The Effect of Final State Interactions on Reaction Cross Sections" *Phys. Rev.*, **88**, p.1163 (1952).

[17] Lüscher, M. "Volume Dependence of the Energy Spectrum in Massive Quantum Field Theories I: Stable Particle States", *Comm. Math. Phys.* **104**, p.177 (1986).

[18] Nakanishi, N. *Graph theory and Feynman integrals*, New York: Gordon and Breach. (1971).

[19] Lüscher, M. "Two particle states on a Torus and their relation to the scattering matrix", *Nucl. Phys. B* **354**, p.531 (1991).

[20] DeWitt, B. "Transition from Discrete to Continuous Spectra", *Phys. Rev.* **103**, p.1565 (1956).

[21] Lüscher, M. and Wolff, U. "How to calculate the elastic scattering matrix in two dimensional quantum field theories by numerical simulation", *Nucl. Phys. B* **339**, p.222 (1990).

[22] Reed, M. and Simon, B. *Methods of Modern Mathematical Physics*, Vol. II, New York: Academic Press. (1975).

[23] Bros, J. and Lassalle, M. "Analyticity properties and Many-Particle structure in General Quantum Field Theory III: Two-Particle Irreducibility in a single channel", *Comm. Math. Phys.* **54**, p.33 (1977).

[24] Lüscher, M. "Volume Dependence of the Energy Spectrum in Massive Quantum Field Theories II: Scattering States", *Comm. Math. Phys.* **105**, p.153 (1986).

[25] Gattringer, C.R. and Lang, C.B. "Resonance scattering phase shifts in a 2d lattice model" *Nucl. Phys. B.* **391** p.463 (1993).

[26] Fiebig, H.R., Linsuain, O., Markum, H. and Rabitsch, K. "Extraction of hadron-hadron potentials on the lattice within 2+1 dimensional QED" *Phys.Lett. B* **386** p.285 (1996).

[27] Goeckeler, M., Kastrup, H.A., Viola, J. and Westphalen, J. "Scattering phases for fermion-fermion scattering in the Gross-Neveu model" *Nucl.Phys.Proc.Suppl.* **47** p.831 (1996).

[28] Ishii, N., Aoki, S. and Hatsuda, T. "Nuclear Force from Lattice QCD" *Phys. Rev. Lett.* **99** p.022001 (2007).

[29] Yamazaki, T. et al."$I = 2\pi\pi$ scattering phase shift with two flavors of O(a) improved dynamical quarks" *Phys. Rev. D* **70** p.074513 (2004).

[30] Dudek, J.J, Edwards, R.G., Peardon, M.J., Richards, D.G., and Thomas, C.E. "Phase shift of isospin-2 $\pi\pi$ scattering from lattice QCD" *Phys. Rev. D* **83** p.071504 (2011).

[31] Budapest-Marseille-Wuppertal Collaboration (Frison, J. et al.) "Rho decay width from the lattice" *PoS Lattice 2010* p.139 (2010).

[32] Rummukainen, K. and Gottlieb, S. "Resonance scattering phase shifts on a non-rest-frame lattice" *Nucl. Phys. B.* **450** p.397 (1995).

[33] Lüscher, M. "Selected topics in lattice field theory", as part of *Fields, strings and critical phenomena; Les Houches (1988)*, Ed. Brézin, E. and Zinn-Justin, J., North Holland Publishing, Amsterdam. (1988).

[34] Aoki, S. "Lattice QCD and Nuclear Physics", as part of *Modern Perspectives in Lattice QCD: Quantum Field Theory and High Performance Computing; Les Houches (2009)* Ed. Lellouch, L., Sommer, R., Svetitsky, B., Vladikas, A. and Cugliandolo, L.F., Oxford University Press. (2011).

[35] Ishii, N. "An extension to the Lüscher's finite volume method above inelastic threashold (formalism)" *PoS Lattice 2010* p.145 (2010).

[36] Liu, C., Feng, X. and He, S. "Two Particle States in a Box and the s-Matrix in Multi-Channel Scattering" *Int. J. Mod. Phys. A* **21** p.847 (2006).

[37] Morningstar, C. "Exploring Excited Hadrons" *PoS Lattice 2008*, 009. (2008).

[38] Drummond, I.T. "Singularities of Feynman Amplitudes", *Nuovo Cimento* **29**, p.720 (1963).

[39] Eden, R.J. and Polkinghorne, J.C. *Lecture notes of the Brandeis Summer Institute*, Vol. I, New York: Academic Press. (1961).

[40] Hörmander, L., *The analysis of linear partial differential operators I*, Grundl. Math. Wissenschaft., **256**, Springer. (1983).

[41] Bernard, V., Meißner U.G. and Rusetsky, A. "The Δ-resonance in a finite volume" *Phys. Lett. B*, **788**, p.1 (2008).

[42] Giudice, P., McManus, D. and Peardon, M. "Extracting resonance parameters from lattice data." *PoS Lattice 2010* p.105 (2010).

[43] Giudice, P. and Peardon, M. "Hadronic decay width from finite-volume energy spectrum in lattice QCD." *AIP Conf. Proc.* **1257** p.784 (2010).

[44] Gockeler, M., Kastrup, H.A., Westphalen, J. and Zimmermann, F., "Scattering phases on finite lattices in the broken phase of the four-dimensional O(4) ϕ^4 theory" *Nucl. Phys. B* **425**, p.413 (1994).

[45] DeGrand, T. and Detar, C.E. *Lattice methods for quantum chromodynamics*, World Scientific. (2006).

[46] Levenberg, K. "A Method for the Solution of Certain Non-Linear Problems in Least Squares". *Quarterly of Applied Mathematics* **2** p.164 (1944).

[47] Lellouch, L. and Lüscher, M. "Weak transition matrix elements from finite-volume correlation functions" *Comm. Math. Phys.* **219** p.31 (2001).

[48] Knecht, M., Moussallam, B., Stern, J. and N.H. Fuchs "The low energy $\pi\pi$ amplitude to one and two loops" *Nucl. Phys. B* **457** p.513 (1995).

[49] Bernard, V., Polejaeva, K. and Rusetsky, A."Extraction of Resonance parameters at finite times" *Nucl. Phys. B*, **846**, p.1 (2011).

[50] Asakawa, M., Hatsuda, T., Nakahara, Y. "Maximum Entropy Analysis of the Spectral Functions in Lattice QCD", *Prog.Part.Nucl.Phys.* **46** p.459 (2001).

[51] Schindler, M.R. and Phillips, D.R. "Bayesian Methods for Parameter Estimation in Effective Field Theories" *Annals Phys.* **324**, p.682 (2009) [Erratum-ibid. **324**, p.2051 (2009)].